HIGH-THROUGHPUT MICROFLUIDIC SCREENING PLATFORMS FOR MICROALGAE STUDY

A Dissertation

by

HYUN SOO KIM

Submitted to the Office of Graduate and Professional Studies of
Texas A&M University
in partial fulfillment of the requirements for the degree of

DOCTOR OF PHILOSOPHY

Chair of Committee,	Arum Han
Committee Members,	Timothy P. Devarenne
	Byung-Jun Yoon
	Jun Kameoka
Head of Department,	Chanan Singh

December 2014

Major Subject: Electrical Engineering

ABSTRACT

Microalgae have been envisioned as a future source of renewable energy. Both fossil fuel depletion and environmental concern have drawn more interest in microalgal biofuels, but the production cost of these biofuels are not yet economically competitive. Significant improvements such as development of better performing microalgal strains, optimization of culture conditions, and better understanding of microalgal biology are required for commercial viability. To resolve these limitations, massively parallel studies are needed, however, current microalgae culture systems are lack of high-throughput screening capabilities, and thus not suitable for the parallel studies. Here, three different high-throughput microfluidic microalgae screening platforms have been developed, each of which addresses major bottlenecks towards economically feasible microalgal biofuel.

The first platform, a high-throughput microfluidic photobioreactor array has been developed to investigate the effect of different culture conditions on microalgal growth and oil production. This platform can provide up to 64 different culture conditions on-chip, such as combinations of different light intensities, light cycles, and culture media/chemical compositions. Single cell/colony trapping sites in culture compartments allowed for long-term analysis of microalgal growth and oil production with single cell/colony resolution. The light conditions that induced 1.8-fold higher oil accumulation over the typically used culture conditions were successfully identified.

The second platform, as a microalgae library screening tool, a high-throughput microfluidic single-cell screening and selection platform has been developed to examine

growth and oil production of various microalgal strains, followed by selective extraction of particular microalgae showing desired traits to off-chip reservoirs for further analysis. Single microalga was isolated and cultured, and its growth and oil accumulation were analyzed through 1024 single-cell trapping/culturing sites in the platform, where opening and closing of each trap can be individually controlled with integrated microfluidic control layers. By opening only a specific site out of the 1024 trapping sites, microalgae in particular trapping sites were selectively released and successfully collected off-chip.

The third platform, a high-throughput droplet microfluidics-based microalgae screening platform has been developed to investigate the growth and the oil production of microalgal libraries with much higher throughput. Growth was characterized by encapsulating a single microalga into a droplet (functions as an independent bioreactor) and tracking its behavior over time. Oil production was also quantified through on-chip staining process, the key feature of the platform, where oil content in microalgae can be stained and measured through on-chip fluorescent tagging. Growth and oil accumulation under different culture conditions were successfully analyzed and compared, demonstrating the capability of the platform as a high-throughput screening tool.

We have developed series of high-throughput microfluidic screening platforms for microalgae study, which provides the capabilities of analyzing microalgal growth and oil production under different culture conditions or among large numbers of microalgal library. The developed platforms will serve as powerful tools to accelerate research in addressing the limitations of microalgal biofuels as well as to significantly advance the current state of microalgal biofuel production.

To my family, for their love and support

ACKNOWLEDGEMENTS

I would foremost like to express my heartfelt gratitude to my advisor, Dr. Arum Han for all his contributions of time, ideas, guidance, and support throughout my research and Ph.D. experiences. He provided me with an excellent atmosphere to be an independent thinker, an engineer as well as a researcher. This dissertation could not have been written without him.

I also thank Dr. Timothy Devarenne not only for his guidance and valuable input throughout the research, but also for allowing me to collaborate and work with my friends Taylor Weiss and Hem Thapa. I look forward to many years of friendship and research together. Without their help, my project couldn't have developed this far.

I would like to extend my thanks to all of my committee members, Drs. Byung-Jun Yoon and Jun Kameoka for their guidance and support. The advice given me during the projects has inspired me in many ways and helped me to think outside the box.

I thank all our group members in NanoBio Systems laboratory for their support, help, and opinions from different angles. I want to express special thanks to Chiwan Koo, Han Wang, and Adrian Guzman for their valuable advices and precious discussions over years.

My time at Texas A&M was made enjoyable in large part due to many friends that became a part of my life. Time I spent with Sungwook Hong, Jaewon Yoo, Jaewon Park, and Jaewoo Suh is the most pleasant memories I have from College Station and will definitely miss the parties and trips we had together.

“Thank you” is not enough for my family. None of this would have been possible without their love and patience. My parents and younger brother support me no matter what I choose to do. My wife, my love and best friend, always supports and encourages me, no matter how things are going. My beloved daughter, one of the most grateful gift during my life, lightens my life with so much happiness. My parents-in-law, thank you for your support and love. To them I dedicated this dissertation.

TABLE OF CONTENTS

Page

LIST OF FIGURES

Page

LIST OF TABLES

Page

CHAPTER I

INTRODUCTION

1.1. Microalgae as a future source of renewable biofuels

1.1.1. Limitations of fossil fuels

In 2013, the annual world energy consumption was estimated at 12,730 million tonnes of oil equivalent. Fossil fuels accounted for 86.7% of the world energy consumption, with oil (32.9% share), natural gas (23.7%), and coal (30.1%) as the major fuels, while nuclear energy, hydroelectricity, renewables account for 4.4%, 6.7%, and 2.2% of the total energy consumption, respectively.[1] Even though the large portion of world energy is covered from the fossil fuels so far, these fuels are regarded as an unsustainable energy source not only due to depletion of world fossil fuel reserves, but also because of the global warming effect resulting from greenhouse gas accumulation.[2-10] For example, fossil fuels are the largest contributor of greenhouse gases to the atmosphere, and in 2010, associated CO_2 emissions were 31 Gtonnes, which was much higher than 12 Gtonnes, an estimated amount that can be removed by natural processes.[11] So fuel production processes are required to be renewable as well as be capable of sequestering atmospheric CO_2 to achieve environmental and economic sustainability.

1.1.2. Biofuel from oil-producing crops

First generation biofuels, which have now reached economic production level, are mainly extracted from food and oil crops such as rapeseed oil, sugarcane, sugar beet, and maize as well as vegetable oils and animal fats.[2] This first generation biofuels can be renewable and carbon-neutral energy sources since they produce energy while only releasing carbon to the atmosphere, captured during the plant growth. However, the impact of the first generation biofuels on satisfying the global energy needs will remain limited due to challenging in large-scale production, competition with food supply, regionally constrained market structure, and high water and fertilizer requirements. In addition, this plant-based oil production has already contributed to an increase of the price of oil crops over the last few years.[12] So it is required to develop an alternative biofuel source, and microalgae seems to be a next promising renewable energy source capable of overcoming the limitations of the first generation biofuels as well as satisfying the global demand.

1.1.3. Microalgae as a promising biofuel resource

Microalgae are photosynthetic microorganisms that convert sun light and atmospheric carbon dioxide to potential biofuels (oil), foods, feeds, and high-value bioproducts.[2, 8] They are typically characterized by much higher growth rate (for example, their biomass doubling time can be as short as 3.5 hours during exponential growth) and oil content compared to oil-producing crops.[4, 6, 7, 13] Oil levels of 20 ~ 50% are common in microalgae, and even some microalgae have more than 70% oil content

inside (Table 1).[4, 6, 8, 14-22] As shown in Table 2, there are significant variations in biomass productivity between oil crops and microalgae, which result in much higher oil yield and biodiesel productivity and much less land use in microalgae.[6, 8, 23-25] There are more advantages that make microalgae as an attractive biofuel resource; less amount of water is required in microalgae growth, which reduces the demand on freshwater sources[26]; since microalgae can be cultured in brackish water on non-arable land, concerns related to competition with food supply, land usage, and associated environment impact are minimized[6, 27]; as microalgae exist in almost all earth ecosystem, it is feasible to find and grow microalgae species best suitable for local environment which is not possible in crops[8]; microalgae production can effect CO_2 biofixation.[6]

1.1.4. Challenges toward economically viable microalgal biofuel

Despite the promising potential of microalgae as a biofuel resource, there are several challenges to be resolved for attaining commercial viability that would allow sustainable production and utilization. The limitations include: cost for producing microalgal biofuels is not in economic stage[6]; scaling up for mass production is challenging[28]; biology (*e.g.,* gene and metabolic regulation) of most microalgae is not well-known so far.[9] To overcome these limitations (*i.e.,* to produce enough microalgal oil to satisfy fuel demand), it is necessary to develop better oil-producing strains through genetic and metabolic engineering or evolutionary pressure, to improve large-scale cultivation based on understanding of microalgal biology, to improve oil extraction methods, and to optimize the culture environment.[5, 9, 29]

Table 1. Oil content of different microalgae species.

Microalgae species	**Oil content (% dry weight biomass)**
Botryococcus braunii	25 – 75
Chlorella vulgaris	5 – 58
Chlorella sp.	10 – 48
Crypthecodinium cohnii	20 – 51
Cylindrotheca sp.	16 – 37
Dunaliella tertiolecta	17 – 71
Dunaliella sp.	17 – 67
Euglena gracilis	14 – 20
Isochrysis sp.	7 – 33
Monallanthus salina	20 – 22
Nannochloropsis sp.	20 – 56
Neochloris oleoabundans	29 – 65
Nitzschia sp.	16 – 47
Phaeodactylum tricornutum	18 – 57
Spirulina platensis	4 – 17
Tetraselmis sueica	8 – 23

Table 2. Comparison of biodiesel feedstocks.

Crop (oil content, % oil by weight in biomass)	Oil yield (L oil/ha year)	Land use (m^2 year/kg biodiesel)	Biodiesel productivity (kg biodiesel/ha year)
Corn (44)	172	66	152
Soybean (18)	636	18	562
Canola (41)	974	12	862
Jatropha (28)	741	15	656
Sunflower (40)	1070	11	946
Oil palm (36)	5366	2	4747
Microalgae (30)	58700	0.2	51927
Microalgae (50)	97800	0.1	86515
Microalgae (70)	136900	0.1	121104

1.2. Microfluidics and lab-on-a-chip

Microfluidic devices and lab-on-a-chip technologies have become increasingly useful tools in bio/medical applications owing to their various advantages over conventionally used systems[29-56]; for example, the ability to precisely control, monitor and manipulate tiny amounts of samples at the nano- to pico-liter scales. These advantages also include the unique characteristics of microfluidics such as small sample/reagent consumption, large surface to volume ratio, laminar flow, and faster analysis/response of biological samples at low cost. Due to compact system size, massive parallelization can be achieved in microfluidic devices, which allows high-throughput analysis. Also, cells can be cultured, controlled, and analyzed with single-cell resolution under more physically and biochemically controlled environment by utilizing microfluidic devices. The lab-on-a-chip concept, which is building an entire life science or chemistry lab on a chip, enables multiple microfluidic components to be integrated into a single platform where all the necessary steps for a particular procedure, from sample preparation to sample analysis, can be conducted with the minimum manual intervention.

1.3. The need for a high-throughput microfluidic screening platform

Current microalgal studies are conducted by culturing the organism in lab-scale flasks, open raceway ponds, or closed photobioreactors.[5-7, 9] These culture systems have made significant contributions to the understanding of basic algal biology, selecting the best strains for the production of biochemicals, and understanding the effects of various

culture factors (*e.g.,* light intensity, light cycle, temperature, nutrient concentration, CO2, pH) on algal growth and oil production. However a clear understanding of the relationships between oil production and biomass increase in response to these various culture conditions for a variety of algae is still needed. There are two factors hampering these efforts. First, the light intensity and cycle exposed to each microalga changes as microalgal density increases over time in conventional photobioreactors, making it difficult to apply identical conditions to all microalgae in a given culture system for direct side by side comparison. Second, conventional flask-type photobioreactors are inadequate as high-throughput screening systems. The workload created by the combinatorial nature of many culture factors and the numerous microalgal strains to be considered, both natural and engineered, cannot be approached by simply doubling or tripling the throughput of currently available culture systems. Thus, a fundamentally different approach is needed to increase the throughput, and a high-throughput microfluidic screening platform can be a promising solution. The high-throughput microfluidic screening platform that can provide well-controlled culture conditions as well as quickly screen through various culture conditions to identify the best algal strains and conditions for fast growth and high oil production could significantly advance the current state of algal biofuel production.

CHAPTER II

A HIGH-THROUGHPUT MICROFLUIDIC PHOTOBIOREACTOR ARRAY *

2.1. Motivation

Microalgae obtain their metabolic energy by photosynthesis which converts solar energy into chemical form inside, and thereby, microalgal growth and oil production are strongly dependent on light conditions (light intensity and light-dark cycle). Different growth/biomass increases and oil production have been reported under different light intensities and cycles.[57-59] In particular, different ranges of favorable light intensity and cycles for improved growth/biomass increase and oil production have been studied for different strains of the same microalgal species.[60-63] However, the favorable light conditions even for a single microalgal strain can differ depending on culture systems, which makes it challenging to compare the significance of the relationship between light conditions and growth/oil production amongst these previous studies.[64-67] This might result from the different culture systems used for testing and the lack of tools applicable for examining the relationship at a microscopic level, where a high-throughput microfluidic screening platform can become a solution. The microfluidic screening platform can also overcome the limitations of conventional culture systems by applying

---

* [H. S. Kim, T. L. Weiss, H. R. Thapa, T. P. Devarenne, and A. Han, "A microfluidic photobioreactor array demonstrating high-throughput screening for microalgal oil production", *Lab on a Chip*, 14, 1415-1425, 2014] – Reproduced by permission of The Royal Society of Chemistry (http://pubs.rsc.org/en/content/articlelanding/2014/lc/c3lc51396c).

identical conditions to all microalgae in culture chambers and implementing high-throughput screening capabilities.

A few microsystems for characterizing and distinguishing microalgal species have been reported so far[54, 68-72], but they were simply analytic devices that lacked cell culture capability. Microfluidic culture systems to examine microalgal lipid production, density changes, or growth kinetics have also been developed.[73-76] However, these systems could provide only a single culture environment at a time, not suitable for high-throughput screening applications. Recently, a high-throughput optical microplate-based culture platform was developed where growth and lipid production of microalgae under different light conditions could be studied.[77] However it only allowed population-based studies, and long-term analysis was challenging due to the lack of nutrient supply capability.

The high-throughput microfluidic photobioreactor array presented here addresses the significant shortcomings of previous systems by providing single-colony resolution for photosynthetic microorganism under an extremely well controlled environment at high-throughput. The array is composed of a dynamic light controllable cell culture array capable of simultaneously studying the effect of 64 different light exposure conditions on algal growth and oil production with single-colony resolution. Coupled with arrays of 64 miniaturized microalgal culture chambers, 64 independent photobioreactor experiments could be conducted in parallel on a 5 x 7 cm^2 footprint. Continuous perfusion of nutrient to each of the miniaturized photobioreactors having arrays of

single-colony trapping microstructures allowed time-course analysis of algal growth and oil production over long periods of time.

2.2. Design

The microfluidic microalgal photobioreactor array is composed of four poly(dimethylsiloxane) (PDMS) layers stacked on top of each other (size: 5 x 7 cm^2): a culture layer, a light intensity control layer, a light-dark cycle control layer, and a light blocking layer (Figure 1A). The bottom microalgae culture layer has 64 culture compartments (diameter: 900 μm, height: 85 μm) connected to an inlet and an outlet through which microalgae and fresh media is introduced and waste is flushed out, respectively (Figure 1B). Five single-colony trapping structures in the culture compartments enable the capture, culture, and analysis of microalgae with single-colony resolution over long periods of time (opening of each trap: 77 μm, Figure 1B-C). The light intensity control layer employs a microfluidic gradient generator to provide various intensities on a single platform with a single light source. The gradient generator utilizes a series of diffusive-mixing channel networks through which different dilutions of chemicals are automatically generated at outlets from two fluid inlets.[78, 79] By flowing deionized (DI) water and black dye through each inlet, the 8-outlet gradient generator produces 8 different concentrations of black dye into downstream channels. When a single light source is placed on top of these 8 channels, the different concentrations of black dye result in 8 different ranges of light shading effects to the underlying microalgae culture layer (Figure 1A). The control of light-dark cycles is based on

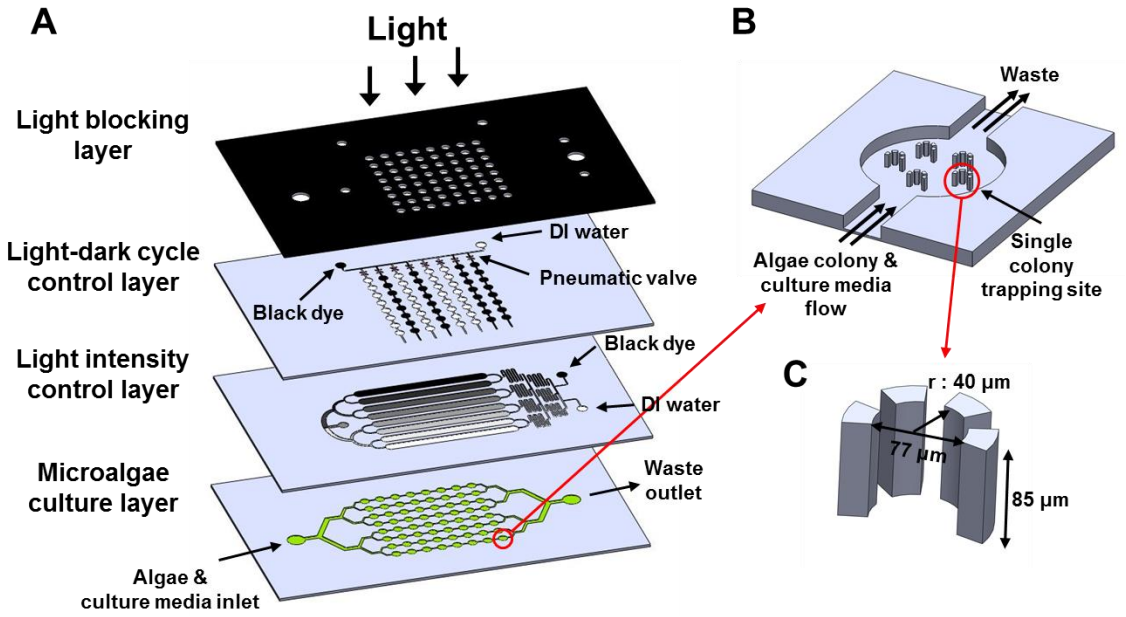

Figure 1. The high-throughput microfluidic microalgal photobioreactor array. (A) The platform was composed of four layers - a light blocking layer, a microfluidic light-dark cycle control layer, a microfluidic light intensity control layer, and a microalgae culture layer. (B) Enlarged view of a single culture compartment having five single-colony trapping sites. (C) A single-colony trapping site composed of four micropillars.

selectively filling each microfluidic channel in the light-dark cycle control layer either with DI water or black dye. When a channel is filled with DI water, 100% of light is transmitted to the underlying culture compartments, resulting in light (or "day") condition. On the other hand, when a channel is filled with black dye, no light is transmitted, creating dark (or "night") condition (Figure 1A). Integrated pneumatic microvalve structures and a microfluidic binary demultiplexer are utilized to individually manage each of the 8 light-dark cycle control channels.[80] This enables switching between DI water (light) and black dye (dark) in a particular channel without affecting the light-dark cycles of other channels. 8 different light-dark cycles can be implemented by periodically filling each channel with either DI water or black dye at 8 different time periods. To screen microalgae against 64 different light conditions in parallel, the 8 light intensity control channels and the 8 light-dark cycle control channels are placed perpendicular to each other for generating 64 unique light conditions to the 64 microalgal culture compartments underneath (Figure 1A). The top light blocking layer in the microfluidic platform is employed to provide isolated light conditions onto each of the underlying microalgae culture compartments.

2.3. Fabrication

The multi-layer microfluidic photobioreactor array was fabricated in PDMS using soft-lithography, a method where hundreds of polymer replicas can be stamped out from a single master mold.[81] The top light blocking layer was made by replicating a black-color PDMS layer (Sylgard® 170, Dow Corning, Inc., Midland, MI) from CNC-

machined acrylic masters (12.5 mm, McMaster-Carr, Atlanta, GA) for blocking all light except for openings for the microalgae culture area and the inlet/outlet interface area.

The master molds for the light intensity control layer, the light-dark cycle control layer, and the microalgae culture layer were all fabricated with photosensitive epoxy (SU-8™, Microchem, Inc., Newton, MA) using a conventional photolithography process. The microfluidic gradient generator channels in the light intensity control layer were made of two SU-8™ layers by spin-coating them at 2200 and 1950 rpm, respectively (SU-8™ 2025: 30 μm, SU-8™ 2075: 90 μm). The light-dark cycle control channels in the light-dark cycle control layer were 90 μm thick, and the master mold was fabricated by spin-coating SU-8™ 2075 at 1950 rpm. The pneumatic binary demultiplexer in the light-dark cycle control layer was 150 μm thick, and the master mold was obtained by spin-coating SU-8™ 2075 at 1000 rpm. These three masters were soft-baked at 65°C for 24 hours, followed by another soft-baking step at 95 °C for 40 minutes. The master mold for the microalgae culture layer, 85 μm thick, was patterned with SU-8™ 2050 by spin-coating at 1500 rpm and soft-baking in two steps at 65°C and 95°C for 60 and 20 minutes, respectively. All masters were exposed to ultraviolet (UV) light followed by a two-step post-exposure baking at 65°C for 10 minutes and at 95°C for 20 minutes. Before PDMS replication, all SU-8™ master molds were coated with a surfactant, (tridecafluoro-1,1,2,2-tetrahydrooctyl) trichlorosilane (United Chemical Technologies, Inc., Bristol, PA), to facilitate PDMS release without damaging the master molds, followed by rinsing with isopropyl alcohol (IPA) to remove excessive coating residues.

PDMS layers forming the microfluidic gradient generator channels and the light-dark cycle control channels (both 130 μm thick) and the pneumatic binary demultiplexer (300 μm thick PDMS) were replicated from the SU-8™ masters by spin-coating 8 g of PDMS pre-polymer at the speed of 700 rpm and 300 rpm for 40 seconds, respectively. To create high-aspect-ratio trapping structures (85 μm/25 μm = 3.4) in the PDMS microalgae culture layer, an SU-8™ master mold having corresponding high-aspect-ratio holes were required. However, a two-step PDMS casting method with a SU-8™ master having raised trapping structures was utilized rather than a typical single-layer casting method that resulted in severe crack to the structure due to the very long developing process. First, a PDMS master having deep holes was cast from the SU-8™ master by pouring 7 g of PDMS pre-polymer and curing it at 85 °C for 3 hours. The PDMS master was then coated with trichlorosilane and rinsed with IPA. A PDMS microalgae culture layer (around 300 μm thick) having the same features with the SU-8™ master was replicated from the PDMS master by pouring 2.5 g of PDMS pre-polymer and curing it at 85 °C for 4 hours.

All PDMS layers were treated with oxygen plasma (Plasma cleaner, Harrick Plasma, Ithaca, NY) before assembly. This PDMS assembly forming the microfluidic microalgal photobioreactor array was then bonded with an acrylic frame, which provided a CO2-controlled environment required for microalgae culture. The overall fabrication steps and assembly processes are summarized in Figure 2.

Figure 3 shows images of the microfabricated high-throughput microfluidic microalgal photobioreactor array. The light blocking layer (Figure 3A), the light-dark

cycle control layer, the light intensity control layer, and the microalgae culture layer (Figure 3B) were successfully replicated from the master molds and assembled together. Also, the high-aspect-ratio trapping structures in the microalgae culture layer were successfully fabricated without damaging pillar structures through the two-step PDMS casting method (Figure 3C-D). Figure 3E illustrates the scanning electron micrograph (SEM) of the single culture chamber with five trapping sites.

2.4. Microfluidic control of light intensity

2.4.1. Characterization of on-chip light intensity control

The microfluidic gradient generator was utilized in the light intensity control layer to generate various intensities of light on a single platform with a single light source. First, a 16-outlet gradient generator was employed instead of the 8-outlet design to characterize the relationship between the concentrations of black dye and resulting light intensities. Light transmission (and light intensities) through different concentrations of black dye (different shading effects depending on black dye concentrations) were measured using a quantum sensor (LI-190 Quantum Sensor with LI-250A Light Meter, LI-COR Bioscience, Lincoln, Nebraska) by filling the light intensity control layer with 19 different black dye (black ink kit for Epson 78 printer) concentrations (0, 0.1, 0.3, 0.5, 1, 1.5, 2, 2.5, 3.5, 4, 5, 6.5, 8.5, 10, 15, 20, 40, 60, 80, 100%). A 14-W compact fluorescent light bulb (65K) was placed on top as a light source, and the transmitted light intensity was measured by first changing the

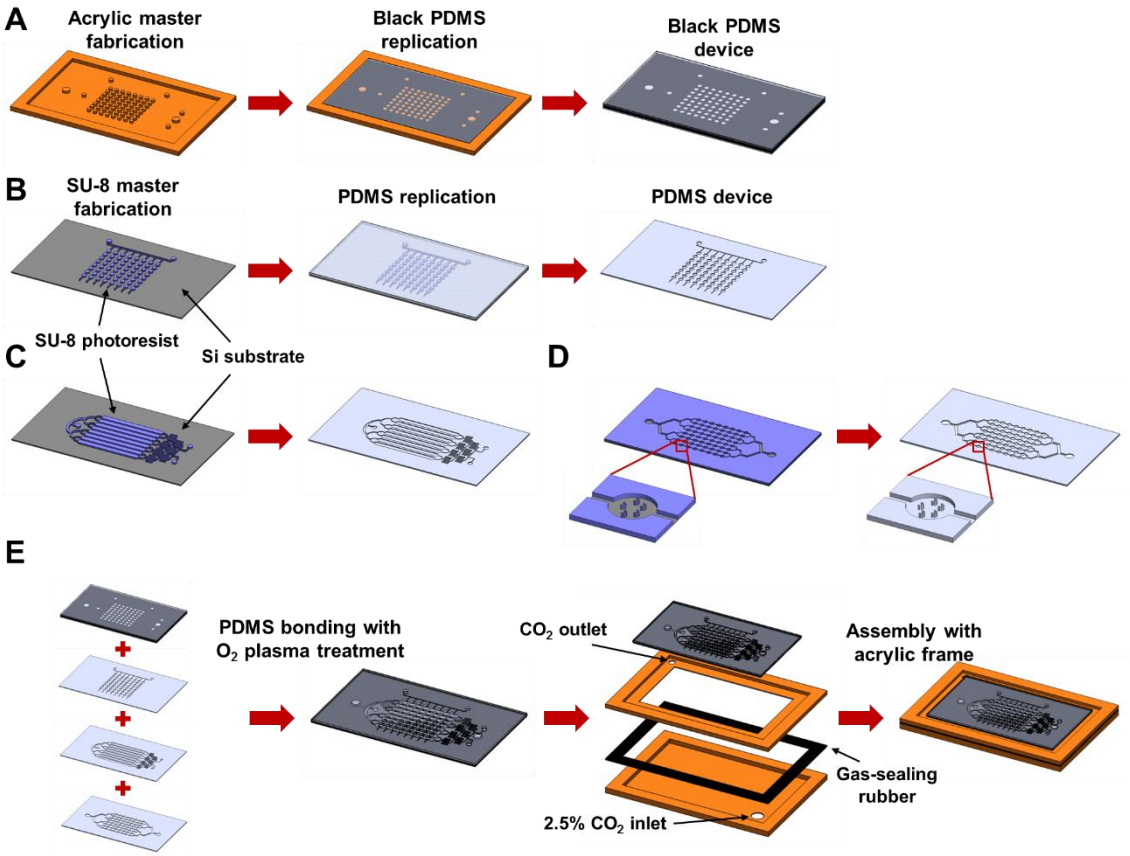

Figure 2. Fabrication process of the microfluidic microalgal photobioreactor array. (A) Light blocking layer. (B) Microfluidic light-dark cycle control layer. (C) Microfluidic light intensity control layer. (D) Microalgae culture layer. (E) Bonding of all PDMS layers using O_2 plasma treatment and assembly into a gas-tight acrylic frame for CO_2-controlled environment.

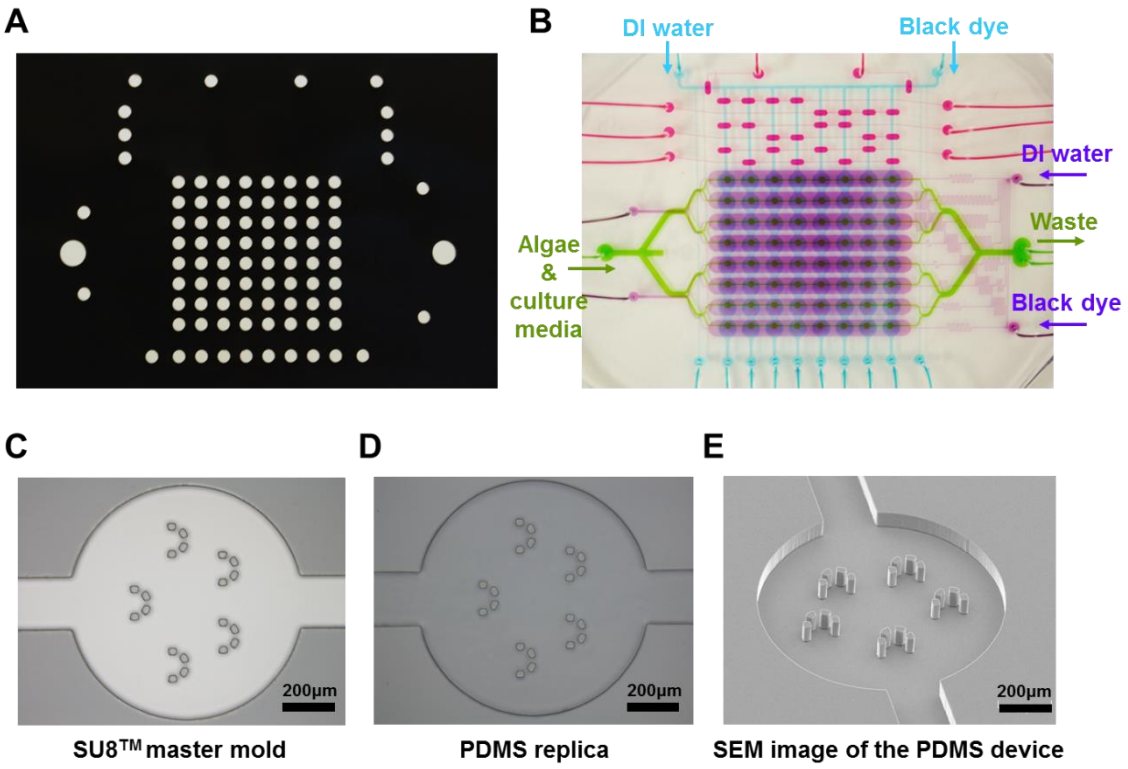

Figure 3. Microfabricated high-throughput microfluidic microalgal photobioreactor array. (A) Light blocking layer. (B) Fully assembled system. Light-dark cycle control layer (cyan: cycle control channels, pink: pneumatic binary demultiplexer) + light intensity control layer (purple) + microalgae culture layer (green) stacked on top of each other. Micrographs showing (C) the SU8™ master mold of the microalgae culture layer and (D) the PDMS replica having the same features with the master. (E) SEM image of a single culture chamber with five *B. braunii* colony trapping sites.

concentration of black dye inside the light intensity control channels and then by changing the distance between the device and the light source (from 4.5 cm to 25 cm) to control the maximum light intensity.

Stronger light intensities (*i.e.,* higher light transmissions) were observed as the concentration of black dye dropped and the distance between the light source and the platform became closer (Figure 4 and Table 3). When a particular concentration of black dye was filled in the channel, regardless of the intensity of the light source, the transmission rate through the particular black dye concentration was almost consistent (less than 2% standard deviations for each black dye concentration from 6 different incident light intensities, Table 3). Thus, each row of the culture compartments in the underlying microalgae culture layer was exposed to one of the 16 light intensities generated (Figure 5A). The gradient generator was designed so that a linear range of light intensities can be generated (Figure 5B, generated transmission rate from 0% to 100% ($R^2 = 0.9991$), corresponding to 0 – 132 μmol photons$\cdot m^{-2} \cdot s^{-1}$). The absolute light intensity on this platform can be easily changed, if needed, by simply adjusting the input black dye concentrations or the distance between the light source and the platform. When the light intensity control layer was used in combination with the light-dark cycle control layer, the 8-outlet gradient generator was used instead of the 16-output design (Figure 3B).

2.4.2. Design of light intensity controlling scheme

A typical gradient generator that creates linearly-distributed gradient profile of

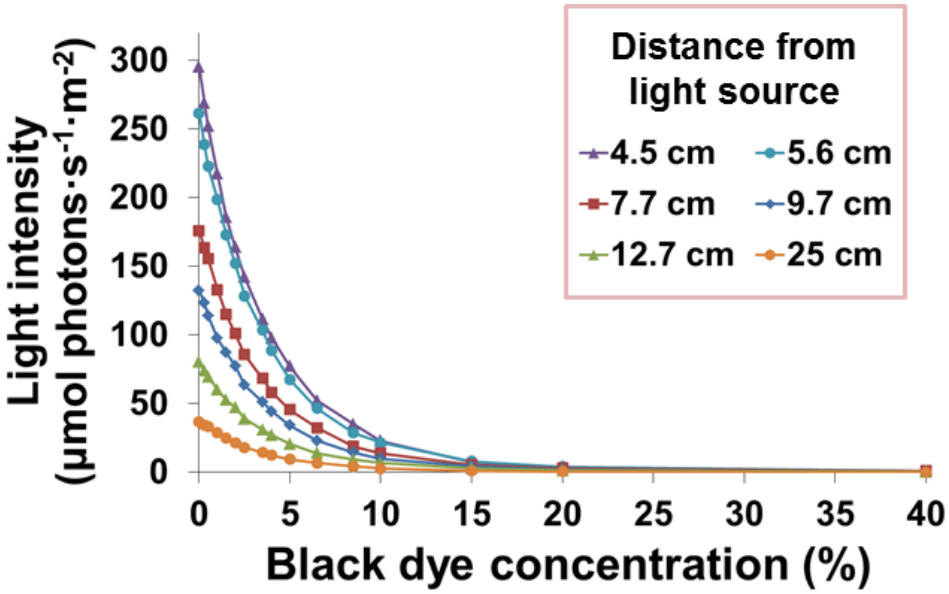

Figure 4. Correlation between measured light intensities and black dye concentrations. Distances between the light source and the platform were adjusted to control the incident light intensity.

Table 3. Light intensity measured through black-dye-filled light intensity control channel in the microfluidic platform and corresponding light transmittance rate.

Light-to-platform distance (cm)	Black dye concentration (%)								
	0 (DI water)	0.3	0.5	1	1.5	2	2.5	3.5	4
	Light intensity (μmol photons·m^{-2}·s^{-1})								
4.5	295.40	269.23	252.12	217.31	185.65	163.82	142.05	111.69	97.93
5.6	261.40	238.68	222.86	198.93	172.92	151.98	128.46	103.49	88.76
7.7	175.78	163.50	155.67	132.87	114.87	101.07	85.71	68.44	58.12
9.7	132.44	123.27	114.14	97.68	87.24	77.51	63.35	51.22	44.35
12.7	80.21	73.90	69.54	60.14	52.44	47.25	38.91	30.98	27.01
25	37.01	34.12	33.27	29.06	24.70	21.63	18.03	14.34	12.40
	Transmittance rate (%)								
4.5	100.00	91.14	85.35	73.56	62.85	55.46	48.09	37.81	33.15
5.6	100.00	91.31	85.26	76.10	66.15	58.14	49.14	39.59	33.96
7.7	100.00	93.01	88.56	75.59	65.35	57.50	48.76	38.94	33.06
9.7	100.00	93.08	86.19	73.76	65.87	58.52	47.83	38.67	33.49
12.7	100.00	92.14	86.70	74.98	65.38	58.90	48.52	38.63	33.68
25	100.00	92.20	89.90	78.52	66.75	58.44	48.72	38.75	33.50
Average	100.00	92.15	86.99	75.42	65.39	57.83	48.51	38.73	33.47
Standard deviation	0.00	0.82	1.86	1.82	1.35	1.25	0.48	0.57	0.33

Light-to-platform distance (cm)	Black dye concentration (%)									
	5	6.5	8.5	10	15	20	40	60	80	100
	Light intensity (μmol photons·m^{-2}·s^{-1})									
4.5	77.36	52.23	34.96	22.72	7.43	3.98	0.26	0.00	0.00	0.00
5.6	67.54	46.54	28.71	21.46	8.00	3.97	1.04	0.75	0.00	0.00
7.7	45.69	32.48	18.93	13.89	5.58	3.03	1.03	0.54	0.15	0.00
9.7	34.10	23.00	14.30	9.88	4.42	2.12	0.47	0.00	0.00	0.00
12.7	20.51	14.00	9.20	6.70	2.78	1.27	0.28	0.16	0.12	0.00
25	9.42	6.63	4.21	2.84	1.14	0.52	0.09	0.05	0.00	0.00
	Transmittance rate (%)									
4.5	26.19	17.68	11.84	7.69	2.52	1.35	0.09	0.00	0.00	0
5.6	25.84	17.80	10.98	8.21	3.06	1.52	0.40	0.29	0.00	0
7.7	25.99	18.48	10.77	7.90	3.17	1.73	0.58	0.31	0.08	0
9.7	25.75	17.37	10.80	7.46	3.34	1.60	0.36	0.00	0.00	0
12.7	25.57	17.46	11.47	8.36	3.46	1.58	0.35	0.20	0.15	0
25	25.45	17.90	11.38	7.67	3.07	1.41	0.26	0.13	0.00	0
Average	25.80	17.78	11.21	7.88	3.10	1.53	0.34	0.15	0.04	0.00
Standard deviation	0.27	0.40	0.43	0.34	0.33	0.14	0.16	0.13	0.06	0.00

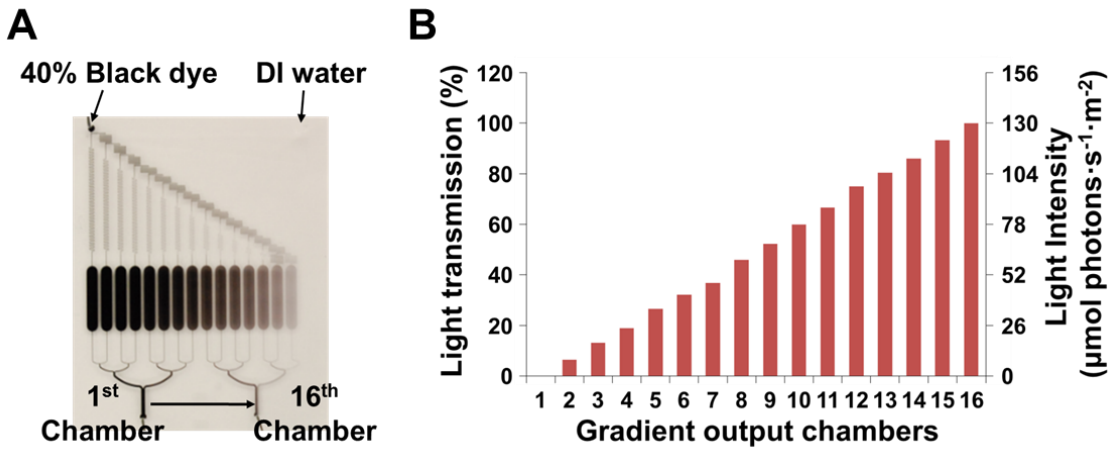

Figure 5. On-chip control of light intensity. (A) Light intensity control layer producing 16 different concentrations of black dye through the microfluidic gradient generator, where DI water (flow rate: 0.8 μl/min) and 40% black dye (flow rate: 5 μl/min) were used as the two inputs. (B) Corresponding transmitted light intensities showing 16 different light intensities within a single microfluidic platform.

black dye concentrations was not appropriate here because the corresponding light intensities were not in the linear range due to the non-linear relationship of black dye concentrations and light transmission, as shown in Figure 4. Thus, a modified gradient generator capable of producing a linear range of light intensities was designed based on the mathematical model of a serial-dilution gradient generator.[82] By deciding the output concentrations ($C_0 \sim C_{N+1}$), output flow rates ($Q_0 \sim Q_{N+1}$), a mixing channel resistance (R_M) and a serial-cascading channel resistance (R_S), all other channel resistances were calculated with below equations (Figure 12), and thereby, a gradient generator having objective output concentrations was designed with channel lengths converted from the calculated channel resistances. Objective output concentrations and channel lengths converted from calculated channels resistances are summarized in Table 4.

However, some channel lengths in Table 4, such as $L_{L,1}$ and $L_{L,2}$, were more than 2m long, and this length was practically impossible to fabricate on 3 or 4 inch diameter substrates, which resulted from large numbers of outputs and a large difference between black dye concentrations for 0% and 6.67% light transmission. The resistance of rectangular microchannel is typically dependent on channel configuration, that is, length (L), width (w), and height (h) of the microchannel[83]:

$$R = \frac{12\mu L}{\omega h^3}\left[1 - \frac{h}{\omega}\left(\frac{192}{\pi^5}\sum_{n=1,3,5}^{\infty}\frac{1}{n^5}\tanh\left(\frac{n\pi\omega}{2h}\right)\right)\right]^{-1}$$

Since most of long channel lengths in previous calculation were to form a certain

Table 4. Target concentrations and channel length calculated from channel resistances.

Target concentrations	C_0	C_1	C_2	C_3	C_4	C_5	C_6	C_7
(%)	0	0.24	0.51	0.79	1.09	1.43	1.85	2.24
	C_8	C_9	C_{10}	C_{11}	C_{12}	C_{13}	C_{14}	C_{15}
(%)	2.68	3.37	4.02	4.88	6.08	7.85	11.3	40
Channel length required for single height gradient generator (90 µm)								
Unit	L_1	L_2	L_3	L_4	L_5	L_6	L_7	L_8
(mm)	20	21.4	53.7	96.4	149.7	212.8	284.1	365.5
	L_9	L_{10}	L_{11}	L_{12}	L_{13}	L_{14}	L_{15}	L_m
(mm)	455.2	549.4	650.6	755.9	862.1	965.7	1054	20
	$L_{L,0}$	$L_{L,1}$	$L_{L,2}$	$L_{L,3}$	$L_{L,4}$	$L_{L,5}$	$L_{L,6}$	$L_{L,7}$
(mm)	1172	2234	2067	2013	1825	1495	1613	1344
	$L_{L,8}$	$L_{L,9}$	$L_{L,10}$	$L_{L,11}$	$L_{L,12}$	$L_{L,13}$	$L_{L,14}$	L_s
(mm)	884.1	930.1	659.4	458.4	296.5	150.2	39.2	2.8
Channel length required for two different height gradient generator (30 µm + 90 µm)								
Unit	L_1	L_2	L_3	L_4	L_5	L_6	L_7	L_8
(mm)	20	21.4	3 + 4	6 + 4	9 + 4	13 + 4	18 + 4	23 + 4
	L_9	L_{10}	L_{11}	L_{12}	L_{13}	L_{14}	L_{15}	
(mm)	29 + 4	35 + 4	41 + 4	48 + 4	55 + 4	61 + 4	67 + 4	
	$L_{L,0}$	$L_{L,1}$	$L_{L,2}$	$L_{L,3}$	$L_{L,4}$	$L_{L,5}$	$L_{L,6}$	$L_{L,7}$
(mm)	75 + 8	143 + 4	132 + 4	128 + 4	116 + 4	95 + 4	102 + 4	85 + 4
	$L_{L,8}$	$L_{L,9}$	$L_{L,10}$	$L_{L,11}$	$L_{L,12}$	$L_{L,13}$	$L_{L,14}$	
(mm)	55 + 4	58 + 4	40 + 4	27 + 4	16 + 4	7 + 4	39.2	

channel resistance, this length could be drastically reduced by decreasing the channel height while maintaining the same channel resistance. For example, when channel heights are reduced to 1/3 in $L_{L,1}$ and $L_{L,2}$, their length can be as short as less than 5 mm. By lowering some portions of long microchannels to 1/3 of its original height (90 μm → 30 μm), the modified gradient generator inducing a linear range of light intensities could be designed with a suitable size for 3 or 4 inch diameter silicon substrate. All channel lengths converted from the calculation of resistances when having two different height microchannels are summarized in Table 4.

2.5. Microfluidic control of light-dark cycle

2.5.1. Microfluidic pneumatic binary demultiplexer

The microfluidic pneumatic binary demultiplexer[80] was composed of two distinct PDMS layers where the control layer containing control lines (H0 – H7 in Figure 6) to actuate microvalve patterns were placed on top of the flow layer comprising of input and output channels to be controlled (V0 – V15 in Figure 6). The microvalve patterns were formed at the junction where the top control lines crossed the bottom flow channels so that the thin membrane between the top and the bottom channels could be deflected by pneumatic actuation. This resulted in opening (negative pressure applied) or closing (positive pressure applied) of the bottom flow channels (Figure 6A).

The pneumatic binary demultiplexer was used to choose one particular channel out of the 16 output channels through which input solution could flow (Figure 6B). Each

pair of control channels (4 pairs in total) was connected to a group of microvalves regulating half of the flow channels. Thus, a pair of control channels formed a complementary pair (*e.g.,* H0–H1, H2–H3, H4–H5, and H6–H7), and constituted one selection bit. To open (or select) a single output channel, only one control channel from each complementary valve pair had to be opened (actuated with a negative pressure, "open") while the other was closed (actuated with a positive pressure, "close"). Thus, the open-close states of the two control channels forming a selection bit were always opposite. For instance, if the selection bit was 0, H0 was closed while H1 was open. On the other hand, if the selection bit was 1, H0 was open and H1 was closed. By deciding the state of each selection bit, opening and closing of the 16 output channels could be independently controlled. For example, when selection bit 1, 2, 3, and 4 were in state 0, 1, 0, and 1, input solution could flow through the selected output channel V10 (0101_2 = 10; Figure 6B). Due to the complementary microvalves organized in a binary architecture, 16 output microchannels (N) could be controlled with 8 control microchannels ($2log_2N$).

For our developed microalgae photobioreactor array to control the different light-dark cycles, a modified microfluidic pneumatic binary demultiplexer having two inputs (DI water and black dye) instead of a single input as described above was used. The overall working principle in the modified schematic was same, with the only difference being that two additional microvalve structures (A1 and A2 in complementary state) were used to control the two inputs (Figure 6C). Depending on whether A1 was open and A2 was closed, or A1 was closed and A2 was open, either black dye (input 1) or DI

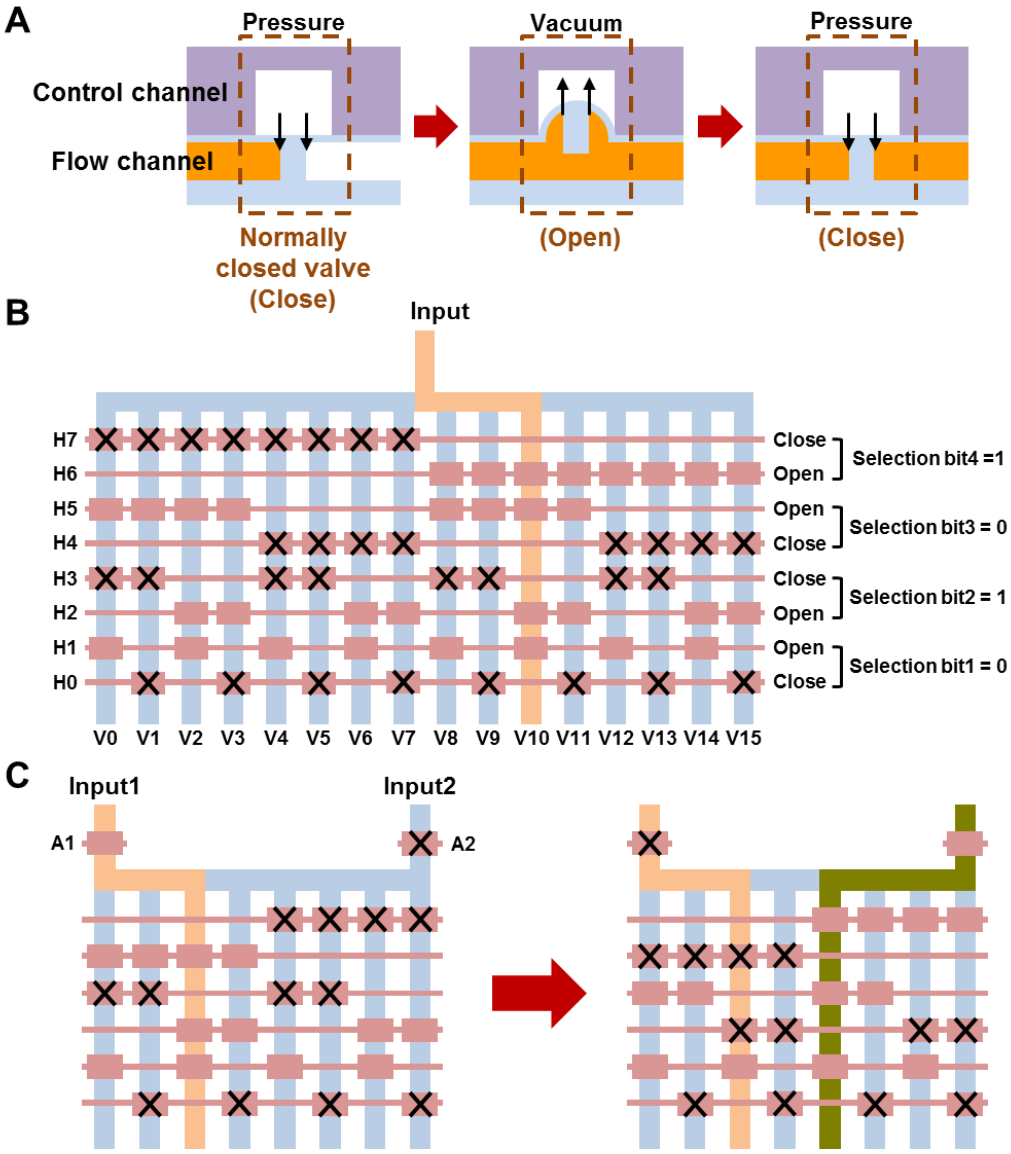

Figure 6. Operation principle of a microfluidic binary demultiplexer. (A) Microvalve composed of a control layer and a flow layer utilized in this demultiplexer. (B) Binary demultiplexer in which 16 output channels were regulated with 8 control microchannels. (C) Modified binary demultiplexer having two inputs and two additional microvalves, which was utilized in the high-throughput microfluidic microalgal photobioreactor array to control different light-dark cycles.

water (input 2) could flow into the system. This selected input solution could then flow into one of the 8 output channels selected by the pneumatic binary demultiplexer (Figure 6C).

2.5.2. Characterization of on-chip light-dark cycle control

Light (or "day") and dark (or "night") conditions in the light-dark cycle control layer were realized by filling each channels with DI water and black dye, respectively. The intensities of transmitted light through DI water- and black dye-filled channels (height: 90 μm) in the light-dark cycle control layer were measured, and 100% and 0% transmissions were confirmed. The pneumatic binary demultiplexer successfully controlled the light-dark cycles in each of the 8 control channels independently (Figure 7A-C), resulting in 8 different light-dark cycles on-chip; 2, 4, 6, 8, 10, 12, 16, and 24 hours (Figure 7D). A 2-hour cycle means switching between light and dark conditions every 2 hours.

The transition time to switch between DI water (light) and black dye (dark), which determines the shortest possible light-dark cycle in the platform, could be easily adjusted by changing the flow rate of the two solutions. For example, at a flow rate of 1.5 μl/min, the transition time was less than 4 minutes, and at a flow rate of 3.0 μl/min, the transition time was less than 2 minutes, which is the fastest possible transition time under these conditions. During all culture experiments presented here, the flow rate was set to 1.5 μl/min.

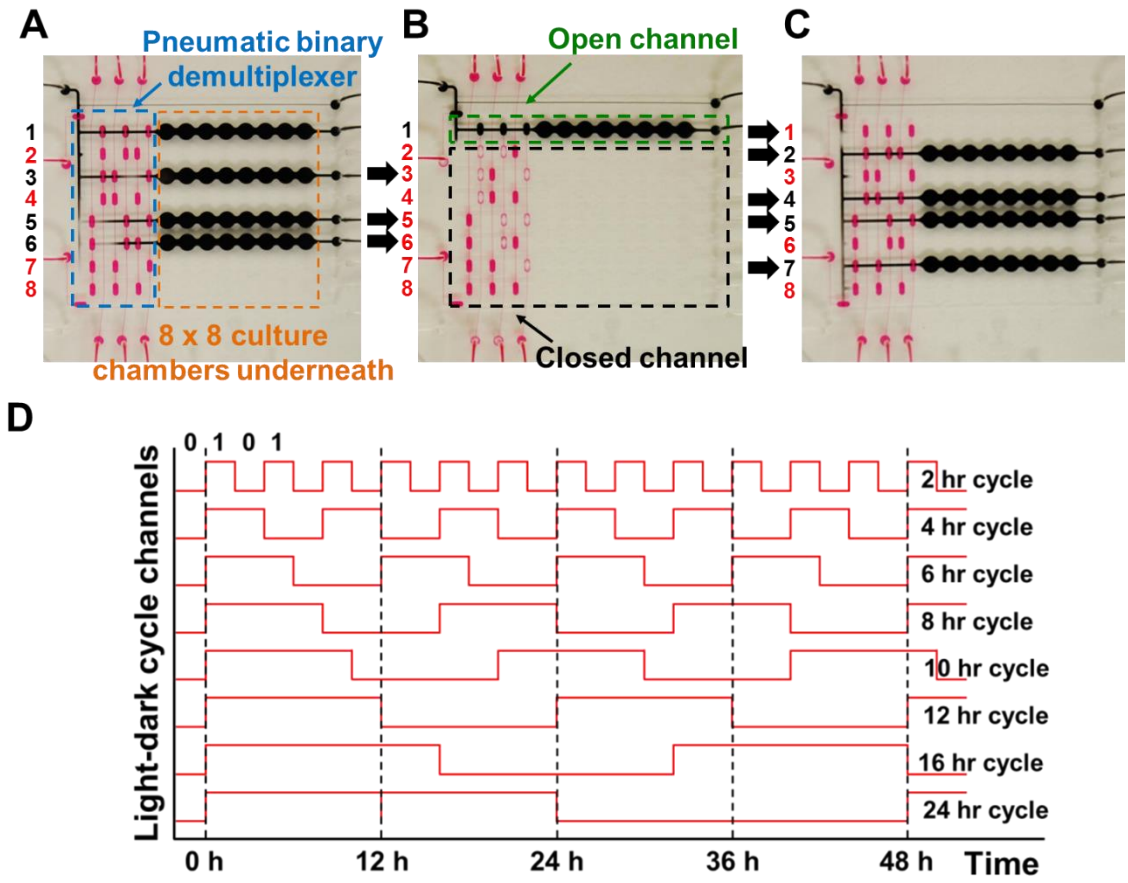

Figure 7. Operation of the microfluidically actuated light-dark cycle control layer. Channels labeled 1 – 8 indicate the 8 individual light-dark cycle control channels controlled by a pneumatic binary demultiplexer. Black and red lettering indicates black dye and DI water filled channels, respectively. (A) Channels 1, 3, 5, and 6 filled with black dye, resulting in a "dark" cycle to the underlying culture chambers, while channels 2, 4, 7, and 8 filled with DI water resulting in a "light" cycle. (B) Only channel 1 in a "dark" cycle. (C) Culture chambers under channels 2, 4, 5, and 7 going through a "dark" cycle, while the rest of the chambers going through a "light" cycle. (D) Eight different light-dark cycles used in the subsequent experiments.

2.6. Isolation of light conditions

The light blocking layer in the microfluidic platform was employed to provide isolated light conditions onto each of the underlying microalgae culture compartments. To validate this capability, all open chambers in the light blocking layer were blocked except for one chamber (highlighted as "Open" in Figure 8A) to which light could penetrate. The intensities of light underneath the open chamber as well as adjacent blocked chambers were measured using the quantum sensor, and these measured intensities were compared to examine whether the light passing through the open chamber affected the neighboring chambers. The measurements were conducted at a light intensity of 165 μmol photons·m^{-2}·s^{-1} by changing the distance between the light blocking layer and the quantum sensor, from 0.5 to 1.5 mm, corresponding to the gap between the microalgae culture layer and the light blocking layer (Figure 8B).

By creating 64 circular open chambers smaller than both the light-dark cycle and the light intensity control channel widths, the top light blocking layer was successfully utilized to prevent any light that was not passing through both the light-dark cycle and the light intensity control layers from reaching the underlying microalgae culture layer (Figure 8A). This layer also isolates the light conditions between chambers by blocking potential scattered light from neighboring chambers. A negligible amount of light interference between adjacent chambers (less than 1.5%) was observed (Figure 8B).

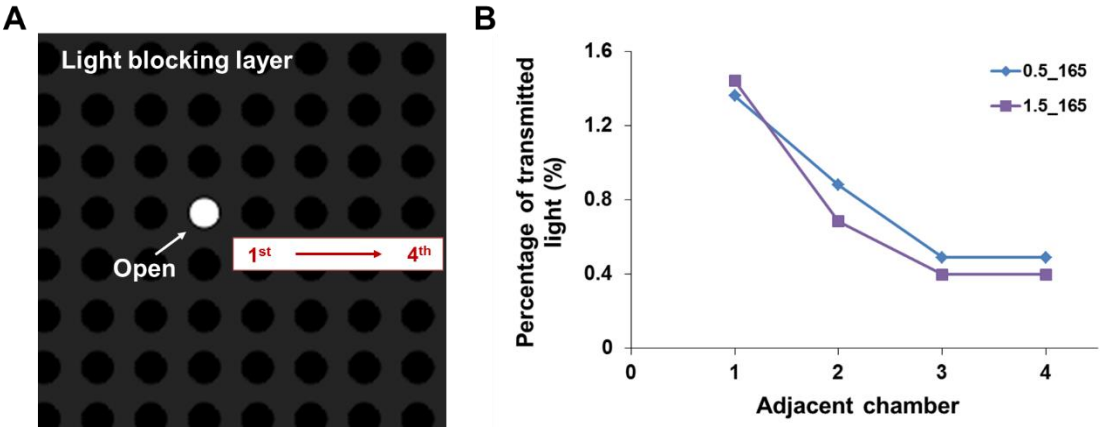

Figure 8. Light interference among neighboring chambers. (A) Schematic showing the setup for this measurement. All chambers in the light blocking layer were blocked except for one chamber (highlighted as "Open"), and the intensities of light underneath this particular chamber as well as adjacent chambers were measured and compared. (B) Comparison of the degree of transmitted light from neighboring chambers by changing the distance from the bottom of the platform used (0.5 and 1.5 in the graph legend indicate 0.5 and 1.5 mm). Number 165 in the graph legend indicates the intensity of incident light, 165 μmol photons·m^{-2}·s^{-1}. Less than 1.5% light transmittance was observed, which is negligible.

2.7. *Botryococcus braunii (B. braunii)* as a microalga model

2.7.1. Biology of *B. braunii*

Botryococcus braunii (B. braunii) is a green colonial microalga with a significantly higher hydrocarbon content compared to other microalgae, which have made this microorganism as a promising source of renewable fuels.[60, 61, 84] Depending on the strain and growth conditions, up to 86% of algal dry weight can be hydrocarbons, most of which are retained in colony extracellular matrix while the remaining is found intracellularly.[60, 84-86] Three races (A, B, and L) of *B. braunii* can be classified on the basis of the type of hydrocarbons they produce. The A race produces alkadienes and alkatrienes derived from fatty acids, and the L race accumulates tetraterpene, known as lycopadiene. The B race, analyzed in the platform, produces triterpenes, called botryococcenes. The three races also can be differentiated based on morphological and physiological characteristics. The individual cell size of L race (8 ~ 9 μm x 5 μm) is relatively smaller than that of A and B races (13 μm x 7 ~9 μm). These races can be distinguished based on colony color in the stationary phase and the nature of biopolymers present in the cell wall.[60, 64, 66, 87-93]

The B race has attained a great interest among the three races on behalf of several characteristics which make it more attractive. First, large quantities of botryococcene derivatives, which are originating from the B race, are observed in current petroleum deposits.[94] Second, the botryococcenes can be easily converted into biofuels suitable for internal combustion engines, including the petroleum-equivalent products such as gasoline, diesel, and kerosene using a single chemical process (hydrocracking).[95, 96]

Finally, the B race can typically accumulate botryococcenes up to 30 ~ 40 % of their dry weight.[97] Thus, *B. braunii* race B, Berkeley strain was selected as our model microalga and its growth and oil accumulation under different light conditions were characterized with the developed microfluidic platform as a demonstration case. Microscopic images of *B. braunii* race B are shown in Figure 9.

2.7.2. *B. braunii* preparation

Prior to loading into the microfluidic platform, *B. braunii* race B, Berkeley (or Showa) strain[98] was cultured in 800 ml of modified Chu 13 media[99], grown under 13-W compact fluorescent (65 K) lighting at a distance of 9.5 cm, which results in a light intensity of 80 μmol photons·m^{-2}·s^{-1}. The cultures went through a 12 hour light-dark cycle at 22.5°C, and were continuously aerated with filter-sterilized air containing 2.5% CO_2. Subsequent subcultures were conducted every 4 to 6 weeks by inoculating 750 ml of new media with 50 ml of mature culture.[64, 65] *B. braunii* in rapid growth phase (6 – 8 days after every subculture) were collected and used for analysis in the microfluidic platform.

2.8. Experimental setup and on-chip culture

The microfluidic platform was sterilized with UV light for at least one hour prior to a culture experiment. The microalgae culture layer and the light intensity/cycle control layers were flushed with culture media and DI water, respectively. *B. braunii* loading

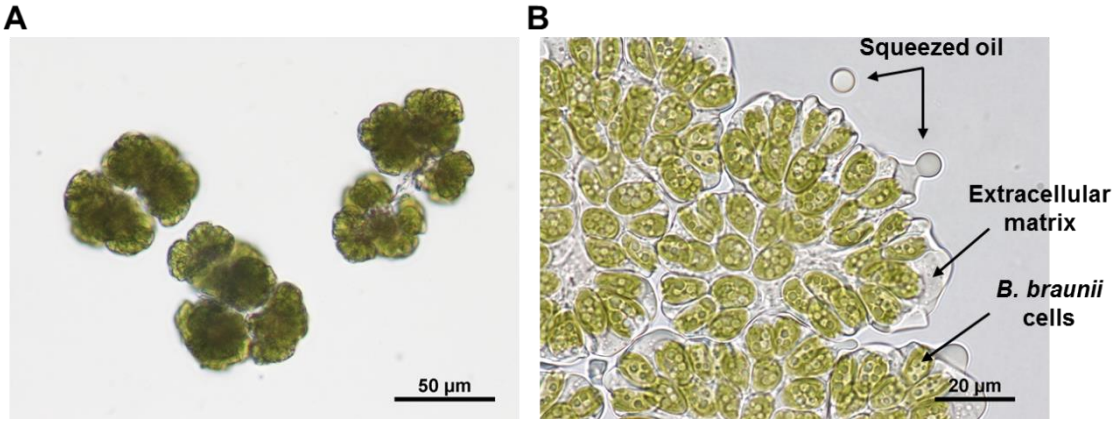

Figure 9. Microscopic images showing *B. braunii* race B colonies (A) suspended in culture media and (B) squeezed between glass slides.

was performed with a syringe pump (Fusion 200, Chemyx Inc., TX, 1 – 3 μl/min), and monitored under the microscope. Since two inlets for microalgae loading and culture media perfusion in the microalgae culture layer face each other, there was possible contamination resulting from microalgae solution flowing into the inlet of culture media perfusion. To minimize this potential contamination, two microvalve structures were utilized in microalgae loading process (Figure 10). During the cell loading, the culture media channel was blocked with the valve actuation, where the flow of microalgae solution can be minimized. Also, the microalgae loading channel can be completely separated during the culturing period by closing it with the microvalve structure. Once *B. braunii* colonies were loaded and captured at all of the trapping sites, any excessive algae that were not captured by the trapping sites were flushed out with culture media (10 – 15 μl/min for 10 minutes). During the culture, the platform was placed under a single light source at a distance of 9.7 cm (132 μmol photons$\cdot m^{-2} \cdot s^{-1}$) for the 16 different light intensity condition experiments and at 10.7 cm (120 μmol photons$\cdot m^{-2} \cdot s^{-1}$) for the 8 different light-dark cycle condition experiments. Fresh culture media was continuously perfused with the syringe pump at a flow rate of 1 μl/min, and 2.5% CO_2 enriched air was provided at a flow rate of 500 ml/min to the acrylic frame holding the microfluidic platform. Since PDMS is gas permeable[100], the gas concentration inside the microfluidic platform is identical to the gas concentration inside the acrylic frame. The entire operation of the system is automatically controlled by a Labview™ interface controlling syringe pumps and pneumatic solenoid valves. The overall experimental setup is illustrated in Figure 11.

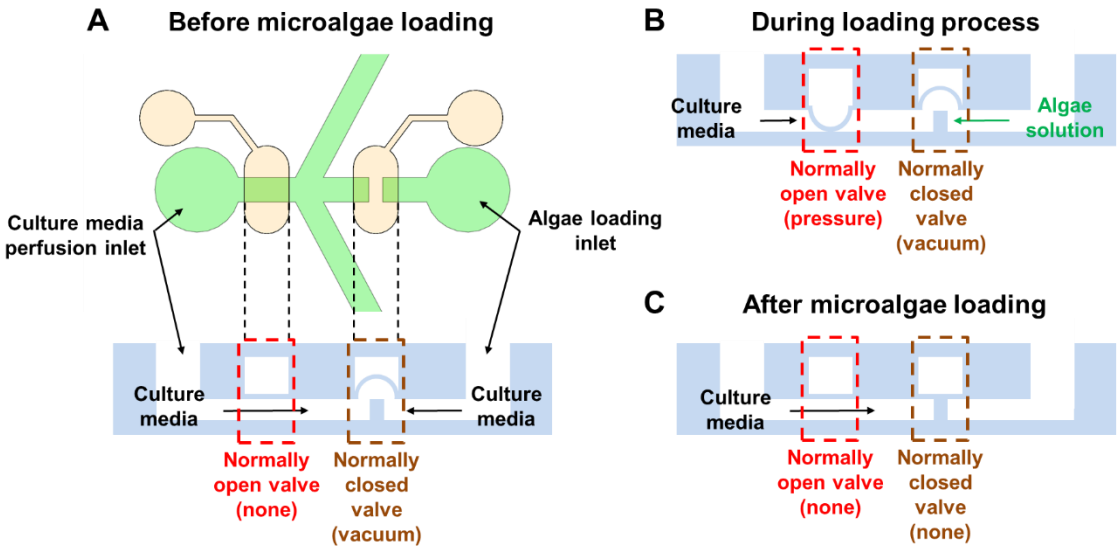

Figure 10. Microvalve operation during microalgae loading process. (A) Before introducing microalgae into the platform, both channels were open and filled with culture media. (B) During loading process, normally open valve on culture media channel was blocked with pressure to minimize the flow of microalgae solution toward culture media inlet. (C) After loading, algae loading channel was blocked with the normally closed valve by releasing a negative pressure.

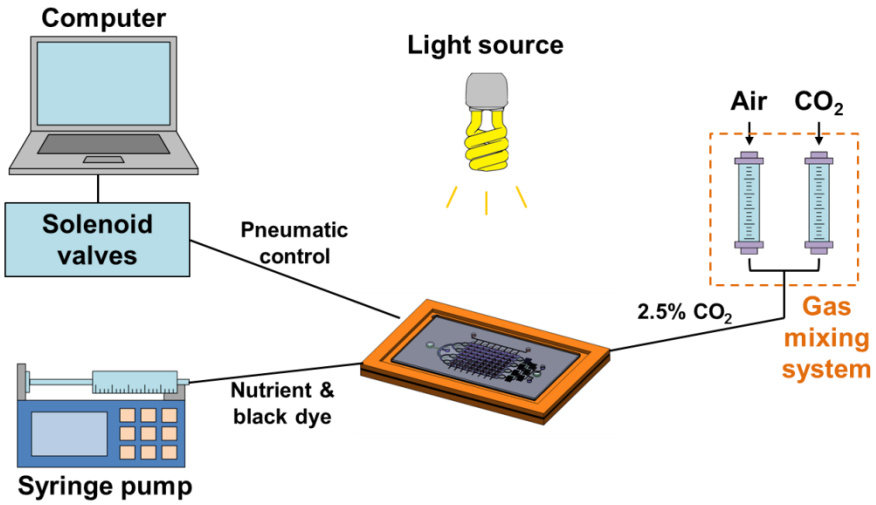

Figure 11. Experimental setup. Air containing 2.5% CO_2 was generated by mixing atmospheric air and 99.9% CO_2 in the ratio of 40 to 1 by controlling each gas flow with compact shielded flowmeters (VWR). This mixed gas was then sterilized through a filter, and flowed into the acrylic culture frame, where CO_2 could diffuse into the microalgae culture compartments through the exposed thin PDMS layer. A 14-W compact fluorescent light bulb (65 K), which could provide different incident intensities of light depending on the distances from the microalgae culture platform, was used. Nutrients were continuously supplied by a syringe pump (1 µl/min, Chemyx Inc.), which introduced fresh culture media into the platform and flushed any waste products out of the platform. The flow of DI water and black dye to produce different light intensities and different light-dark cycles were also controlled with syringe pumps, where different flow rates were used for intensity control (5 µl/min : 0.8 µl/min = DI water : black dye) and light-dark cycle control (1.5 µl/min for both solutions). All control lines in the pneumatic binary demultiplexer to regulate the light-dark cycles were operated automatically by an array of solenoid valves and a programmable Labview™ interface.

2.9. Growth analysis with single colony resolution

Growth of *B. braunii* inside the microfluidic platform was characterized by tracking the sizes of colonies captured in each of the trapping sites over time. Immediately after the cell loading process, all *B. braunii* were imaged using an Eclipse TS 100F microscope (Nikon Instruments, Inc.) equipped with a digital camera (DS-2MV), and these images were used as references (day 0). Once the culture started, images were taken every 2 – 3 days. To quantify the size change, the size of each *B. braunii* colony was first analyzed with an image analysis software package (Image J) by measuring its area. Then, the sizes of *B. braunii* colonies were compared to its initial size to characterize the growth. The single-colony trapping site allowed time-lapse imaging of the exactly same colony over the entire culture period, providing single-colony resolution growth data.

2.10. Quantifying oil production

To analyze and quantify the amount of oil accumulated by *B. braunii* under different light conditions, Nile red fluorescence staining was utilized. Nile red, a lipid-soluble fluorescent dye that binds to neutral lipids, has been shown to efficiently stain *B. braunii* oil in the extracellular matrix as well as in intracellular oil bodies,[64, 65] and has been used to accurately evaluate the oil content in *B. braunii*.[101, 102] It has been also reported that the fluorescence intensity of cells stained with Nile red and the lipid content in *B. braunii* determined by a conventional solvent extraction system shows a linear relationship ($R^2 = 0.998$).[102] Thus, in our microfluidic microalgae platform, the oil

amount in *B. braunii* was analyzed by staining with Nile red and estimating the oil content based on the fluorescent intensity.

However, due to PDMS absorbing hydrophobic small molecules, Nile red staining inside the PDMS microalgae platform can cause severe background fluorescence.[103] To resolve this issue, the PDMS platform was first filled with 3% Bovine Serum Albumin (BSA) and incubated at room temperature for 3 – 5 hours, followed by rinsing with culture media (Figure 12). For oil content measurement both before and after the culture period, a Nile red solution in acetone was diluted in culture media to a concentration of 0.75 μg/ml Nile red and 0.5% acetone, and this diluted solution was flowed through the culture chambers where microalgae were captured for 1 hour at a flow rate of 1 – 10 μl/min. The channels were then rinsed with fresh culture medium for 10 minutes.

An alternative method is to selectively extract desired microalgal colonies off-chip for Nile red staining and oil quantitation. By applying a backflow to the culture compartment, *B. braunii* colonies that were captured inside the trapping sites could be sequentially released and collected to off-chip reservoirs and then stained with Nile red. This process still allowed us to trace a specific colony to its original position due to the sequential nature of the release process into off-chip reservoirs. Even though this protocol was more time-consuming than on-chip staining, it ensured that all colonies were exposed to the same amount of Nile red solution, thus minimizing potential fluorescence intensity variations due to different degree of Nile red staining. Thus, this protocol was used to obtain accumulated oil data as well as oil per unit area data in the

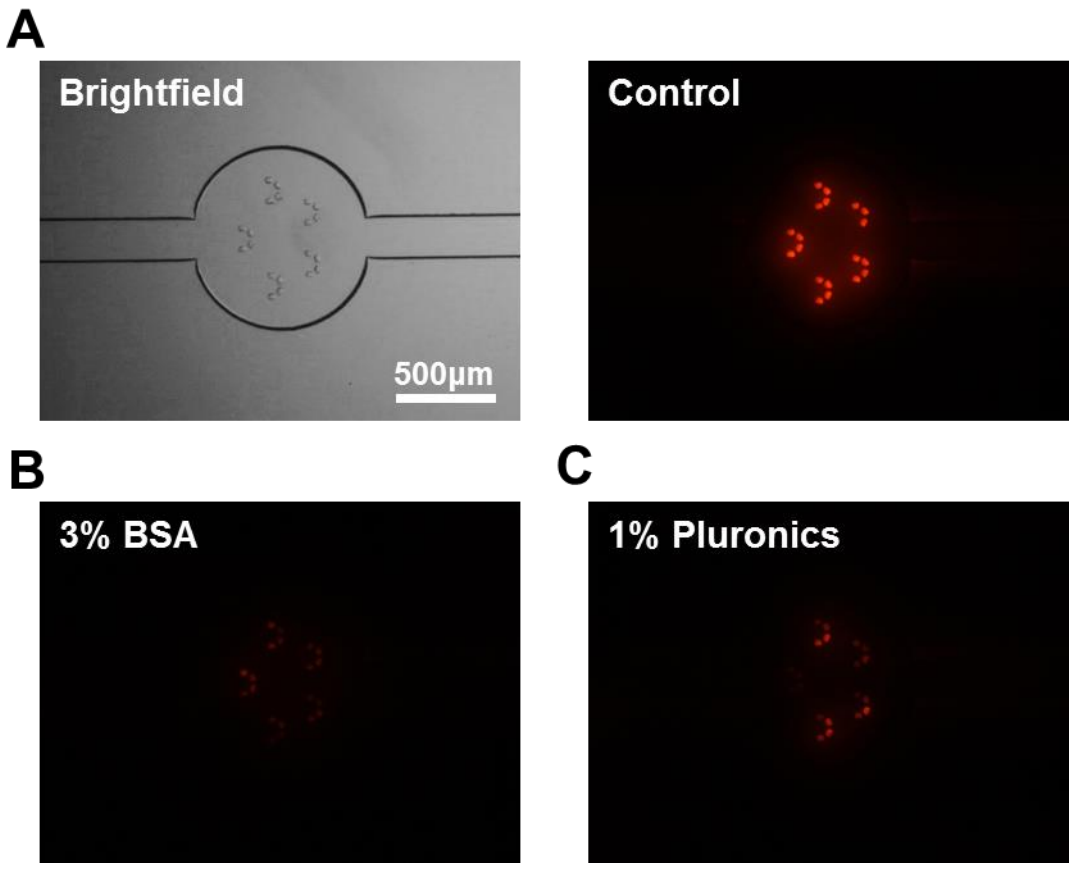

Figure 12. Comparison of background noise in PDMS microalgae culture layer after Nile Red staining. (A) No treatment (Control: bare PDMS substrate). PDMS surface was treated with (B) 3% Bovine Serum Albumin (BSA) in Phosphate Buffer Saline (PBS) and (C) 1% Pluronics F-108NF in water prior to the Nile Red staining.

result section. We are currently in the process of fully characterizing various on-chip staining protocols to minimize such potential variations.

After Nile red staining, microscopic images were obtained using a Zeiss Axio Observer Z1 microscope equipped with a digital camera (Orca Flash2.8 CMOS Camera) and a filter set (excitation: 450 – 490 nm, emission: 500 – 550 nm). To characterize the oil per unit area in *B. braunii*, first, Nile red fluorescence intensity per unit area of each *B. braunii* colony was measured using the Image J software, and then compared to the value measured at day 0. The increase in overall oil amount accumulated during the culture was also analyzed by calculating the ratio of the initial oil amount (initial *B. braunii* size x fluorescence intensity per unit area measured at day 0) and the final oil amount (final *B. braunii* size x fluorescence intensity per unit area measured at the end of the culture).

2.11. Single microalga colony trapping

Single-colony trapping structures in the culture compartments, each consisting of 4 standing pillars with a gap between them, allowed the capture, culture, and analysis of microalgae with single-colony resolution over long periods of time (Figure 1B-C and 3D-E). During the cell loading process, *B. braunii* suspended in culture media was flowed into the platform and the colonies were hydrodynamically captured by the trapping sites. Owing to the gaps and a slightly larger opening size (77 μm) of the trapping site compared to *B. braunii* colony size (Berkeley strain, typical diameter: 50 – 70 μm), single colonies could be successfully captured (Figure 13A). Efficiency of fully

occupying all trapping sites with *B. braunii* was 98.4 ± 1.1% (315 out of 320 trapping sites on a single device). Since captured colonies could not escape the trapping sites under continuous perfusion, continual monitoring of the same *B. braunii* throughout a long-term culture was possible. As the microfluidic platform is compatible with light and fluorescence microscopy, algal colonies captured inside the trap could be analyzed in real-time by examining their growth based on bright-field imaging (Figure 13A) and Nile red-based fluorescence imaging (Figure 13C) for quantifying biomass and oil production, respectively.

2.12. Analysis of microalgal growth and oil production under different light intensities

B. braunii colonies in the microfluidic platform were cultured for 12 days under 16 different light intensities (Figure 5B), all under a 12-hour light-dark cycle (*i.e.*, 12h light and 12h dark), to study the effect of light intensity on growth and oil production. The growth of *B. braunii* was characterized by tracking its size changes over time, where the size was analyzed by measuring the area of each colony. Nile red fluorescence staining was utilized to monitor and quantify oil (botryococcenes) content. Oil per unit area from each colony was defined as Nile red fluorescence intensity per unit area, and the total oil amount accumulated inside a colony was quantified by multiplying the colony size and the oil per unit area. Time-lapse microscopy showed that different light intensities resulted in different size increases (Figure 14A) and analysis of Nile red

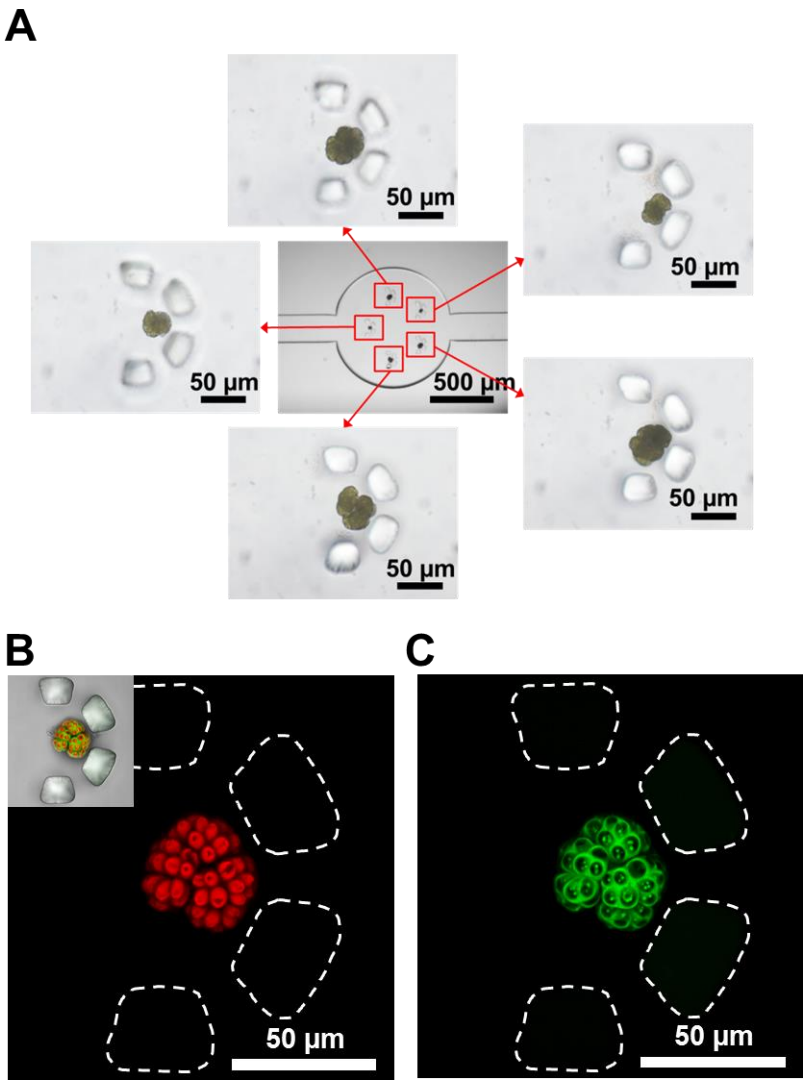

Figure 13. Single *B. braunii* colony trapping in the microfluidic photobioreactor array. (A) A single microalgal cultivation compartment where five *B. braunii* colonies were captured inside each of the trapping sites. (B) Chlorophyll autofluorescence and (C) lipid-stained images (through Nile red treatment) of a single *B. braunii* colony inside the trapping structure. Inset shows merged image of corresponding bright-field, chlorophyll autofluorescence, and Nile red fluorescence. Dotted lines indicate micropillar structures that formed a single trapping site.

stained *B. braunii* also showed differences in oil accumulation under varying light intensities (Figure 14B).

The average colony size increase under the 12-hour cycle after 12 days of growth and compared to day 0 increased up to a certain light intensity level (229% increase at 113 μmol photons·m^{-2}·s^{-1}), but then showed a lower size increase as light intensity increased (171% increase at 132 μmol photons·m^{-2}·s^{-1}, Figure 15A), possibly due to photoinhibition. The size increase trend under different light intensities was similar throughout the time-course experiment (5, 7, 10, and 12 days of culture) (Figure 15B). This growth trend indicates that culture periods between 10 and 12 days may be sufficient to evaluate the effects of light intensity on the growth characteristics of *B. braunii*.

Oil per unit area became higher as the light intensity increased (maximum increase: 51 % compared to day 0), but then started to plateau or slightly decrease as the light intensity was raised (99 μmol photons·m^{-2}·s^{-1} and higher, Figure 15C). Interestingly, maximum oil per unit area was observed at a slightly lower light intensity level (99 μmol photons·m^{-2}·s^{-1}, Figure 15C) compared to the intensity under which maximum size increase was observed (113 μmol photons·m^{-2}·s^{-1}, Figure 15A). Thus, even at a light intensity under which maximum size increase was observed, oil production per unit area seems to have already saturated, possibly due to the stress response to increased light intensity. However, maximum total oil accumulation during culturing still occurred under the same light intensity that produced the maximum size increase (113 μmol photons·m^{-2}·s^{-1}, Figure 15C).

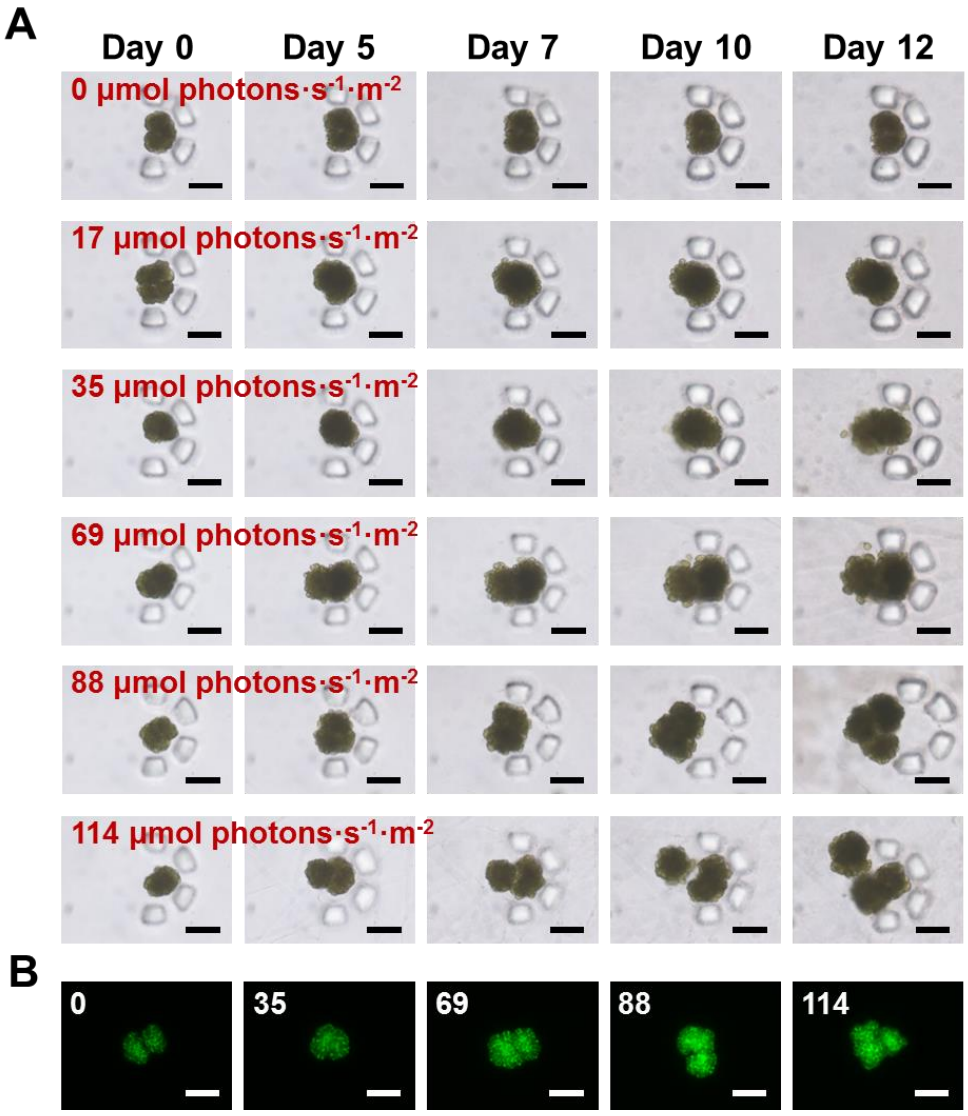

Figure 14. Micrographs showing *B. braunii* growth and oil production under 16 different light intensities with a 12-hour light-dark cycle. (A) Example images of *B. braunii* colonies at days 0, 5, 7, 10, and 12 from six of the 16 light intensities used. (B) Example images of *B. braunii* colonies stained with Nile red after 12 days of culture. The number in each image indicates light intensity. Scale bar = 50 µm.

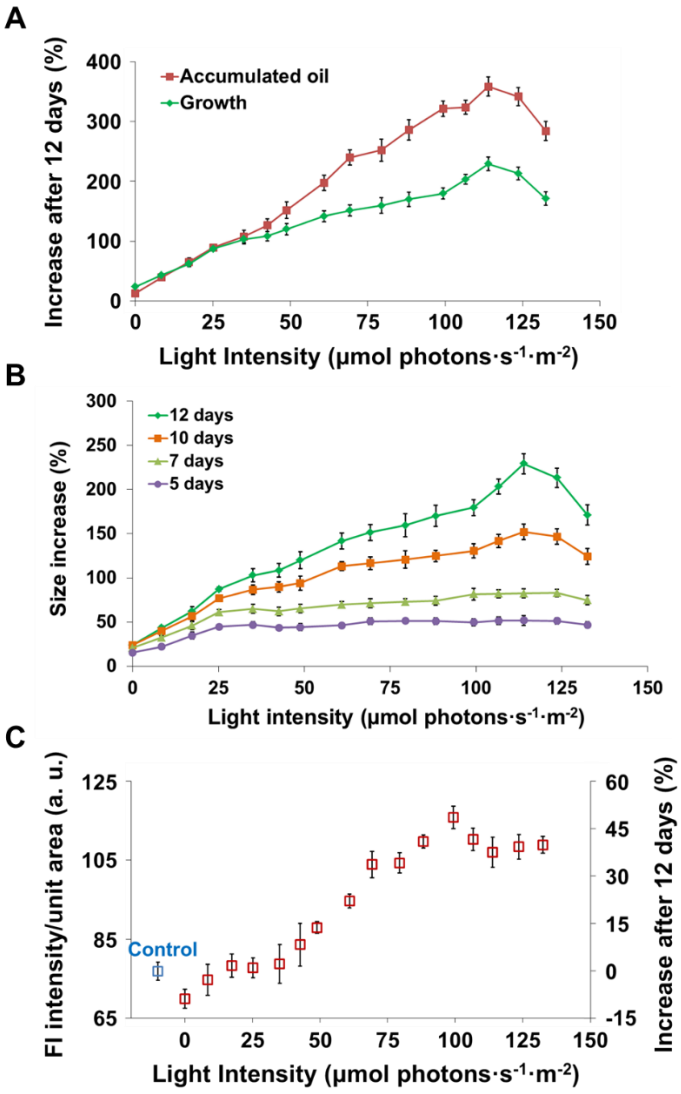

Figure 15. Analysis of *B. braunii* growth and oil production under 16 different light intensities with a 12-hour light-dark cycle. (A) Increase in average *B. braunii* colony size and oil amount after 12 days of culture and (B) time-course analysis of average size increase of *B. braunii* at days 5, 7, 10, and 12 under 16 different light intensities (n = *18*). (C) Average oil per unit area (Nile red fluorescence intensity per unit area) in *B. braunii* after 12 days of culture (n = 23). Control indicates the average oil per unit area measured at day 0. All data shown are mean ± standard error.

The trends of growth and oil production observed from different light conditions matched well with recent research[67], where increasing growth rate was observed with increasing light intensity, but then decreased beyond a specific light intensity. In typical flaks culture, *B. braunii* biomass increase over a 12-day culture period has been reported to be 26%,[66] which is much lower to that observed under this microfluidic platform. It is also known that oil accumulation increase over a 12-day culture period is in the range of a 28% increase[66], again much lower to that observed under this microfluidic platform. Thus, this platform may provide better growth conditions (more direct light exposure to the colony) over the standard culturing system. It has also been reported that a linear relationship exists between hydrocarbon content (oil amount) and growth rates[67]. A similar relationship was obtained from our platform where the highest oil accumulation was observed under the light condition that also showed maximum growth. Our study also shows a decrease in growth and oil production beyond the light intensity of 113 μmol photons$\cdot m^{-2}\cdot s^{-1}$. While this level of light intensity may be low for photoinhibition compared to that seen in land plants, studies have shown that photoinhibition can occur even at low light levels and is related to the total irradiance received by the cell, not the amount of excess light[104]. Additionally, photoinhibition in the green microalga *Neochloris oleoabundans* has been shown to occur at light levels above 180 μmol photons$\cdot m^{-2}\cdot s^{-1}$, a level very similar to that presented in this study[105]. As a matter of fact, this finding of light level that causes photoinhibition in *B. braunii* has not been previously reported.

The growth characteristics of algae in the current study were evaluated through size tracking using bright field microscopy, although this method is useful, it makes automated image analysis challenging. Measurement of chlorophyll autofluorescence is one of the most widely used and convenient methods to estimate algal biomass[106, 107]. The chlorophyll autofluorescence of *B. braunii* colonies captured inside the microfluidic platform was also characterized to analyze the relationship between the colony sizes and fluorescence intensities. Microscopy for quantifying chlorophyll autofluorescence was conducted using a Zeiss Axio Observer Z1 microscope (Carl Zeiss MicroImaging, LLC) equipped with a digital camera (Orca Flash2.8 CMOS Camera) and a filter set (excitation: 460 – 500 nm, emission > 600 nm). The size of *B. braunii* and its corresponding intensity sum of chlorophyll autofluorescence were measured using an image analysis software (Image J), and the correlation between these measurements was analyzed. Our study shows that there is a strong correlation ($R^2 = 0.9937$) between the intensity sum of chlorophyll autofluorescence and the size of *B. braunii* (Figure 16). This suggests that algal growth analysis can be conducted through fluorescent imaging in the future, which is much more amenable for fully automatic image processing to minimize the analysis time.

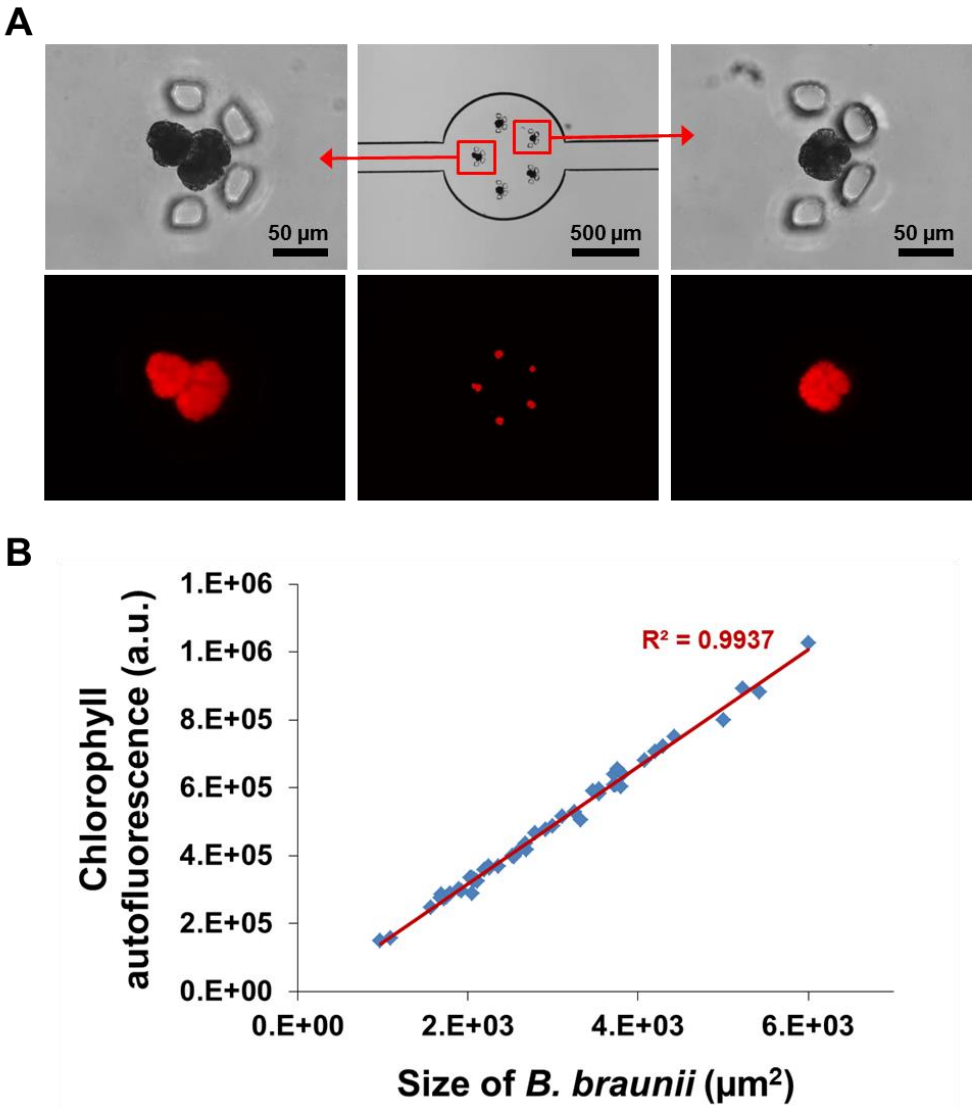

Figure 16. Correlation between size and chlorophyll autofluorescence of *B. braunii* colonies. (A) Chlorophyll autofluorescence and bright field images of captured *B. braunii* colonies inside the platform. (B) Strong linear correlation (R^2=0.9937) between *B. braunii* size and intensity sum of its corresponding chlorophyll autofluorescence, which also indicates strong linear relationship between size and biomass.

2.13. Analysis of microalgal growth and oil production under different light-dark cycles

To investigate the effect of different light-dark cycles on growth and oil production, *B. braunii* colonies in the microfluidic platform were cultured under 8 different cycles (2, 4, 6, 8, 10, 12, 16, and 24 hours of day and night) for 17 days at a light intensity of 120 μmol photons·m^{-2}·s^{-1} (Figure 17A-B). The light intensity of 120 μmol photons·m^{-2}·s^{-1} was selected since that intensity was close to the level where maximum growth and oil accumulation was observed (Figure 15A). Over a 17 day analysis, the colony size increase compared to day 0 peaked under the 8-hour cycle at 191%, and then rapidly dropped to about a 148% increase under the 12-hour cycle (Figure 18A), a light cycle commonly used in conventional *B. braunii* cultures[64-66]. The size increase further dropped to a 108% increase at the 24-hour cycle (Figure 18A). Further time-course analyses of size increase after 4, 7, 11, and 14 days of culture period showed that a similar trend was observed after 11 days of culturing (Figure 18B). Combined with our light intensity studies above that showed an optimal culturing period of 10 – 12 days, the 11 day time point should be sufficient to fully understand the growth characteristics of *B. braunii*, a tremendous reduction in time compared to the conventional 4 – 6 week laboratory-scale culture[64-66].

The highest amount of oil per unit area was observed under the 2-hour cycle (45% increase compared to day 0), 1.8 times higher compared to the oil per unit area under the typically used 12-hour cycle (25% increase compared to day 0, Figure 18C). Interestingly, maximum total oil accumulation was observed under the 8-hour cycle (261% increase compared to day 0, Figure 18A), the same condition under which the

largest colony size increase was observed (Figure 18A). However, due to the significantly higher oil production per unit area (Figure 18C), total oil accumulation under the 2-, 4-, and 6-hour cycles all showed relatively high increases compared to day 0 (235, 239, and 259% increase, respectively, Figure 18A). The use of our photobioreactor array allowed us to define the conditions to optimize oil production (per unit area and total accumulation) compared to the currently used culture conditions, and more importantly this device will allow for future detailed mechanistic studies to be conducted for direct side-by-side comparisons between growth and oil production for a wide variety of algal strains of interest.

An interesting finding was that the 2-hour light-dark cycle showed higher oil production per unit area compared to conventionally used 12-hour cycle (1.8 times). This was different from the 8-hour cycle under which maximum total oil accumulation and growth were observed. This was due to the fact that a high level of oil production per unit area occurred between the 2-6 hour cycles even though the growth for these cycles was slower than that of the 8-hour cycle. This finding clearly demonstrates the importance of fully understanding the relationship between growth and oil accumulation under combinations of different light intensities and light-dark cycles.

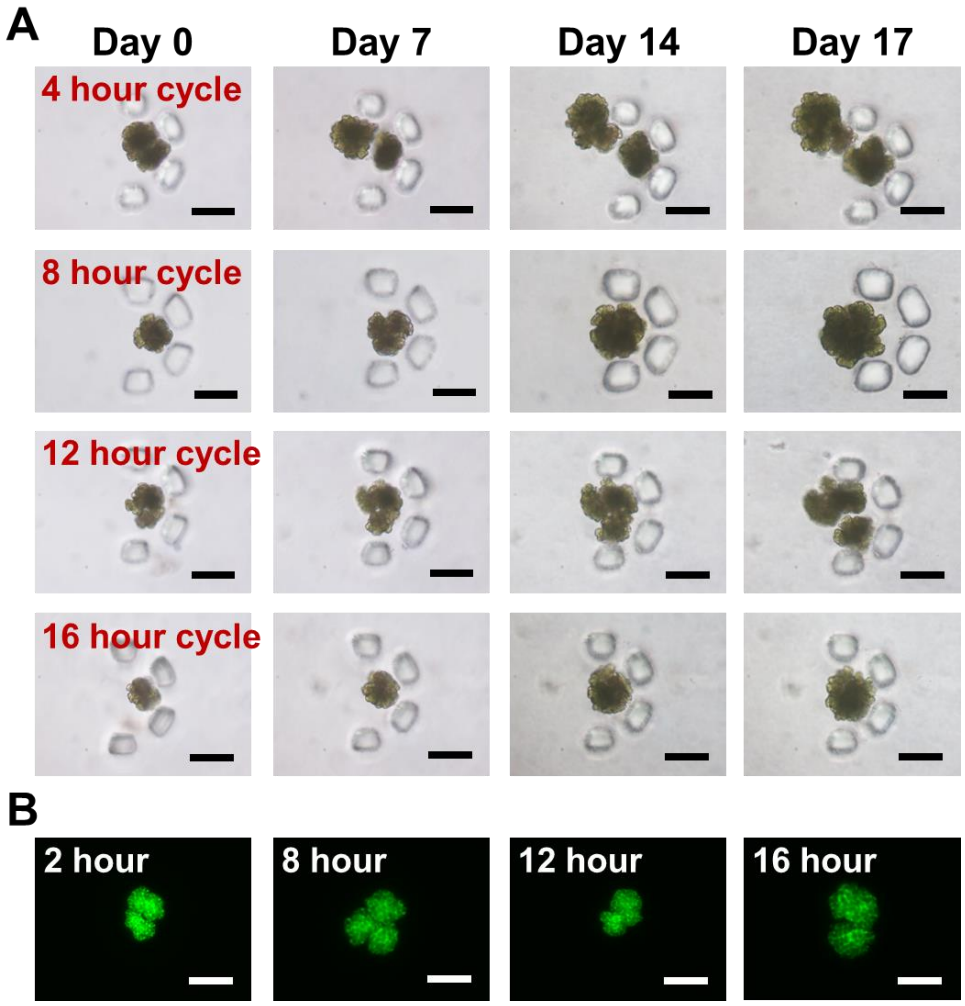

Figure 17. Micrographs showing *B. braunii* growth and oil production under 8 different light-dark cycles at a light intensity of 120 µmol photons·m^{-2}·s^{-1}. (A) Example images of single *B. braunii* colonies at day 0, 7, 14, and 17 days. (B) Example images of *B. braunii* colonies stained with Nile red after 17 days of culture. Scale bar = 50 µm.

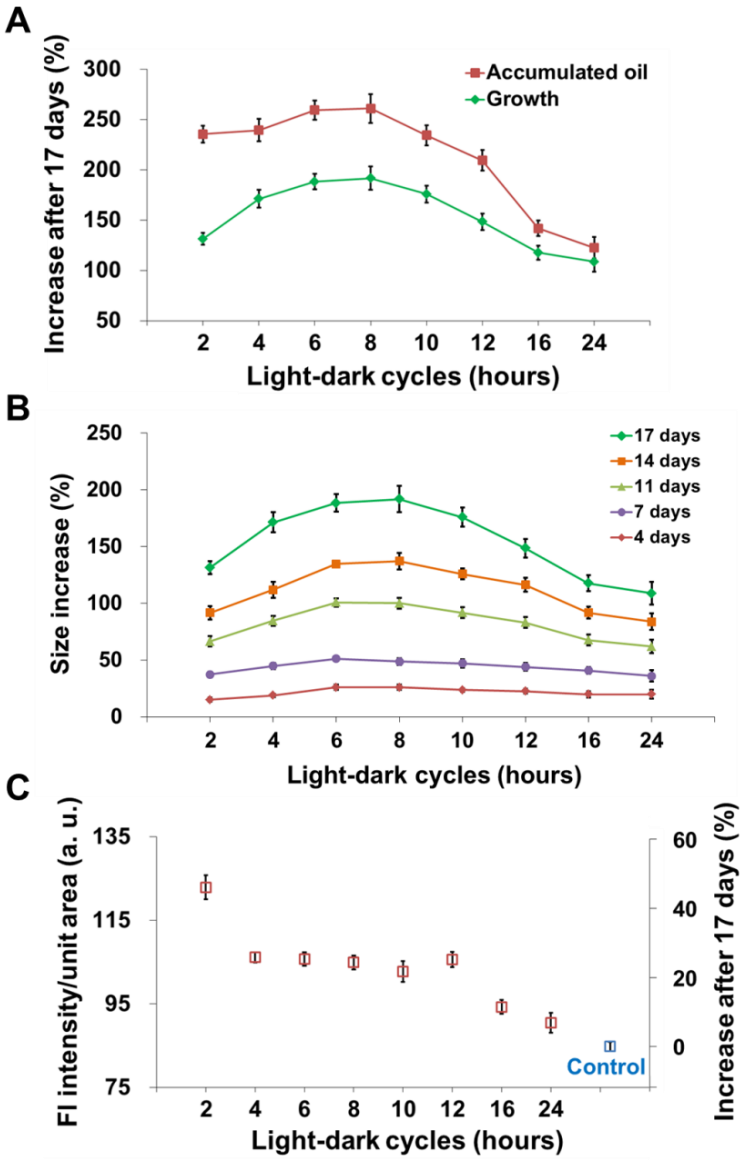

Figure 18. Analysis of *B. braunii* growth and oil production under 8 different light-dark cycles at a light intensity of 120 μmol photons·m^{-2}·s^{-1}. (A) Increase in average size and oil amount after 17 days. (B) time-course analysis of average size increase of *B. braunii* at days 5, 7, 10, and 12 (n = *15*). (C) Average oil per unit area in *B. braunii* after 17 days (n = 21). Control indicates the average oil per unit area measured at day 0. All data shown are mean ± standard error.

2.14. Comparison with conventional flask cultures

Conventional *B. braunii* culture periods are very long (4 – 6 weeks)[64-66] due to their slow growth rate, which makes analysis of optimal growth conditions very time-consuming. Therefore, *B. braunii* is a good model microalga for studying slow-growing microalgae as well as for assessing the long-term culture and analysis capabilities of the developed platform. In conventional flask culture systems, 800 ml of media is required to support 6-weeks of culturing *B. braunii* under a single light condition. However, in the microfluidic platform, 60.48 ml of media is needed to culture *B. braunii* for 6 weeks under 64 different light conditions (continuous media perfusion rate: 1 µl/min, 1 µl/min x 60 minutes x 24 hours x 42 days = 60.48 ml), and thus, each light condition requires 945 µl of media (60.48 ml/64 = 945 µl), almost 850 times less reagent consumption compared to current conditions (800 ml/945 µl = 846.6). More importantly, growth characteristics of *B. braunii* under 64 different light conditions can be analyzed after 11 days of culture inside the microfluidic platform, resulting in almost 250 times higher throughput (64 experiments/11 days x 42 days = 244.4) compared to the conventional flask system (1 experiment/42 days).

2.15. Variation of the microfluidic photobioreactor array

The current platform utilizes arrays of single-colony trapping microstructures for the presented analysis. However, trapping structure design can be easily modified to accommodate different numbers of colonies (Figure 19A-C), which would enable studying the effect of different population densities on growth/biomass/oil production,

which have been reported in some microalgae[108, 109]. Also, the current platform can be modified and applied to investigate unicellular microalgae, where single/multiple *Tetraselmis suecica* cells were captured at the revised trapping structures (Figure 19D-F) and successfully cultured (Figure 19G) and stained with Nile red (Figure 19H) in the platform. Here, the use of this device demonstrates that such detailed characterizations could be conducted for a large variety of different algal strains.

2.16. Microfluidic control of nutrient/chemical compositions

2.16.1. Motivation and design concept

Growth media for microalgae culture is composed of essential elements such as nitrogen (N), phosphorus (P), and iron, and trace elements[6, 60, 92]. Several studies have been done to improve biomass and oil productions by changing compositions of the essential elements; deficiency of nitrogen or phosphorus can lead to higher oil accumulation[60, 110]; different concentration of nitrogen results in different growth rate and oil production[111]. Here, we have developed a high-throughput microalgae analysis platform capable of not only generating different nutrient compositions in culture media, but also providing more growing factors controlled culture environment by combining with light condition control function.

The platform consists of 4 PDMS functional layers; a light blocking layer, a microfluidic light-dark cycle control layer, a microfluidic light intensity control layer, and a microalgae culture layer with media gradient. 4 different culture media

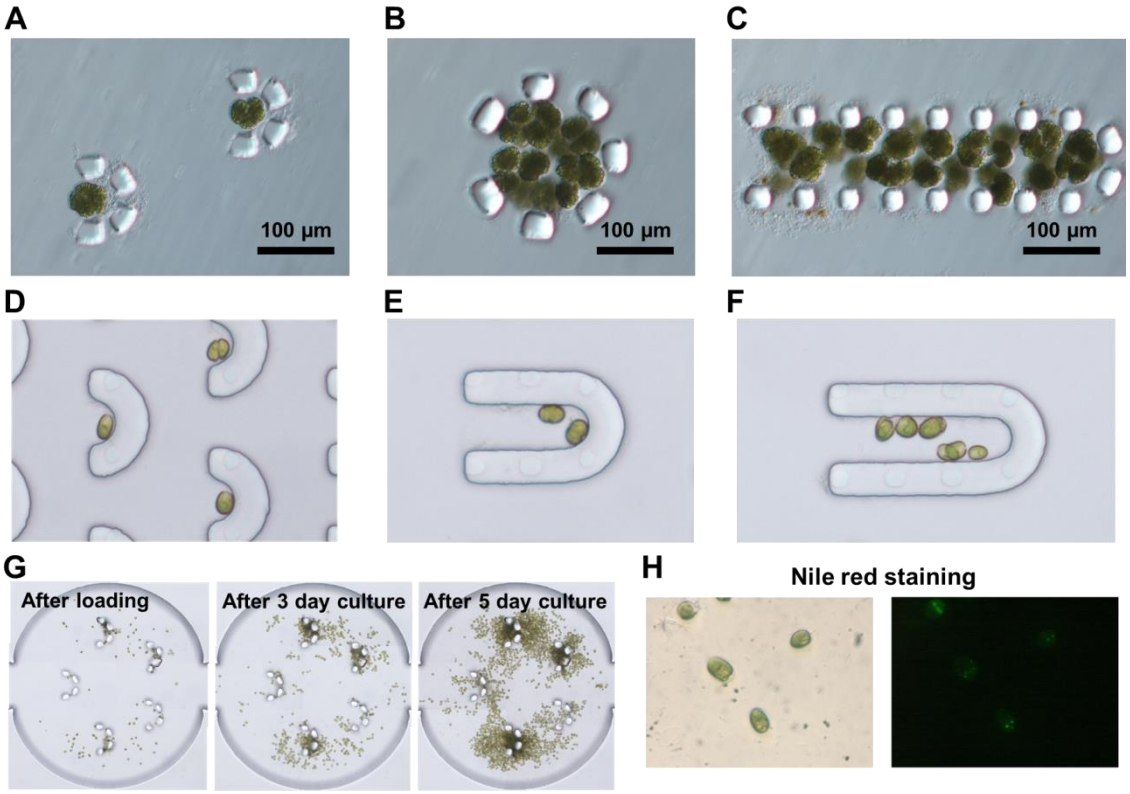

Figure 19. Different designs of algal colony trapping sites. (A) Single-colony trapping design consisting of smaller opening (52 μm). Multiple-colony trapping designs having (B) a large circular structure and (C) a long U-shape structure. (D) Single-cell trapping design showing the successful capture of unicellular microalga, *Tetraselmis suecica*. Multiple-cell trapping designs with (E) a short U-shape structure and (F) a long U-shpae structure. (G) Time-lapse images showing the growth of *Tetraselmis suecica* cells inside the platform. (H) Microscopic images of *Tetraselmis suecica* cells stained with Nile red.

compositions can be produced on the microalgae culture layer through a gradient generator which outputs are connected to microalgae culture compartments. Light intensity control layer and light-dark cycle control layer are designed to generate 4 different light intensities and light-dark cycles, respectively. By combining these four layers, each of 64 unique conditions can be exposed to each of 64 culture chambers in microalgae culture layer (4 different culture media x 4 different light cycles x 4 different light intensities = 64 different culture conditions).

2.16.2. Microalgae analysis platform for screening antibiotics

Interaction with bacteria can be either positive or negative to microalgae[60]; bacteria can enhance microalgae growth and oil production by releasing substance such as vitamin or by producing nitrogen derivatives and inorganic nutrients[112, 113]; on the other hand, they can hinder microalgae growth by competing for nutrients or by secreting algaecides[114, 115]. From previous microalgae culture tests in the platform, severe bacteria and slime mold contaminations were observed during the culture. Although it was not determined whether these bacteria were positive or negative, sometimes these contaminations blocked proper transport of nutrients and chemicals to microalgae, and also clogged the outlet of the platform. In order to overcome these issues, a microfluidic microalgae analysis platform capable of studying the effect of antibiotics combinations on microalgae growth and contamination has been developed.

The microalgae analysis platform is composed of two PDMS layers; a top microalgae loading layer and a bottom microalgae culture/analysis layer with antibiotics

gradient (Figure 20A). First, through the top microalgae loading layer, microalgae can be introduced and captured at the bottom culture/analysis layer by passing a via hole array, which interconnect the top and the bottom layers (Figure 20B). Then, 8 different mixtures of antibiotics, in other words, 8 different concentrations of antibiotics combination are produced through a gradient generator between two inlets and culture/analysis compartments in the bottom layer (Figure 20B-D). By applying these 8 different antibiotics cocktails with culture media perfusion, microalgal growth/oil production as well as contamination inside the platform can be monitored to investigate optimized concentration/combination of antibiotics that only affects contaminants or minimizes bacteria contamination.

As a preliminary test, *B. braunii* was cultured under two different culture media conditions, without antibiotics treatment (control) and with antibiotics treatment, and its growth as well as the contamination level inside the platform were compared each other. Mixture of timentin (15 mg), rifampicin (2 mg), and nystatin (5 mg) in 1% dimethyl sulfoxide (DMSO) (v/v) was diluted in 100 ml culture media, and this solution was used as the antibiotics cocktail. After 10 days of culture, *B. braunii* grown without antibiotics treatment showed growth and had healthy green color, but bacteria contamination was observed inside the platform (Figure 20E). On the other hand, no contamination was found out inside the platform when antibiotics cocktail was provided. However, *B. braunii* colonies were also damaged and its color became brownish, probably due to large amount of antibiotics used, where further optimization of antibiotics is required by utilizing the developed microfluidic analysis platform (Figure 20F).

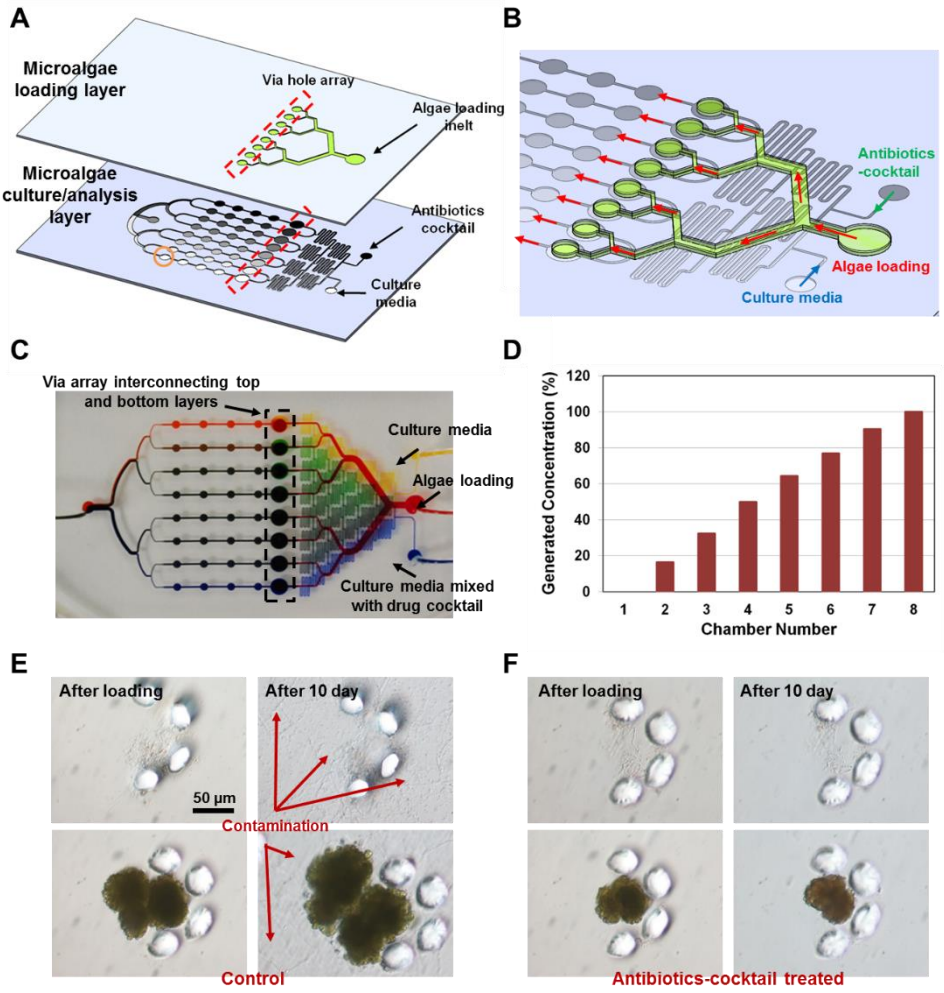

Figure 20. Microalgae analysis platform capable of screening the effect of different antibiotic combinations. (A) Illustration of the platform – a top microalgae loading layer and a microalgae culture/analysis layer. (B) Operation of the platform – microalgae loading and gradient generation of antibiotics cocktail. (C) Fabricated platform showing the gradient generation of antibiotics cocktail. (D) Characterization of concentration profile produced through the gradient generator. Comparison of *B. braunii* growth and contamination (E) without antibiotics treatment (Control) and (F) with antibiotics treatment.

2.17. Conclusion

A high-throughput microfluidic microalgae photobioreactor array was developed to investigate growth and oil production of microalgae under 64 different light conditions in parallel. Continuous perfusion of nutrients to each culture compartment containing multiple single-colony trapping structures allowed long-term analysis with single-colony resolution. This platform also overcame the limitations of conventional culture systems by applying identical conditions to all microalgae in trapping sites and implementing high-throughput screening capabilities. *B. braunii* colonies were successfully characterized using the array platform and resulted in identifying light conditions that showed maximum oil production that differed from conditions typically used in conventional cultures. This screening was achieved at 250 times higher throughput and 850 times less reagent consumption. In addition, the platform was integrated with the capability to create different culture media/chemical conditions for microalgal cells, where the effect of different antibiotics combinations was successfully tested.

The growth and oil production studies conducted through the microfluidic photobioreactor array here is meant to serve as a demonstration of a standardized photobioreactor platform that can be used to examine algal growth and oil production under a combination of different conditions. Additionally, the use of this device demonstrates that such detailed characterizations could be conducted for a large variety of different algal strains, both natural and engineered, at high throughput. The knowledge gained through such studies also has the potential to be directly utilized in

large-scale cultures. We expect that this platform will serve as a powerful tool to investigate how algal growth and oil production are influenced by light conditions as well as screening through various growth conditions against algal strains of interest, all at significantly lower cost and shorter time, which can dramatically accelerate the development of renewable algal energy systems. This work has been published and selected as a HOT ARTICLE as well as a front cover page in Journal of Lab on a Chip[29].

CHAPTER III

A HIGH-THROUGHPUT MICROFLUIDIC SINGLE-CELL SCREENING AND SELECTION PLATFORM

3.1. Motivation

Developing microalgal strains having enhanced growth rates and higher biomolecular production is one of the major strategies to achieve commercially viable microalgae-based bioproduction[5, 9, 116]. Microalgal strain development to obtain better performing microalgae has been achieved through identification of new strains, genetic and metabolic engineering, or evolutionary pressure[5, 9, 117]. These methods involve conventional screening process to select microalgal strains showing desired properties (*i.e.,* enhanced growth and oil production) where sample cell populations are diluted and cultured on their media plates, followed by manually picking the cells of interest. Although this process is useful and widely utilized, it is quite labor-intensive, time-consuming, and requiring long culture periods. The large numbers of samples ($10^3 – 10^6$) to be screened to find out microalgae of interest also make this process very challenging. To resolve these limitations, a different approach is needed to minimize manual intervention as well as to increase the throughput, and a high-throughput microfluidic single-cell screening and selection platform can be one solution.

Various microfluidic single-cell analysis platforms integrated with sorting capabilities have been developed[117]. Microfluidic flow cytometers are one good example, where large numbers of single cells can be analyzed by measuring fluorescence

signals from tagged cells or their dielectric properties, followed by selective sorting of particular cells utilizing dielectrophoretic sorting or acoustophoretic sorting[117-119]. Microdroplet-based microsystems also provide high-throughput single-cell analysis capabilities by encapsulating a single-cell into a monodisperse aqueous droplet, which functions as an independent microreactor. The contents of the microdroplets are then typically identified using fluorescence detection techniques, followed by selective sorting through pneumatic, dielectrophoretic or acoustophoretic forces[50, 53, 120]. Although these platforms have been successfully utilized in detecting and selectively sorting single cells at high-throughput, they are end-point measurements and thus cannot be used to track the exact same single cells over time (*i.e.,* lack of time-course analysis capabilities). Many of the platforms are also limited in single-cell culture capabilities and thus lack the capability to measure certain characteristics such as cell growth rate. Droplet microfluidic systems do have single-cell culture capabilities, but either do not allow long-term culture or require complicated droplet manipulation or processing to enable long-term culture.

Only a few microfluidic single-cell analysis platforms have been developed so far that allow both single-cell time-course analysis and selective cell retrieval capabilities. An optofluidic microsystem has been reported where single cells could be immobilized in a microwell array via sedimentation, and then selectively released with the optical scattering force generated from an infrared laser[121]. Hydrodynamic trapping schemes based on the principle of fluidic resistance have also been developed, where polymer beads or cell-encapsulating alginate beads captured at trapping sites could be

selectively retrieved through an air bubble generated via laser heating that pushed out beads from the trapping sites[122, 123]. However, both methods require expensive laser equipment as well as accurate alignment of the laser to each of the trapping sites. The exposure of intense laser light or heat pulses during the extraction process can also have negative influences on cells. Negative dielectrophoresis (nDEP) combined with cell trapping via microdam structures or mild negative pressure in an array-format has also been proposed[124, 125]. Single yeast cells could be captured through the trapping structures and specific cells could be selectively released by generating nDEP force with the integrated electrodes. Although the exposure of cells to a strong electric field could be reduced, this approach has low throughput, and would require complex on-chip interconnections and off-chip support circuitry, which would be unsuitable for large arrays of trapping sites. Most importantly, all of these cell-trap designs are open-trap structures that do not have enough space for cell growth and division. As soon as cells divide and double, they will escape from the trapping sites, making it impossible to measure growth rates of individual cells.

Here, we have developed a high-throughput microfluidic single-cell screening platform, which provides the capabilities of single-cell trapping in an array format, long-term culture and analysis of the cell's growth rates, on-chip fluorescent tagging, followed by selective retrieval of target cells showing traits of interest. The 1024 individually controllable single-cell trapping and culturing sites allowed hydrodynamic trapping of single cells and had enough space for cells to grow and divide over long periods of time while being directly monitored. Each trapping site had an individually

addressable gate structure, where the closure of the gate structure resulted in a closed compartment that kept the all cells within the trapping site. Opening of the gate structure allowed for retrieving the cells from the trapping site through simple backflow. The individual control of each trapping site enabled selectively extracting only the cells of interest to off-chip reservoirs for further analysis or selection. A microfluidic OR logic gate allowed controlling the 1024 trapping sites using only 22 control channels.

3.2. Design and operating principle of the individually addressable single-cell trap

A platform that can screen through large libraries of cells such as genetically engineered or mutagenized cells requires the capability to capture and isolate single cells, culture the isolated single cells for some period of time while monitoring the cellular properties of interest, and to be able to selectively extract the cell of interest for collection or further analysis, all at high throughput. The proposed microfluidic single-cell screening platform is composed of three PDMS layers; a top microfluidic control layer, a middle microfluidic control layer, and a bottom microfluidic cell culture/analysis array layer (Figure 21A). The bottom microfluidic cell culture/analysis layer (height: 16 μm) has an array of 1024 single-cell trapping sites (32 x 32) where a single cell can be captured, cultured, and analyzed in each of the trapping sites with a continuous perfusion of culture media. After analysis, cells of interest residing in a particular trapping site can be selectively collected to an off-chip reservoir by opening only the particular trapping

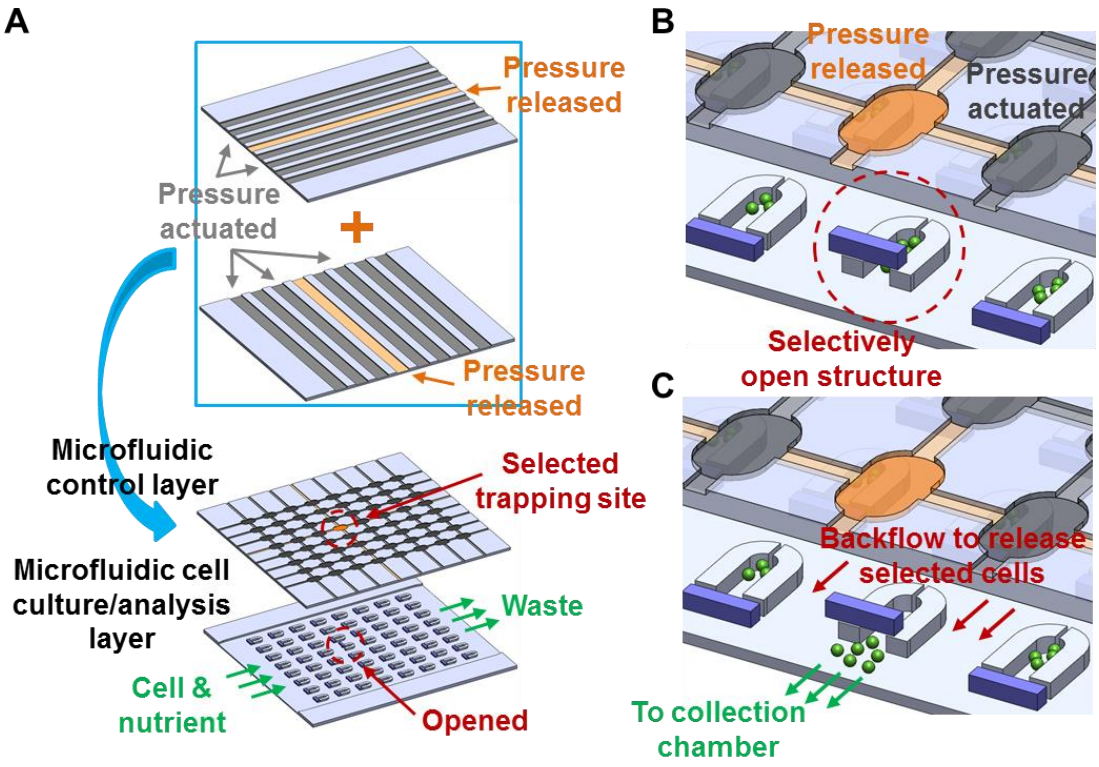

Figure 21. Illustration of the high-throughput microfluidic single-cell screening platform. (A) Two functional layers – a microfluidic control layer and a microfluidic cell culture/analysis layer. (B-C) Enlarged view of three U-shaped cell-trapping sites, each showing multiple cells grown from an initial single cell inside the traps. Bar-shaped gate structures in front of each U-shaped trap function as gates to control the opening and closing of each trapping site. The front gate is only open when pressure in both the row and column control microchannels in the control layer is released simultaneously. Trapped cells from only the cell trapping site with an open gate structure can be extracted when applying a backflow.

site while all other trapping sites remain closed, followed by applying a backflow to release the cells from the selected trapping site (Figure 21B-C). Each trapping site consists of a U-shaped microstructure (height: 16 μm, width: 15 μm) with a narrow opening (3 μm) in the center that functions as a single-cell trap and a top-hanging bar-shaped structure (height: 7 μm) that functions as a gate in front of the U-shaped cell trap (Figure 22A). During cell loading, culturing, and analysis, these gate structures remain open (positioned 9 μm above from the bottom surface), where single cells, nutrients, and chemicals can be delivered into the U- shaped cell traps with a forward flow of culture media. During the cell extraction process, all gate structures except the one at a particular trapping site of interest are closed by pushing down these gate structures toward the bottom surface of the cell culture/analysis layer. The vertical movement of the arrays of gates at each trapping site can be individually controlled by utilizing the top and middle control layers through hydraulic pressure.

The top and the middle control layers have 32 columns and rows of control microchannels, respectively. When these two layers are combined together, 1024 junctions are generated in which each junction area matches with the gate structure of each trapping site in the underlying cell culture/analysis layer (Figure 21A and 22A). Since a thin PDMS membrane (thickness: 20 ~ 25 μm) is formed between each layer, when hydraulic pressure is applied to the middle control microchannels, the thin membrane between the middle control layer and the underlying cell culture/analysis layer is pushed downward. This downward movement pushes the gate structure down, closing the trapping site (Figure 22D). On the other hand, if the hydraulic pressure is

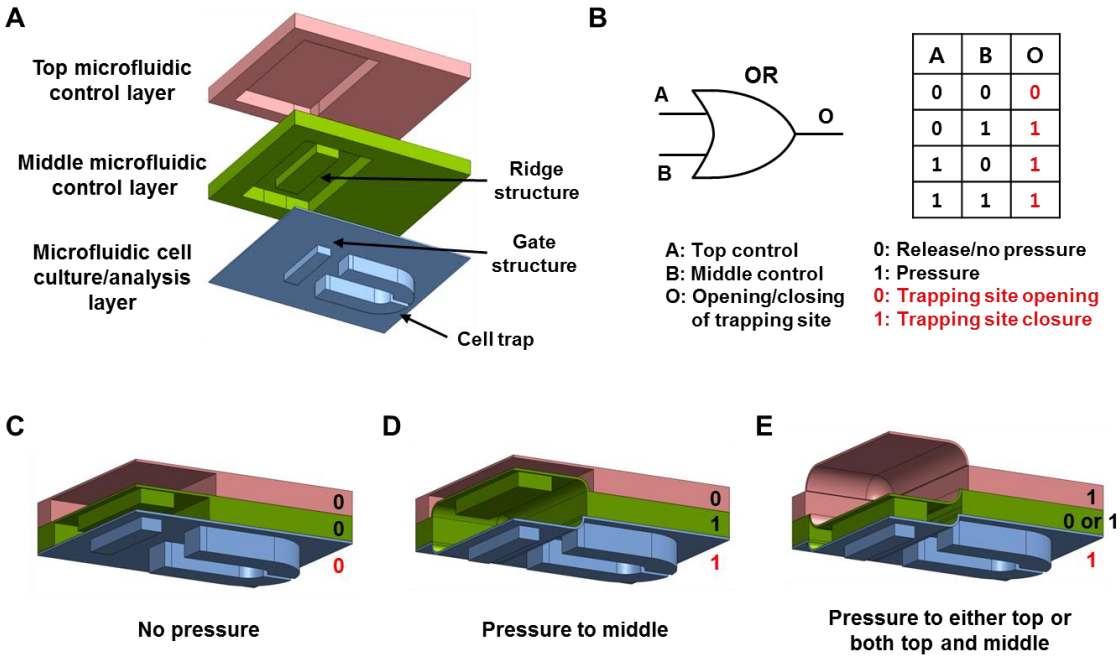

A	B	O
0	0	0
0	1	1
1	0	1
1	1	1

Figure 22. A schematic view of a single trapping site where its opening and closing are controlled through two microfluidic control channels. (A) Each trapping site consists of a U-shaped cell trap where a single cell is hydrodynamically captured and a gate structure that can be selectively opened or closed by actuating the control microchannels with hydraulic pressure. (B) The actuation principle to close the single trapping site, which effectively becomes a microfluidic OR logic gate. (C) The trapping site remains open only when neither the top nor the middle control microchannels are pressurized. (D) When the middle control microchannel is pressurized, the gate structure is pushed down and the trapping site is closed. (E) When both control microchannels or only the top control microchannel are actuated, the trapping site remain closed.

released from the middle control channels, the deformed membrane restores to its original position, lifting up the gate structure to open the trapping site (Figure 22C). When the top control microchannels are actuated with hydraulic pressure, the thin PDMS membrane between the top and the middle control layer is pushed down, and consequently the ridge structures hanging upside down from the membrane pushes down the underlying PDMS membrane between the middle control layer and the cell culture/analysis layer together with the gate structure, closing the trapping site (Figure 22E). To facilitate the closing of the gate structure when the top control layer is pressurized, a top-hanging ridge structure (3 μm above from the bottom) is employed in the middle control layer, which allows the closing of the trapping sites using lower hydraulic pressure.

Thus, the gate structure controlled by the two perpendicular control microchannels stacked on top of each other is designed to close the trap when either one of the top or the middle control microhannels are actuated with hydraulic pressure or when both microchannels are actuated with hydraulic pressure, but to remain open when neither microchannels are pressurized (Figure 22C-E). The opening and closing principle of this gate structure to open or close the cell trapping site is similar to a microfluidic OR logic gate (Figure 22B). Here the output of the microfluidic OR logic gate becomes '0' (trapping site: open) only when both inputs to the gate are '0' (both control microchannels are "open", meaning no pressure applied). However, the output of the gate becomes '1' (trapping site: closed) if either one of the inputs or both are '1' (at least one of the two control microchannels are "closed", meaning pressurized). This

microfluidic OR logic gate implemented here allows independently controlling a large array of trapping sites with minimum number of control lines.

3.3. Independently accessing a large array of single cell traps

In mutant cell library screening, after identifying the few cells (typically less than few %) having a desired feature (*e.g.,* high growth rate, high biomolecule production rate, high or low drug resistance), which can be captured in any of the traps in a large array of trapping sites, the corresponding trapping sites have to be selectively opened for cell retrieval and collection off-chip. Thus it becomes crucial to be able to independently access each of the cell trapping sites. To extract cells of particular interest after analysis, first, hydraulic pressure is applied to both the column-direction control microchannels in the middle control layer and the row-direction control microchannels in the top control layer, closing all trapping sites (Figure 23B). Next, only the row (in the top control layer) and the column microchannels (in the middle control layer) covering the particular trapping site of interest are selected and then, the hydraulic pressure is released, which results in that particular trapping site to be open (Figure 23C-D). Since a trapping site can be opened only when pressure from both control microchannels (row-direction and column-direction) are released, trapping sites where either the row or column-direction control microchannels are depressurized remain closed. Finally, by applying backflow from the outlet, cells from only this particular trapping site can be released and flow into an on-chip or off-chip reservoir for collection and further analysis (Figure 21C and 23D).

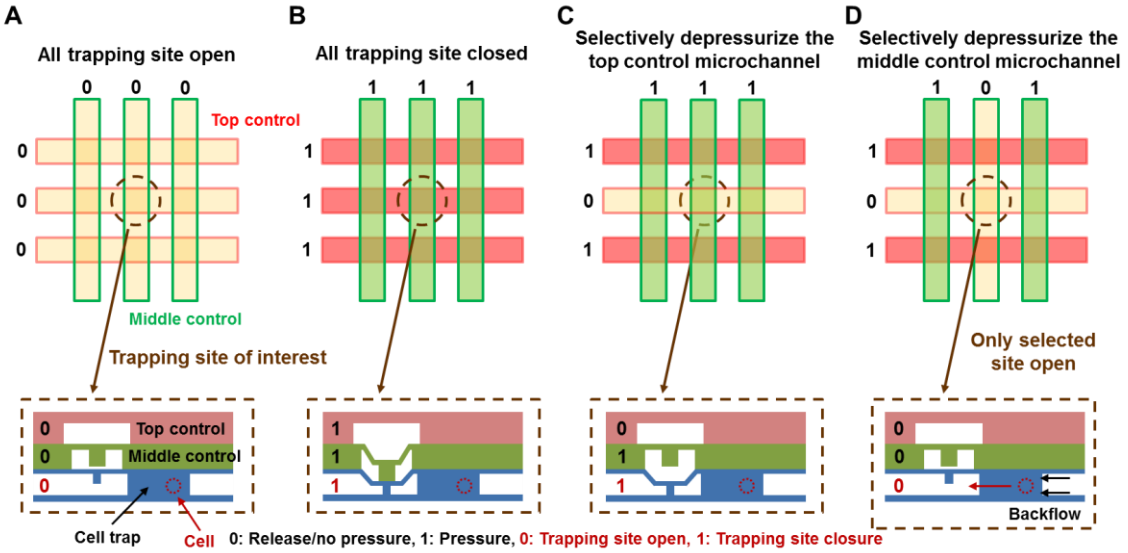

Figure 23. Operation principle and sequence of the selective cell extraction process from a particular trapping site. (A) During cell loading, culturing, and analysis periods, all control microchannels in both control layers are not pressurized, and thus all trapping sites stay open. (B) To extract cells from a particular trapping site (highlighted with a dashed circle), first all trapping sites are closed by pressurizing all control microchannels. (C-D) By releasing the pressure from the second column-control microchannel in the top control layer (red) and the second row-control microchannel in the middle control layer (green), only the gate of the underlying trapping layer at the (2,2) position opens while all other traps remain closed. This allows selective release and collection of cells from the trap position (2,2) with backflow.

To regulate each of the 32 control microchannels with reduced number of inputs, a microfluidic binary demulitplexer scheme was utilized in both the top and the middle control layers[29, 80]. This allowed a total of 64 control microchannels to be regulated with only 22 inputs (10 for the binary demultiplexer control lines + 1 for input source = 11 inputs required for each of the top and the middle control layers). Thus, all of the 1024 trapping sites can be independently controlled and target cells of interest in any of the 1024 trapping sites can be selectively extracted using only 22 tubing connections. All control microchannels in both control layers were regulated by arrays of solenoid valves (SMC, Noblesville, IN) controlled by a custom LabView™ program (National Instruments, TX). All control microchannels were filled with DI water (hydraulic pressure) instead of air in order to prevent bubble formation in the cell culture/analysis layer during the operation.

3.4. Fabrication

The microfluidic platform was fabricated in PDMS (10:1 mixture, Sylgard® 184) using the soft-lithography technique. The master molds for the top control layer, the middle control layer, and the bottom cell culture/analysis layer were fabricated by SU-8™ photoresist using a conventional photolithography process. The top control microchannels and the binary demultiplexer for both control layers were 50 μm deep, obtained by spin-coating SU-8™ 2050 at 3500 rpm. The middle control microchannels with ridge structures were made of two SU-8™ layers by spin-coating them at 1000 and 3000 rpm, respectively (SU-8™ 2002: 3 μm, SU-8™ 2025: 30 μm). In the cell

culture/analysis layer, the gate structures (thickness: 7 μm) were first patterned by spin-coating SU-8™ 2007 at 3500 rpm, followed by the fabrication of the U-shaped single cell traps (thickness: 16 μm, SU-8™ 2015 at 3000 rpm). PDMS layers forming the top control microchannels (thickness: 70 μm, 1300 rpm), the middle control microchannels (thickness: 50 μm, 2000 rpm), and the cell culture/analysis layer (thickness: 40 μm, 2500 rpm) were replicated from the SU-8™ masters by spin-coating PDMS pre-polymer for 40 seconds. The thickness of the SU-8™ masters as well as the replicated PDMS devices was measured using an optical surface profilometer (Veeco NT9100, Veeco, NY). All PDMS layers were aligned and assembled under a microscope upon 90 seconds of exposure to oxygen plasma. For sterilization, the assembled platform was treated with ultra-violet (UV) light for at least one hour. Prior to cell loading, this cell culture/analysis layer was also coated with bovine serum albumin (BSA) for 3 ~ 5 hours by filling the microchannels with 3% (w/w) BSA solution to prevent cell adsorption as well as to minimize the background noise during Nile red staining.

The single-cell screening platform was successfully fabricated by replicating each PDMS layer (the top control layer, the middle control layer, and the bottom cell culture/analysis layer) from the mater molds and assembling all the layers together (Figure 24A-C). Compared to our model microalga, *Chlamydomonas reinhardtii (C. reinhardtii)* (typical diameter: 5 ~ 10 μm), the trapping structure has a slightly larger opening (15 μm) at the front, where single microalgal cells could be successfully captured. The 3D structure of the single trapping site with a captured *C. reinhardtii* is shown in Figure 24D, reconstructed using confocal microscopy by intentionally over-

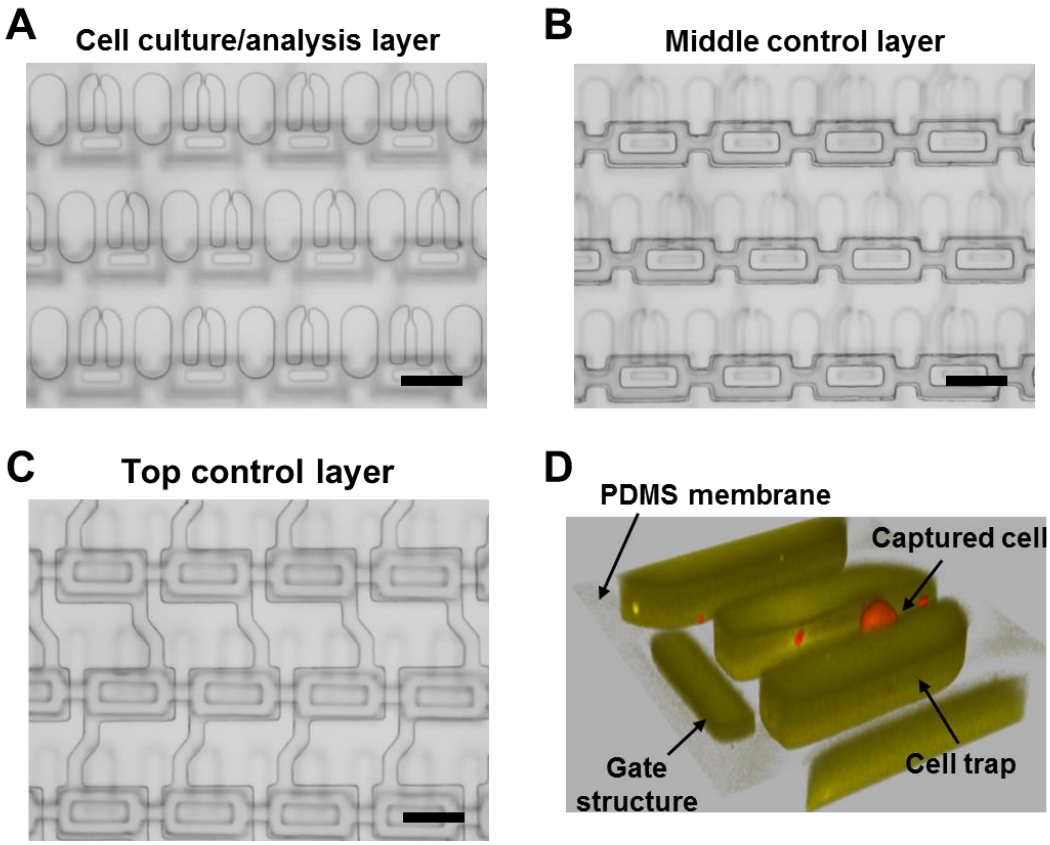

Figure 24. Microfabricated high-throughput screening platform. (A-C) Microscopic images of each PDMS layer. (D) 3D reconstruction of the PDMS cell culture/analysis layer having a single *C. reinhardtii* cell captured within, visualized by imaging its chlorophyll autofluorescence. Scale bar = 100 μm.

staining the PDMS device with Nile red to view the trapping structure and using chlorophyll autofluorescence to view the *C. reinhardtii* cell.

3.5. *Chlamydomonas reinhardtii (C. reinhardtii)* as a microalga model

The capabilities of the developed single-cell extraction platform were tested using a unicellular green microalga *Chlamydomonas reinhardtii (C. reinhardtii)* CC-125 strain, a model microalga widely used for genetic and mutagenic engineering. *C. reinhardtii* has the best developed transgenic methods among algae and has been used as a biofactory to produce fully functional antibodies and other proteins of pharmaceutical interest[126-129]. Additionally, *C. reinhardtii* has been an important model system for studying photosynthesis, motility, and numerous metabolic processes for several decades[130]. Both the nuclear and chloroplast genomes of *C. reinhardtii* have been sequenced and both of these compartments can be readily and stably transformed[131, 132]. Detailed metabolomic and transcriptomic analysis of *C. reinhardtii* have been carried out, giving insight into gene expression and metabolic changes related to oil production[133].

This strain was cultured in Tris-acetate-phosphate (TAP) media[134, 135] at 23°C under a light intensity of 100 μmol photons·m^{-2}·s^{-1} with a 12 hour light-dark cycle. *C. reinhardtii* was collected from an exponentially growing liquid TAP culture. It is well known that *C. reinhardtii* accumulates oil bodies under stressed condition such as nitrogen or phosphate deprivation[134, 136]. To induce oil accumulation, *C. reinhardtii* was

grown in TAP media lacking NH_4Cl or any other N source (TAP-N) for 3 ~ 4 days before use.

3.6. Simulation of various single-cell trap designs

The cell trap for engineered or mutagenized cell library screening has two requirements. First it should have the capability to trap only a single cell with high efficiency, as each of the cells in the library are potentially different and should be tested for the trait of interest. Second, since the trait of interest can typically be only identified after some duration of culture (*e.g.,* cell growth rate), meaning that multiple cells will be produced from a trapped single cell, it is necessary to have a large-enough cell trap to allow room for cell growth and doubling. For example, when looking for genetic variants that show the highest growth rate amongst a mutagenized algal library, single algal cells trapped in each of the trapping sites has to be cultured for some time and cells with the highest doubling time, as identified through the number of cells stemming from a single trapped cell, needs to be selected and extracted. This requirement of cell culture and resulting cell doubling makes many previously developed single-cell assay microfluidic platforms unable to accomplish such cell library screening tasks.

Three different trap designs have been proposed and tested. All trapping sites consist of a U-shaped trapping structure of which the opening width, length, and overall height are 15, 62.5, and 16 μm, respectively (Figure 25). The first design has a 3 μm high supporting structure underneath the 13 μm high U-shaped cell trap. This supporting structure is employed to prevent the collapse of the cell trap as well as to maintain a

small opening (width: 10 μm and height: 3 μm) at the center through which culture media or reagents can flow through (Figure 25A). The second design has the same schematic as the first design except for the width of the bottom supporting structure. Here the width of the supporting structure (12 μm) is narrower than that of the U-shaped cell trap (20 μm), resulting in more culture media flow through the cell trap, which would increase the possibility of cell capture (Figure 25B). The third design has a narrow opening (width: 3 μm, height: 16 μm) at the center of the U-shaped cell trap (height: 16 μm), as described in the previous section (Figure 25C, see '3.2. Design and operating principle of the individually addressable single-cell trap')

Numerical simulations of fluidic flow through the three different trapping structures were conducted using a commercial finite element method (FEM) software (COMSOL Multiphysics®, COMSOL Inc., Los Angeles, CA, USA). To optimize the single-cell capturing efficiencies as well as backflow required for cell release, flow profiles inside each trap design for three situations – before cell capture, after cell capture, and during cell extraction, were simulated and compared (Figure 26; X ~ X': along the flow direction, Y ~ Y': across the center of a gap at each trap design). 3D schematics of each trapping structure design utilized in the simulation are shown in Figure 26A, each having a different gap geometry; the first design has a bottom opening (cross section = 10 (width) x 3 (height) = 30 μm^2), the second design has a bottom opening with supporting structures (cross section = 10 x 3 = 30 μm^2), and the third design has a narrow gap in the center (cross section = 3 x 16 = 48 μm^2). Compared to the flow profiles before capturing a cell (Figure 26B), flow speeds inside the trapping

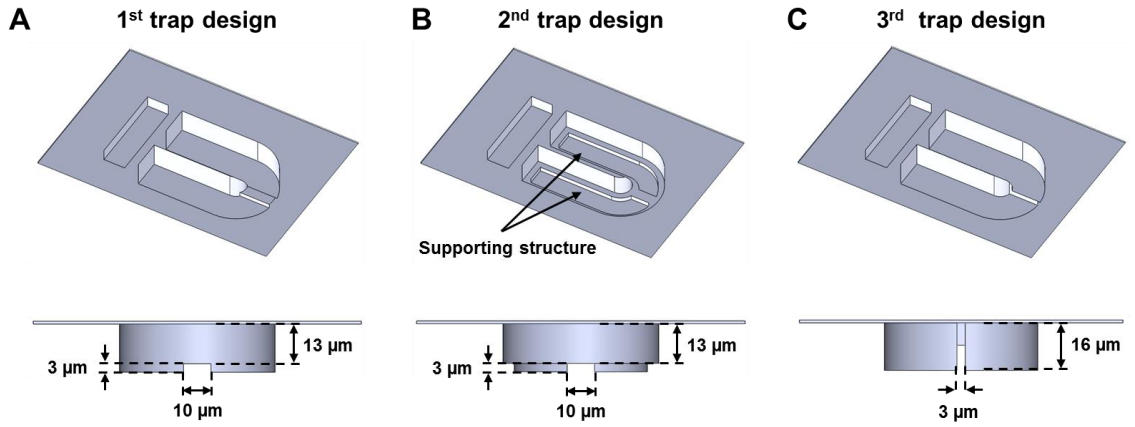

Figure 25. Three different single-cell trapping designs proposed and tested through simulation. All trapping structure designs consist of U-shaped cell traps having a 15 µm wide opening and a length of 62.5 µm, which provide enough room for a captured cell to be cultured. 3D schematics and enlarged rear view of the (A) first trap design having a small opening at the bottom, (B) second design having a small opening as well as supporting structures at the bottom, and (C) third design having a narrow opening in the center of the U-shaped structure.

structures were decreased after capturing a cell, which reduces the chance for other cells to be introduced and captured in the same trap (Figure 26C). Although the variation of flow speeds in each trapping structure design (average speed difference across the gap cross-section before and after cell capture: first design: 0.78 → 0.67 mm/s, second design: 0.72 → 0.29 mm/s, third design: 0.46 → 0.27 mm/s) could provide some valuable information about each trap design itself, this parameter was not appropriate for comparing the three different trapping structure designs due to their different gap geometry. Even under a constant flow condition, fluidic speed flowing through a microchannel can vary depending on the microchannel geometry (*e.g.,* cross-section), and thus, another parameter covering both the flow speed and the gap geometry is needed, that is, fluid flux.

Fluid flux, defined as the amount of fluid passing through the gap cross-section per unit time (m^3/s), was calculated by multiplying the average flow speed across the gap cross-section and the area of the gap cross-section in each trap design (flux = average flow speed passing through the cross section of the gap x cross sectional area of the gap, Figure 26E). Fluid flux provides the volume of fluid flowing through each trap design regardless of gap sizes, which allows for side-by-side comparison of the three different trap designs. Before capturing cells, all three trapping structure designs had almost the same amount of fluid flowing inside. After capturing cells, 60% (first design), 14% (second design), and 50% (third design) of fluid flow was blocked with a captured cell (flux difference before and after cell capture: first design: 2.17×10^{-14} → 0.87×10^{-14}

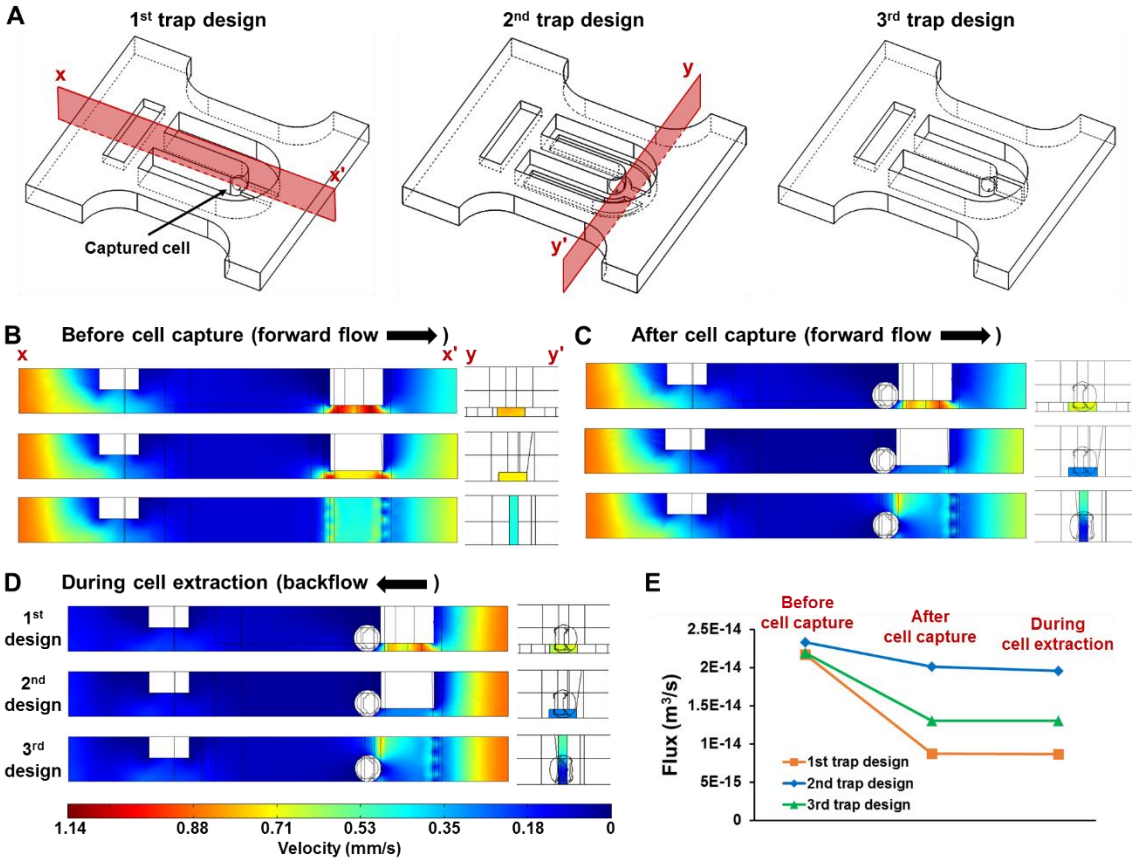

Figure 26. Numerical simulation results of the fluidic flow profiles of the three different trapping structure designs. (A) 3D illustrations of first, second, and third trapping structure designs having three different gap geometries. Flow profiles of the three different trap designs analyzed along the flow direction as well as across the center of a gap (B) before capturing a cell, (C) after capturing a cell, and (D) during cell extraction process (when backflow is applied). (E) Analysis of fluid flux, the amount of fluid flow across the cross-section of a gap for each trap design.

m^3/s, second design: 2.33 x 10^{-14} → 2.02 x 10^{-14} m^3/s, third design: 2.19 x 10^{-14} → 1.31 x 10^{-14} m^3/s). Based on these flux changes, the first design would have the highest single-cell trapping efficiency as less amount of fluid will flow through this trap design once the trapping sites are occupied, compared to the other two designs, resulting in the least probability in capturing more than two cells in a single trap. The second design showed the smallest reduction in fluid volume after capturing a cell (only 14% decrease). This would mainly come from the supporting structures having a narrower channel width, resulting in space between a captured cell and the gap of the trap through which most of fluid can still flow.

Next, fluid flow during the cell extraction process (*i.e.,* when applying backflow to release cells) was analyzed through the three different trap designs with a captured cell inside (Figure 26D). The highest flux and the lowest flux were observed from the second and the first designs, respectively, meaning that more backpressure will be needed for the first design to achieve the same degree of backflow compared to other two designs. For example, approximately 2.3 and 1.5-fold of backflow is required in the third design to obtain the same amount of fluid flow as the first and the third designs (flux in first design: 0.87 x 10^{-14} m^3/s, flux in second design: 1.96 x 10^{-14} m^3/s, flux in third design: 1.30 x 10^{-14} m^3/s). Based on these simulation results, the first design will have the highest single cell trapping efficiency, but will require more backflow during the cell extraction process. The second design will need the least backflow to release cells from the cell trap, but will have the lowest single cell trapping efficiency. The third design will have a slightly lower trapping efficiency compared to the first design, but

will require much less backflow to extract the cells for off-chip analysis. Considering these simulation results, the third trapping design was selected and utilized in the microfluidic single cell screening platform.

3.7. Single cell trapping efficiency

Trapping efficiency of the selected trapping structure design (third design) was evaluated experimentally by measuring the number of trapping sites having no cell, one cell, and more than two cells. *C. reinhardtii* was loaded into the cell culture/analysis layer with a syringe pump (Fusion 200, Chemyx Inc., Stafford, TX, 3 ~ 5 μl/min) to characterize the single-cell trapping efficiencies. Once all of the trapping sites were occupied with *C. reinhardtii* cells, any excessive microalgae were flushed out with fresh culture media (5 ~ 10 μl/min for 10 minutes). The trapping structure design (third design) had an overall cell trapping efficiency of 91.8 ± 2.9% (average ± standard deviation), where 7.7 ± 2.6% sites were empty, 8.7 ± 5.1% sites had more than two cells captured, and 83.2 ± 3.4% had only a single cell trapped (n = 8).

3.8. Capability of culturing and staining microalgae

The capabilities of culturing and analyzing cells are essential requirement for the developed system to be used as a cell screening platform. The culture capability of the platform was tested by growing *C. reinhardtii* inside the platform, where its growth rate was characterized by its doubling time. *C. reinhardtii* cells inside the trapping sites were

cultured under a light intensity of 100 μmol photons·m^{-2}·s^{-1} with a 12 hour light-dark cycle. Fresh TAP media was continuously perfused with a syringe pump at a flow rate of 1 μl/min. Cell doubling time of *C. reinhardtii* was analyzed by counting the number of cells under a microscope. Compared to conventional culture systems (lab-scale flasks), the developed single-cell screening platform has several advantages. In the microfluidic single-cell screening platform, the growth profile of *C. reinhardtii* can be obtained with single-cell resolution. For example, as shown in Figure 27A, single-cell level behavior of *C. reinhardtii*, such as cell size increase and cell division, could be observed in real time. This microalga is known to undergo 2 ~ 4 rounds of mitosis before daughter cells are divided and separated from a mother cell[134]. Based on this information, the doubling time of *C. reinhardtti* inside the platform was determined to be 6 ~ 8 hours, which was consistent with previous studies using conventional flask systems[137]. In addition, identical light exposure conditions could be applied in the developed platform unlike the conventional culture systems that are hampered by light blocking problems caused by self-shading. Thus, information obtained through this platform is consistent and could be used in mechanistic studies that require accurate and a consistent cellular microenvironment.

The on-chip fluorescence staining capability of the platform was also characterized. For example, in microalgae screening applications the production and accumulation of lipids inside the cell body are one of the most interesting features due to its potential as a future renewable biofuel source[5, 9, 29]. Analysis of oil accumulation in N-starved *C. reinhardtii* was carried out using Nile red fluorescence staining inside the

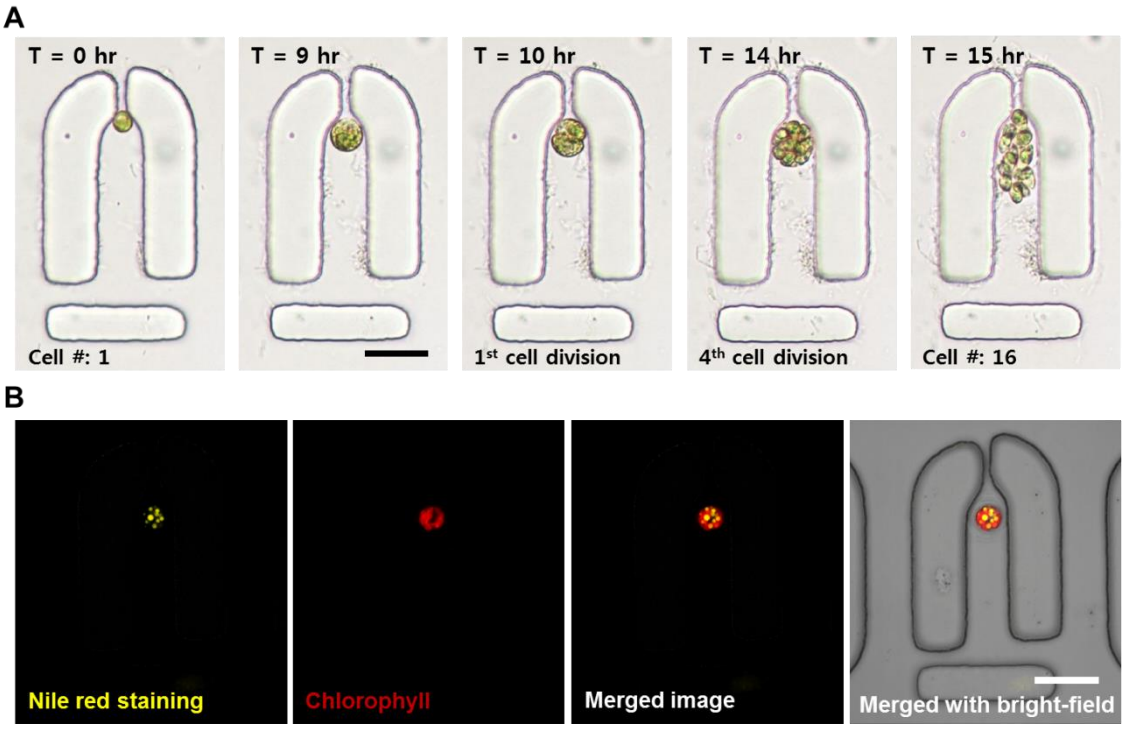

Figure 27. Microscopic images showing culture and on-chip staining capabilities of the platform. (A) Single-cell resolution growth profile of *C. reinhardtii* showing size increase, followed by cell division inside the cell trap over a 15-hour period. (B) Oil accumulation in *C. reinhardtii* grown under N-limited condition was analyzed inside the cell trap through Nile red fluorescenct dye staining. Chlorophyll autofluorescence (red) indicates biomass and Nile red staining (yellow) shows lipid content. Scale bar = 25 μm.

platform. Nile red solution in dimethyl sulfoxide (DMSO) was diluted in TAP media to a concentration of 0.75 μg/ml Nile red and 0.5% DMSO, and this diluted solution was provided through the cell culture/analysis layer for 10 minutes at a flow rate of 1 – 10 μl/min, followed by rinsing with fresh media for 5 minutes. Microscopy for Nile red fluorescence (excitation: 460 – 500 nm, emission: 560 – 600 nm) as well as chlorophyll autofluorescence (excitation: 460 – 500 nm, emission > 610 nm) were conducted using a Zeiss Axio Observer Z1 microscope (Carl Zeiss Micro Imaging, LLC) equipped with a digital camera (Orca Flash2.8 CMOS Camera). Figure 27B shows microscopic images of oil bodies successfully stained with Nile red (yellow) and autofluorescence from chlorophyll (red, biomass indicator), demonstrating the on-chip analysis capability of the developed platform.

3.9. Operation (closing and opening) of the single cell trapping site

Each of the 1024 trapping sites is open only when both control microchannels are not actuated with hydraulic pressure, but are otherwise closed if at least one of the control microchannels is pressurized. This working principle was tested and characterized by observing the lowering of the gate structure in each trapping site with incremental actuation pressure. First, when only the middle control microchannel was pressurized under a pressure of less than 90 kPa, the gate structure was pushed down, but did not touch the bottom surface, thus the trap remained open (Figure 28A). However, the trapping site was completely closed at a pressure of 90 kPa or higher, in which the overall gate structure tightly contacted the bottom surface (Figure 28B-C, total

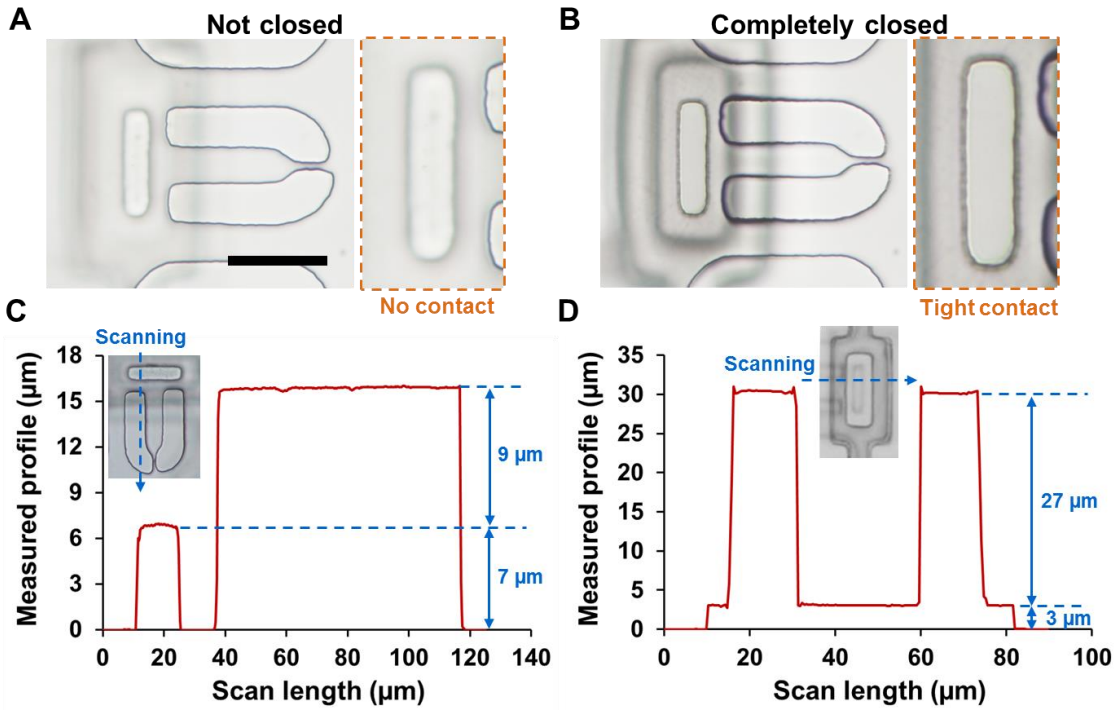

Figure 28. Microscopic images showing the opening and closing of the trapping site. (A) Trapping site remaining open, where the gate structure had no contact with the bottom surface of the cell culture/analysis layer. (B) Trapping site closed as the gate structure formed a tight contact with the bottom surface. Inset images (orange dashed line) show the enlarged view of the gate structure. The thicknesses of (C) the fabricated cell culture/analysis layer consisting of the cell trap and the gate structure, and (D) the middle control layer with the ridge structure. Scale bar = 50 μm.

deformation length required to fully close the trapping site: 9 μm).

When only the top control microchannel was actuated, a fairly high pressure of more than 360 kPa was required to fully close the trapping site. This is because the PDMS membrane between the top and the middle control layers had to be sufficiently pushed down to subsequently deform the underlying membrane between the middle control layer and the cell culture/analysis layer, which then lowered the blocking structure to close the cell trap (total deformation length required to fully close the trapping site: 30 (microchannel height in the middle control layer) + 9 = 39 μm). However, often this high pressure broke the bonding or damaged the PDMS membrane between the top and the middle control layers, making robust and repeated operation of the system a challenge. To reduce the required pressure (or the required deformation length) for the top control microchannel actuation, a 30 x 82 μm^2 ridge structure hanging upside down from the membrane and positioned 3 μm above the underlying membrane was utilized in the middle control microchannels (Figure 28D). When the top control microchannel was actuated with hydraulic pressure and the membrane between the top and the middle control layers was deformed, the ridge structure made contact with the underlying membrane, and thus pushed down the gate structure to close the cell trapping site. By employing this ridge structure, total Z-directional deformation length required was 12 μm (3 + 9 μm) and the trapping site could be completely closed with significantly lower actuation pressure of 155 kPa. When applying pressure of less than 155 kPa to the top actuation channel, the cell trap was not closed (Figure 28A), however was fully closed when pressure of 155 kPa or higher was applied (Figure 28B). This

significantly lower actuation pressure compared to the previous 360 kPa significantly increased the system stability by minimizing the membrane damage. Thus, successful closing and opening of the gate structure through actuating the top and the middle control microchannels enabled a microfluidic OR logic gate. Thus a pressure of 155 kPa was used in all subsequent experiments.

3.10. Selective cell extraction

During the cell loading, culture, and analysis periods, the gate structure in each trapping site remained open to provide cells with nutrients through continuous perfusion of culture media at a flow rate of 1 μl/min. To extract the cells of interest from a particular trapping site after analysis, first, all trapping sites ($S_{1,1} \sim S_{3,3}$) were closed by actuating all microchannels in the top and the middle control layers ($T_1 \sim T_3$ and $M_1 \sim M_3$, Figure 29A-B) with hydraulic pressure. To release cells from trapping site $S_{3,2}$, pressure from the top control microchannel T_2 and the middle control microchannel M_3 were released. Since each trapping site is designed to remain closed even if the pressure in one of the control microchannels is released, only this particular trapping site ($S_{3,2}$) was opened out of the 1024 sites in the cell culture/analysis layer. With the backflow (flow rate: 3 – 5 μl/min), the *C. reinhardtii* cell inside the particular trapping site ($S_{3,2}$) was successfully extracted to an off-chip reservoir without affecting cells captured in other trapping sites (Figure 29C).

This process could be repeated to sequentially release cells from other trapping sites of interest. For example, all trapping sites were closed again when all

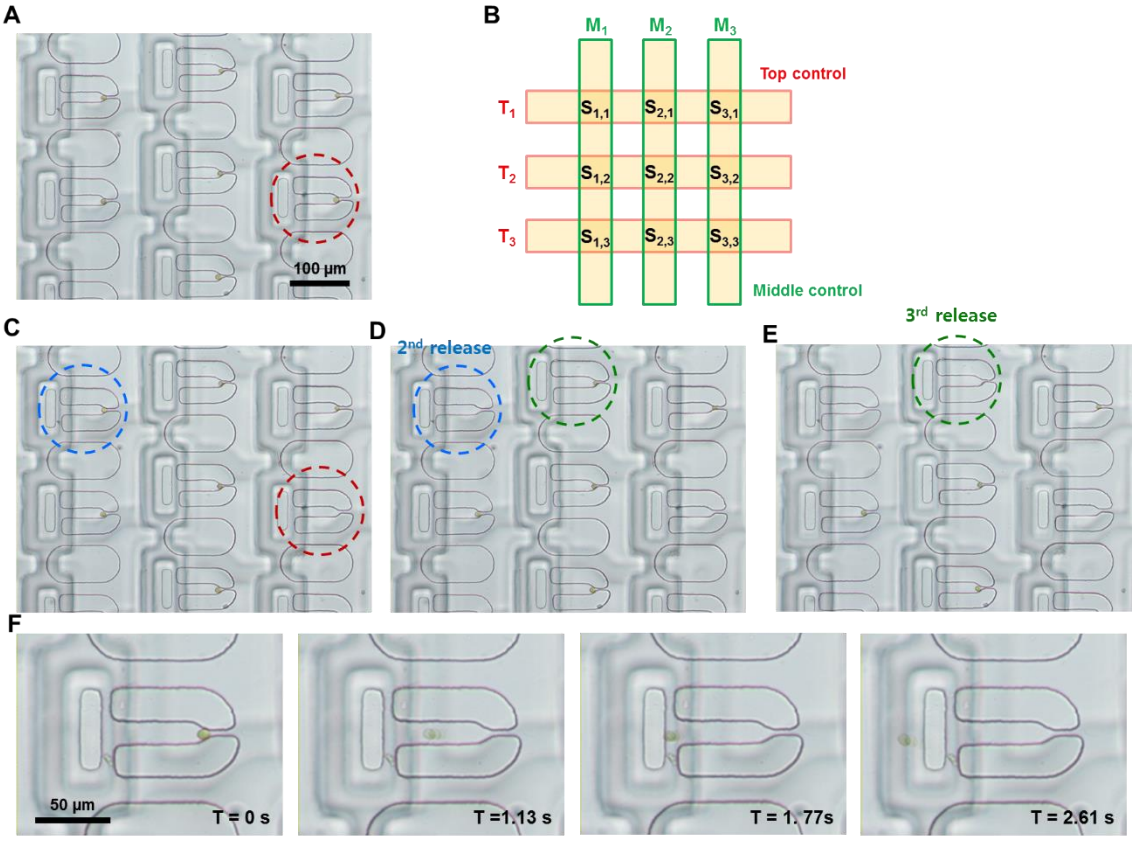

Figure 29. Microscopic images showing selective cell extraction from a particular trapping site of interest. (A) Before extracting cells, all trapping sites were closed. (B) Illustration showing 3 top and 3 middle control microchannels on top of 9 single-cell trapping sites ($S_{1,1}$ ~ $S_{3,3}$). (C) By selectively releasing pressure from the M_3 and T_2 control microchannels, a cell captured at trapping site $S_{3,2}$ was successfully released. (D-E) By releasing pressure only from the chosen top and middle control microchannels on top of the target trapping sites, cells inside the target site could be released without affecting other trapping sites. (F) Time-lapse images showing a cell from site $S_{1,1}$ being released when a backflow was applied.

microchannels in both control layers were pressurized after releasing the cell from position $S_{3,2}$ (Figure 29C). Then, a second cell trapping site ($S_{1,1}$) was selectively opened by releasing pressure from the top and the middle control microchannels (T_1 and M_1) controlling this trapping site, and the *C. reinhardtii* cell could be successfully released once backflow was applied (Figure 29D). This process was repeated for trapping site $S_{2,1}$ (Figure 29E) by releasing pressure from the microchannel T_1 and M_2. Time-lapse images showing the cell being releasing from the selected trapping site ($S_{1,1}$) with backflow were displayed in Figure 29F. In summary, by selectively releasing pressure from the control microchannel combinations in both the top and the middle control layers, any of the 1024 trapping sites in the cell culture/analysis layer could be selectively opened and captured cells inside the selected trapping site could be successfully extracted without affecting other trapping sites.

3.11. Conclusion

We have developed a microfluidic high-throughput single-cell screening platform with the capability of capturing, culturing, and analyzing cells with single-cell resolution, followed by selectively extracting particular cells of interest off-chip for further study. Two microfluidic control layers regulated by a binary demultiplexer scheme and a microfluidic OR logic gate enabled independent control of the opening and closing of each of 1024 trapping sites with a much reduced complexity. By opening only a particular trapping site while others remained all closed, cells of interest could be successfully retrieved among cell populations in the platform by applying a backflow.

The growth profile of a captured single *C. reinhardtii* cell was monitored over time and its oil accumulation was also analyzed through on-chip Nile red fluorescent lipid staining. Finally, single *C. reinhardtii* cells from a particular trapping site were successfully isolated and extracted to an off-chip reservoir. We expect that this system will serve as a powerful high-throughput single-cell screening and analysis tool in broad ranges of applications where screening through large libraries of genetic variants is needed, particularly a mutagenized or engineered microalgae screening.

CHAPTER IV

A HIGH-THROUGHPUT DROPLET MICROFLUIDICS-BASED MICROALGAE SCREENING PLATFORM

4.1. Motivation

Previously developed microfluidics-based screening systems such as the growth condition screening photobioreactor array and the single-cell screening and selection platform were successfully developed and utilized to investigate microalgal growth and oil production under different growth conditions (light intensity, light-dark cycle, and culture media composition) and among different microalgal strains. However, the throughput of these systems is somewhat limited (from a few hundred to several thousand range) when screening through large numbers of microalgal library that may have to be tested for more than one million cells. To overcome this limitation, a droplet microfluidics-based microalgae screening platform was developed and applied in microalgae study.

Droplet microfluidic-based systems have shown the capability to outperform conventional biological assays by providing the ability to conduct complex and highly repeatable screening applications at high-throughput[52, 53, 120, 138-151]. Droplet microfluidics entails microdevices that produce and manipulate discrete droplets of one fluid within a second immiscible carrier fluid (*e.g.,* water-in-oil droplet emulsion). This method generates highly monodisperse microscale diameter droplets (typically in the range of tens to hundreds of micrometer) at the formation rates of over 10 kHz. Each droplet

having femto-, pico-, or nano-liter aqueous volume functions as an independent bioreactor, and moreover, these droplets can be individually transported, mixed, and analyzed, where massive parallel processing and experimentation can be achieved within a short period of time. In addition, this system can provide encapsulation of a single cell within a droplet, which allows for high-throughput single cell screening and analysis capabilities. Volumetric confinement in droplets also prevents dilution of chemicals, improves sensitivity, and facilitates faster reaction time due to the large surface to volume ratios. The droplet microfluidic-based systems have been successfully utilized in a variety of applications, such as drug discovery, polymerase chain reaction (PCR), synthesis of biomolecules, diagnostic testing, and other screening applications such as enzyme activity and engineered proteins for directed evolution.

Only a few droplet microfluidics-based microalgae screening platforms have been emerged so far. Droplet generators integrated with downstream culture chambers were employed to encapsulate single microalga into a droplet and to monitor these droplets over time[74, 75]. Although growth profile of microalgae inside droplets was successfully analyzed, these platforms are limited in characterizing oil contents inside microalgae. Alginate hydrogel-based microcapsules encapsulating BODIPY-stained microalgae were introduced to analyze oil content of a single microalga, and the heterogeneity of oil accumulation among species and among individual cells within the same species were investigated[72]. However, this system cannot provide a culturing capability and requires an additional sample preparation step (off-chip BODIPY staining) to conduct on-chip oil analysis. To be utilized as a screening tool for

investigating numerous microalgal strains, the platform needs to have capabilities of analyzing both growth and oil production on-chip. However, all of the previous droplet microfluidics-based platforms were lack of either on-chip culture or oil analysis capabilities, not suitable for microalgal strain development.

Here, we have developed a high-throughput droplet microfluidics-based microalgae screening platform capable of analyzing both microalgal growth and oil production on-chip. Independent bioreactors encapsulating a single microalga with its media were produced through a droplet generator in the platform, and microalgal growth in each droplet was monitored by tracking the number of cells inside the same droplet over time. One of crucial features in the developed platform is the on-chip oil analysis capability, where fluorescence tagging and quantification of oil bodies in microalgae were all carried out through on-chip Nile red merging and rinsing processes. The functionalities of the developed microalgae screening platform were characterized and demonstrated using a unicellular microalga *C. reinhardtii* as well as a colonial microalga *B. braunii*.

4.2. Design

The PDMS droplet microfluidics-based screening platform is composed of three functional parts; a droplet culturing region, an on-chip droplet staining region, and a droplet rinsing/analysis region (Figure 30). In the culturing region, first, droplets (240 μm in diameter) containing a single microalga and culture media were generated through a T-junction droplet generator. The T-junction generator was comprised of a 200 μm

wide channel for continuous oil phase (carrier oil) and a perpendicular 160 μm wide orifice for microalgae suspended culture media, where viscous oil having a higher flow rate shears cells and media solution (Figure 31B). Then, these droplets were held at a downstream culture chamber to monitor the growth of microalgae inside the same droplets over time. As the culture chamber, a 200 μm wide serpentine microchannel was utilized in order to maintain spacing between neighboring droplets as well as to prevent unexpected droplet merging during the culturing period (Figure 31C).

One of the crucial innovations in the developed platform is the on-chip oil staining capability of microalgae within droplets. Nile red fluorescence dye was utilized in the on-chip staining process to quantify the oil accumulation in microalgae. In order to achieve the on-chip staining functionality, droplets containing Nile red molecules in DMSO (240 μm in diameter) were created through another T-junction droplet generator in the on-chip staining region, and were synchronized with droplets containing microalgae (released from the culture chamber) through a railroad-like structure (Figure 31D)[152]. This railroad-like structure equalized flow resistance between two trains of droplets (microalgae-containing droplet and Nile red solution droplet), which formed a one-to-one pair at the end of the synchronization region. These synchronized droplets were then merged inside a merging chamber (500 x 500 μm^2) by applying an electric field using two integrated electrodes, exposing microalgae inside the droplet to Nile red dye, which stained oil bodies within microalgae (Figure 31E). The applied electric field destabilized the droplet surface and induced merging of two adjacent droplets[52, 141, 142, 153]. For complete staining, the merged droplets were stored in an incubation chamber for

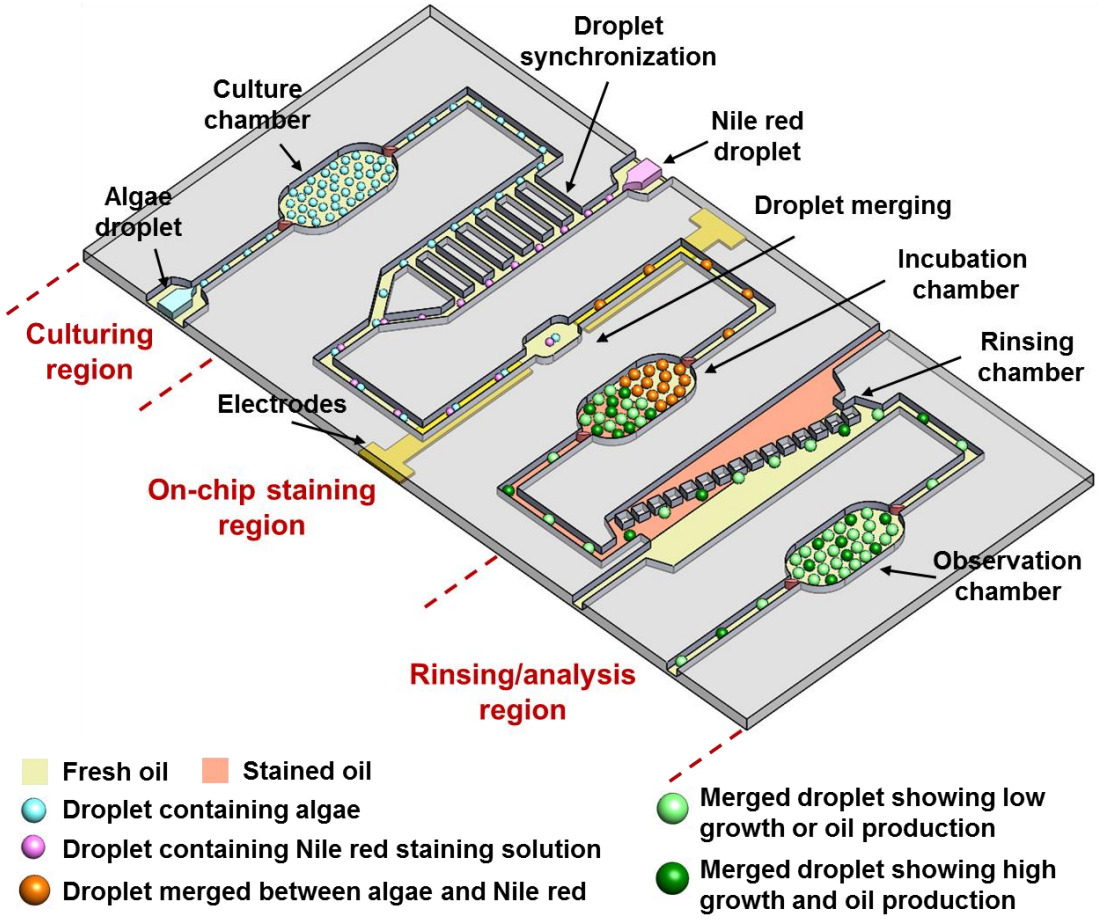

Figure 30. Illustration of the high-throughput droplet microfluidics-based microalgae screening platform for analyzing microalgal growth and oil production. The platform is composed of three functional parts – the culturing region for microalgae culture and their growth monitoring, the on-chip staining region for tagging Nile red fluorescent dye to oil bodies of microalgae, and the rinsing/analysis region for oil quantification.

for 0 – 10 minutes (Figure 31C).

Due to the nature of Nile red molecules diffusing into hydrophobic carrier oil, the carrier oil was also stained with Nile red during the on-chip staining process. This created severe background noise, which prevented an appropriate observation of stained microalgal oil through fluorescence imaging/detection. To remove this background noise, an angled 400 x 400 μm^2 micropost array (3°) was utilized in the rinsing/analysis region, which guided Nile red-stained droplets in the stained carrier oil into the neighboring fresh oil flow, effectively rinsing the droplets (Figure 31F). Finally, droplets were collected at an observation chamber and oil production was analyzed (Figure 31G).

4.3. Fabrication

The droplet microfluidic-based screening platform was fabricated in PDMS (10:1 mixture) using a soft-lithography technique. First, the master molds for a bottom channel layer (height: 160 μm) and a top valve layer (height: 250 μm) were fabricated by spin-coating SU-8™ photoresist (SU-8 2075, Microchem Inc., MA) on silicon wafers. These masters were patterned using conventional photolithography process. Before replicating PDMS layers from the masters, the SU-8™ patterns were coated with (tridecafluoro-1,1,2,2-tetrahydrooctyl) trichlorosilane (United Chemical Technologies, Inc., Bristol, PA) for 20 minutes to prevent the master mold damage during PDMS release. A PDMS layer containing the channel layer (250 μm thick) were made by spin-coating PDMS pre-polymer at the speed of 300 rpm for 40 seconds, and a thick PDMS valve layer (4 mm thick) was replicated by pouring 24 g of PDMS pre-polymer. The electrodes used to

induce on-chip droplet merging were patterned on a 50.8 mm x 76.2 mm glass slide (Micro Slides 2947-75x50, Corning Inc., NY) by first depositing a Cr/Cu layer (200 Å and 3000 Å thick, respectively) using an electron beam evaporator (PVD-75, Kurt J. Lesker, PA). Positive photoresist (Shipley 1818, Microchem Corp., MA) was used to define the electrode as an etch mask, followed by a metal etching process (TFE and CE-100, Transene Company Inc., MA). A thin PDMS layer (thickness: 30 μm) was then spin-coated on the electrode-patterned glass slide to create hydrophobic bottom surface (3000 rpm for 40 seconds). All three layers (the channel layer, the valve layer, the electrode layer) were aligned and bonded through an oxygen plasma treatment. After assembly, the devices were kept at room temperature for at least 2 days to recover hydrophobic surface inside the channel layer. The microfabricated droplet screening platform is shown in Figure 31.

4.4. Cell preparation

Two different microalgae strains were selected as model organisms to demonstrate the on-chip analysis capabilities of microalgal growth and oil accumulation in the developed droplet screening platform. Frist, as a unicellular microalga, *C. reinhardtii* CC-125 strain was used here to characterize the on-chip Nile red staining process as well as to validate the growth and oil production screening capabilities of the platform. This microalga was grown in Tris-acetate-phosphate (TAP) media at 23°C under a light intensity of 80 μmol photons$\cdot m^{-2} \cdot s^{-1}$ with a 12 hour light-dark cycle, and

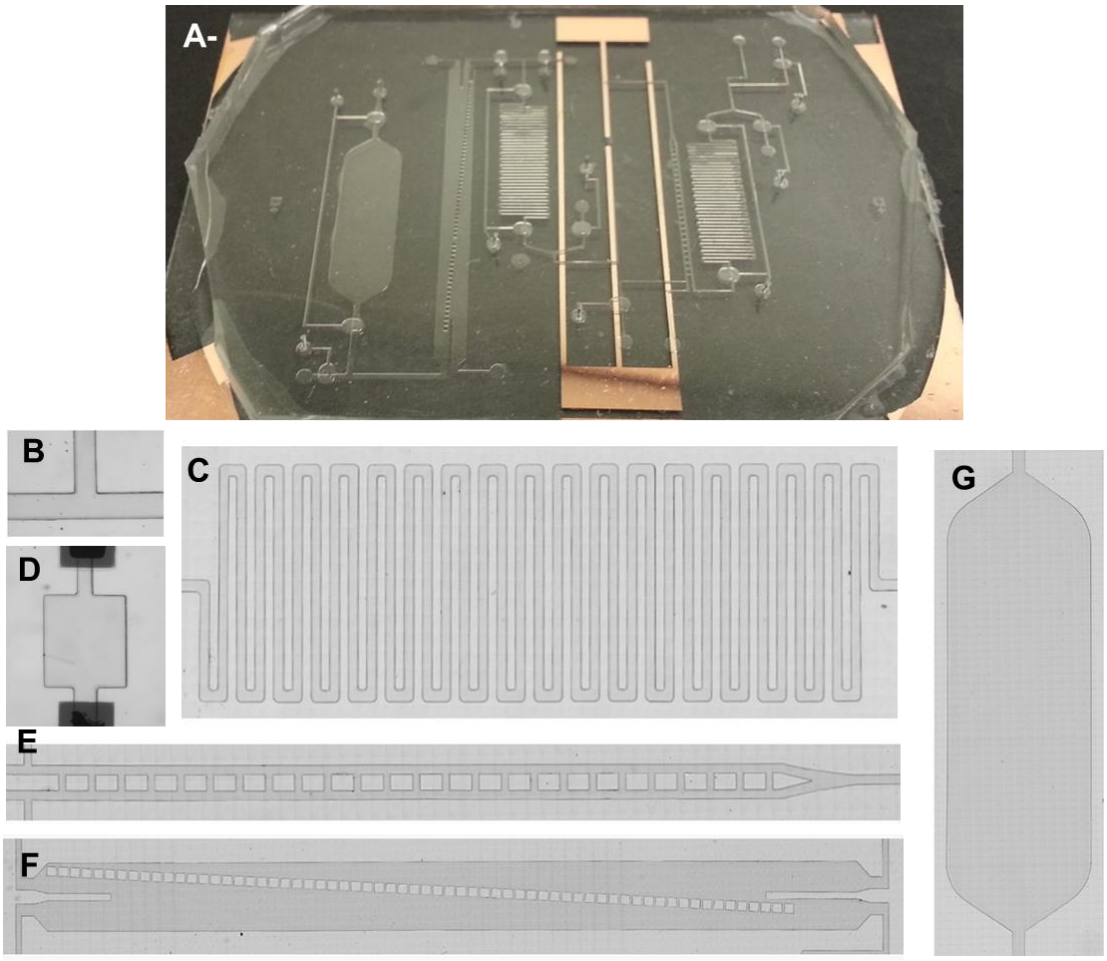

Figure 31. Microfabricated high-throughput droplet-based microfluidic microalgae screening platform. (A) Photographs of the assembled device. Micrographs of (B) T-junction droplet generator for both cell solution and Nile red solution droplets, (C) culture chamber or incubation chamber, (D) on-chip droplet merging chamber, (E) railroad-like structure to adjust the flow resistance between droplets, (F) droplet rinsing region consisting of an angled micropost array (3°), and (E) observation chamber.

was collected in exponential growth phase. This collected sample was centrifuged at 4400 rpm for 2 min, washed with fresh TAP media, and diluted at a concentration of 1.38 x 10^5 cells/ml to encapsulate a single *C. reinhardtii* cell into a droplet. To induce oil accumulation, *C. reinhardtii* was cultured in TAP media lacking NH4Cl (TAP-N) for 4 ~ 5 days before use since this strain is known to accumulate oil bodies under stressed condition such as nutrient depleted culture conditions (*e.g.,* nitrogen and phosphate). Sample solution with a density of 8.85 x 10^6 cells/ml was prepared and loaded into the droplet screening platform to encapsulate approximately 64 cells in a single droplet.

To show the on-chip Nile red staining capability of colony-forming microalgae, *B. braunii* race B, Berkeley (or Showa) strain was selected. *B. braunii* was cultured in modified Chu 13 media at 22.5°C under a light intensity of 80 μmol photons·m^{-2}·s^{-1} with a 12 hour light-dark cycle. The cultures were continuously aerated with filter-sterilized air containing 2.5% CO_2. *B. braunii* colonies in exponential growth phase (6 – 8 days after every subculture) were collected, filtered (diameter of *B. braunii* colonies after filtering: 70 – 100 μm) and utilized here.

4.5. On-chip droplet generation, synchronization, and merging

Droplets containing a single microalga (240 μm in diameter) were successfully generated by flowing the oil (J217 Mineral Oil Light White, Amresco, OH) with surfactant (2% wt/wt, Abil EM90, Evonik, TX) and microalgae suspending culture media at a flow rate of 272 μl/hr and 55 μl/hr, respectively (Figure 32A). The same size of droplet containing Nile red molecules in DMSO (240 μm in diameter) was produced

using the flow rate of 180 μl/hr for the oil and 55 μl/hr for the Nile red solution (Figure 32A). Different flow rates of oil were used to obtain the same size of droplets between microalgae solution and Nile red solution, which resulted from the large difference in viscosity between culture media and DMSO (0.886 vs. 1.990 cp at 25°C).

When considering the fusion between droplets, the proximity of two adjacent droplets is one of critical parameters which determines the merging efficiency. For example, if a pair of droplets are separated by a certain distance, the merging cannot take place in some cases. Thus, the synchronization of two droplets is of great importance in droplet merging applications. In the developed screening platform, a railroad-like structure was utilized to synchronize two trains of droplets (microalgae solution and Nile red solution). The pressure difference between two trains of droplets (top and bottom channels in Figure 32A-B) induce the crossflow of the carrier oil through the perpendicular channel network (between the top and the bottom channels) until the pressure in each channel is balanced, which results in automatic synchronization of two droplet trains[152]. By flowing the droplet with microalgae solution and generating Nile red droplet at a flow rate of 325 and 235 μl/hr, respectively, the two droplet trains was successfully synchronized and introduced to the droplet merging chamber (Figure 32C).

In the droplet merging chamber, around 30 to 40% of droplet merging efficiency was observed between synchronized two droplets (microalgae solution and Nile red solution) even without applying the electric field, probably resulting from DMSO in Nile red droplet. When synchronized droplets entered the merging chamber, the electric field was formed using a function generator (DG4102, Rigol Technologies Inc., OH) to

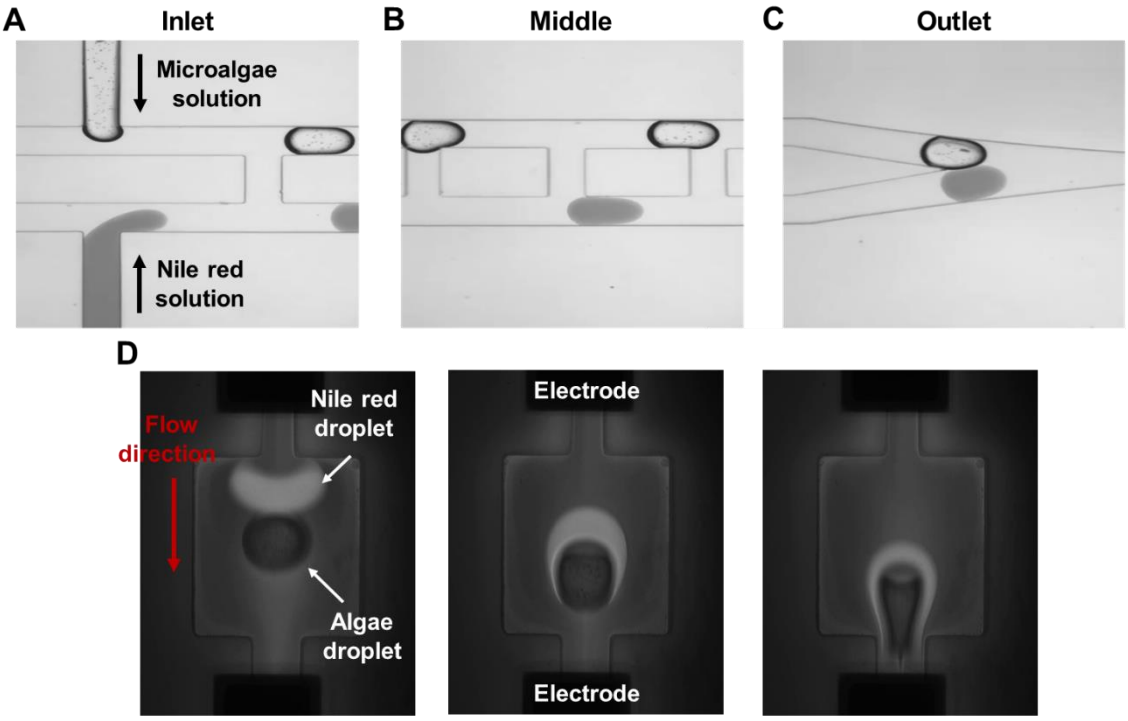

Figure 32. Micrographs showing on-chip droplet generation, synchronization, and merging in the developed platform. (A) Inlet of the railroad-like structure where droplets were generated through the T-junction droplet generator. (B) Middle of the railroad-like structure. (C) Outlet of the railroad-like structure where synchronization of two droplets were achieved. (D) Time-lapse micrographs showing on-chip Nile red lipid staining. Synchronized droplets (algae-containing droplet and Nile red solution droplet) were merged into a single droplet by applying electric field in which algae inside the droplet were exposed to Nile red solution.

generate a .1 V to 1 V square wave (10 kHz) that was amplified with a high voltage amplifier (2210-CE, TREK, Inc., NY) producing a 100 V to 1000 V AC signal. Due to this effect of DMSO, around 95% of one-to-one droplet merging efficiency was achieved at lower voltage (150 ~ 250 V) (Figure 32D). Sometimes, more than two droplets were merged together, or only one droplet passed by the merging chamber, which were included in the remaining 5%.

4.6. On-chip droplet rinsing

Nile red molecules for staining oil bodies in microalgae started to diffuse into and stain the surrounding carrier oil right after the droplets were created in the on-chip staining region (Figure 32C). This stained oil formed severe background noise, and made it challenging to examine oil production through fluorescence microscopy. Also this stained carrier oil eventually stained the PDMS platform where this platform cannot be utilized any more. To resolve this issue, the droplet rinsing chamber integrated with a 3° angled micropost array was designed where Nile red stained droplets could be transferred from stained oil flow to fresh oil flow, which would remove the background noise as well as excessive Nile red molecules in the stained droplets (Figure 33A)[152, 154].

The rinsing effect was characterized by changing the combinations of flow rates between stained oil and fresh oil, followed by conducting image analysis (light intensity profile measurement, Image J software) to confirm that no Nile red molecules were diffused into the fresh oil. Three different flow rates (225, 452, and 562 μl/hr) of stained oil were selected, each indicating a slow rinsing speed (225 μl/hr), a rinsing speed with

the droplet incubation after staining (no microalgae & Nile red solution flow, only oil flow, 272 + 180 = 452 μl/hr), and a rinsing speed without incubation step for high-throughput analysis (all solution flow including microalga, Nile red, and oil, 55+ 55 + 272 + 180 = 562 μl/hr). The 4 different ratios between the stained oil flow and the fresh oil flow were compared, that is, 1 : 2, 1 : 2.5, 1 : 3, 1 : 3.5, and 1 : 4. For example, when a flow rate of 452 μl/hr was used for stained oil flow, flow rates of 904, 1130, 1356, 1582, and 1800 μl/hr were used for fresh oil.

Regardless of flow rates used for the stained oil, the stained carrier oil was completely removed and Nile red stained droplets were successfully guided into the fresh oil, if more than 3 times higher flow rate was used for the fresh oil flow compared to the stained carrier oil flow (Figure 33B). The profile of Nile red fluorescence intensity measurement along the droplet rinsing chamber (the ratio of flow rates between stained and fresh oil = 1 : 3) also showed the complete rinsing of the stained oil, where no Nile red fluorescence signal was detected at the outlet of the chamber (Figure 33C). The effect of this rinsing process is also shown in Figure 33D where no background noise was observed after the droplet rinsing process while severe background fluorescence signal was found without this step.

4.7. Characterization of on-chip staining for oil analysis

The capability of oil analysis in the platform was characterized through the on-chip Nile red staining of N-starved *C. reinhartii* cells. Droplets containing 64 N-starved *C. reinhartii* cells were utilized here to represent droplets after 2 days of culture,

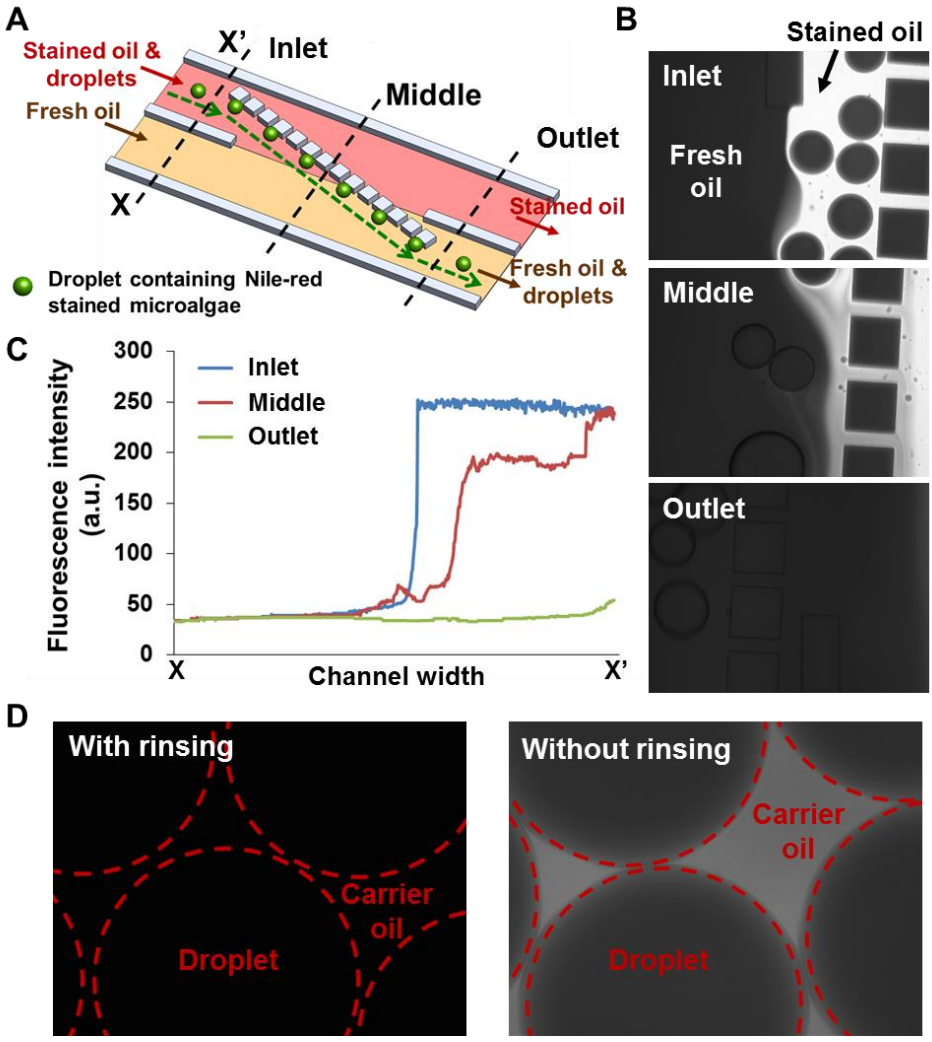

Figure 33. Characterization of the droplet rinsing process. (A) Enlarged schematic of the droplet rinsing chamber. (B) Microscopic images showing the rinsing of stained oil through the rinsing chamber – at the inlet, the middle, and the outlet of the chamber. (C) Intensity profile through the rinsing chamber, which shows the rinsing of stained oil with fresh oil. (D) Droplets collected at the observation chamber showing the effect of rinsing process.

which would be the required time for comparison among different microalgal strains or mutants, considering that doubling time of *C. reinhartii* inside droplets are 8 hours. To validate the on-chip oil staining capability of the platform, oil bodies in *C. reinhartii* cells were stained and measured by changing the concentrations of Nile red solution (1, 5, 10, 25, and 100 μg/ml in DMSO) as well as incubation time (0, 3, 6, and 10 minutes), and were compared with off-chip Nile red stained samples. For off-chip staining, 100 μl of *C. reinhartii* cells suspended media were treated with 20 μl of Nile red dissolved in DMSO (25 μg/ml) for 10 minutes, where the actual concentrations of Nile red and DMSO were 5 μg/ml and 20%, respectively. The efficiency of on-chip Nile red staining was confirmed by measuring the Nile red fluorescence intensity per unit area in *C. reinhartii* oil bodies, and then comparing this value to that obtained from off-chip stained samples. Microscopy for Nile red fluorescence (excitation: 460 – 500 nm, emission: 560 – 600 nm) and chlorophyll autofluorescence (excitation: 460 – 500 nm, emission > 610 nm) were conducted using a Zeiss Axio Observer Z1 microscope (Carl Zeiss Micro Imaging, LLC) equipped with a digital camera (Orca Flash2.8 CMOS Camera), and all microscopic images were analyzed with the Image J software.

Figure 34A shows example images of N-starved *C. reinhartii* cells stained through the on-chip Nile red staining process, and variations in fluorescence intensity could be observed depending on different concentrations of Nile red solution and incubation time used. At a concentration of 1 μg/ml, Nile red fluorescence intensity of *C. reinhartii* was lower than the control (stained through the off-chip staining protocol), where less than 92% staining efficiency was obtained (Figure 34B). With the Nile red

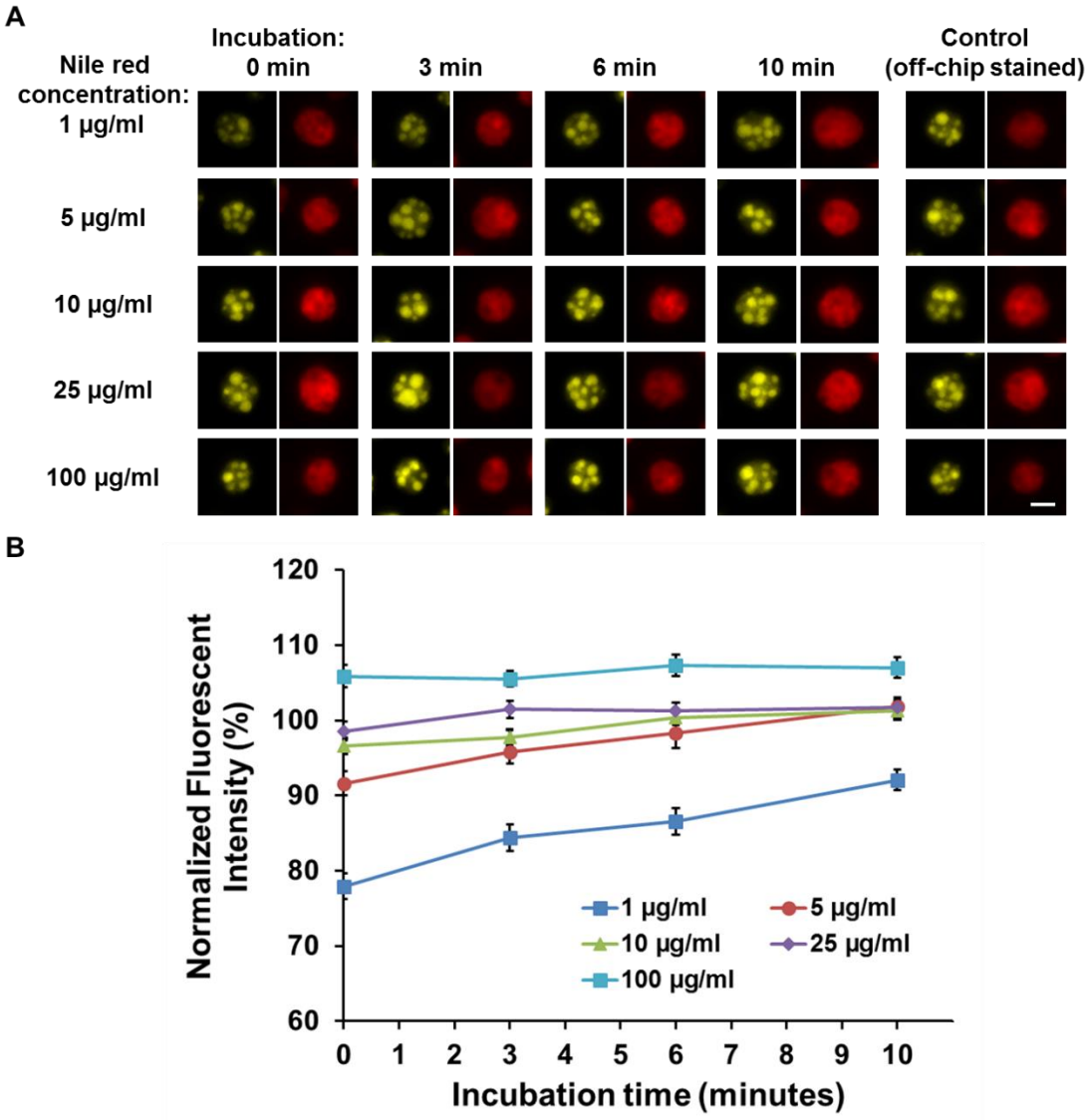

Figure 34. Characterization of on-chip Nile red staining process. (A) Nile red stained *C. reinhartii* cells (yellow) showing different fluorescence intensities of oil bodies inside when using different Nile red concentrations and incubation time. Red color indicates chlorophyll autofluorescence of stained *C. reinhartii* cells (B) Analysis of average fluorescence intensities of oil bodies stained with different concentrations of Nile red dye and incubation time (n = 100). Scale bar = 5 µm.

solution having a concentration of 5 μg/ml, more than 95% staining efficiency was observed at an incubation time of 3 and over, comparable to the off-chip staining (Figure 34B). Nile red concentrations higher than 10 μg/ml led to the comparable staining result against the off-chip staining regardless of the incubation time, where all staining efficiencies were more than 95% even under no incubation condition (Figure 34B). This implies the capability of analyzing oil content even without the incubation step, which will allow more number of droplets to be examined within the same screening time.

4.8. Oil quantification of colonial forming microalga, *B. braunii*

To exhibit the applicability of the on-chip Nile red staining function toward other microalgae, colony-forming microalga *B. bruanii* was selected and analyzed. The oil content in *B. braunii* colonies were stained and measured through on-chip Nile red staining, and were compared with off-chip Nile red stained samples. Optimized concentration of Nile red solution and staining time for the on-chip staining was found experimentally. For off-chip staining, 100 μl of *B. braunii* colonies suspended media were treated with 20 μl of Nile red dissolved in DMSO (25 μg/ml) for 20 minutes, where the actual concentrations of Nile red and DMSO were 5 μg/ml and 20%, respectively. The efficiency of on-chip Nile red staining was confirmed by measuring the Nile red fluorescence intensity per unit area in *B. braunii*, and then comparing this value to that obtained from off-chip stained samples. On-chip stained *B. braunii* colonies were also collected to an outlet reservoir for further analysis, where the collected samples were squeezed between glass slides in order for examining whether oil content inside

individual cells as well as in the extracellular matrix was sufficiently stained. All microscopic images were taken using a Zeiss Axio Observer Z1 microscope (Carl Zeiss Micro Imaging, LLC) equipped with a digital camera (Orca Flash2.8 CMOS Camera) and filter sets (Nile red – excitation: 450 – 490 nm, emission: 500 – 550 nm, chlorophyll autofluorescence – same as described above) and were analyzed with the Image J software.

B. braunii colonies used in the platform are typically composed of 100 – 200 individual cells, and have significantly higher oil amount compared to other microalgae. Individual cells in the colony are held together by an extracellular matrix in which 90 – 95% of oil amount is stored while the rest is found inside cells. Due to larger numbers of cells as well as higher amount of oil to be stained compared to previous *C. reinhartii* staining, higher concentration of Nile red solution and longer incubation time were required. Among various conditions tested, 1000 μg/ml in DMSO of Nile red concentration and 20 min of incubation time were selected and used throughout the experiment with *B. braunii*. As shown in Figure 35A, same level of Nile red staining was achieved in B. braunii through the on-chip Nile red staining compared to off-chip stained samples (control). Also, the staining of oil bodies in individual *B. braunii* cells were verified by collecting on-chip stained droplets between glass slides and then squeezing them (Figure 35B).

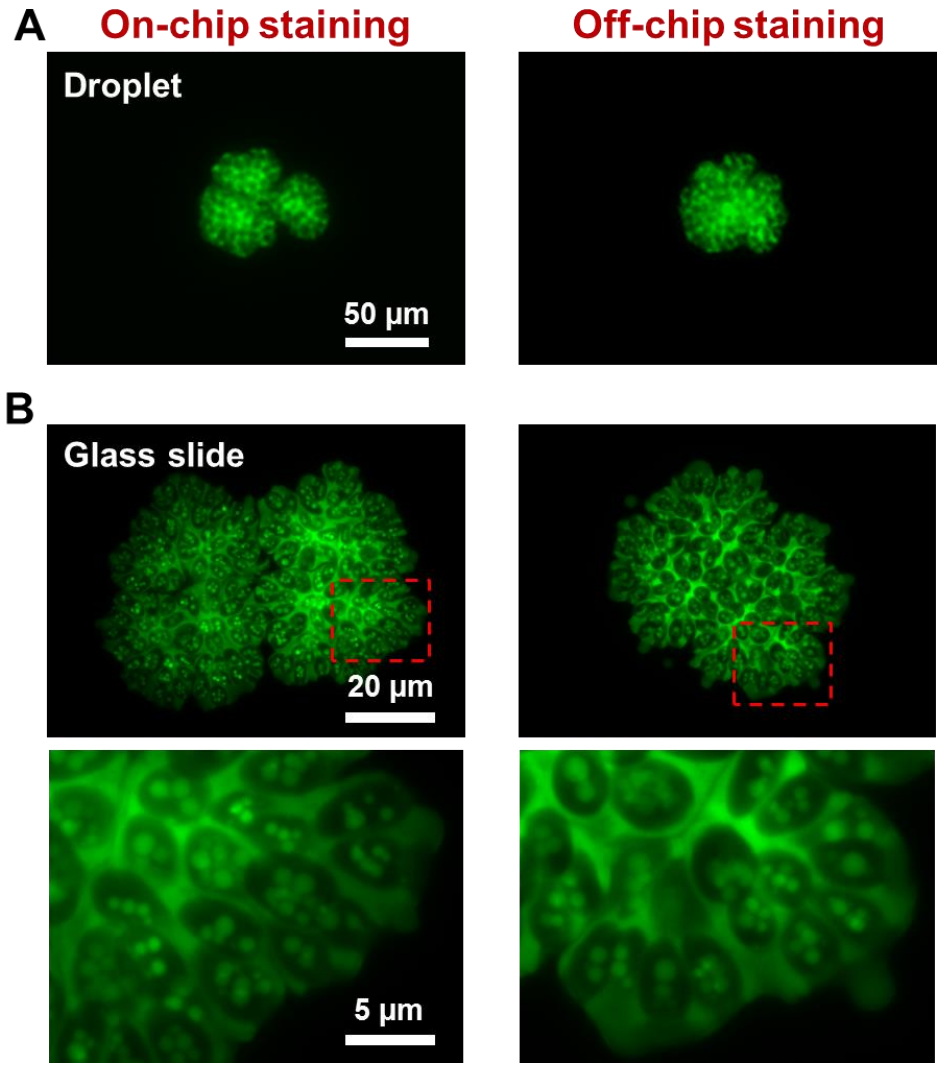

Figure 35. Microscopic images showing the comparison of on-chip Nile red stained and off-chip Nile red stained *B. braunii*. (A) Observation inside droplets. (B) Observation between glass slides to verify the staining of oil bodies inside individual *B. braunii* cells.

4.9. Analysis of growth and oil accumulation in *C. reinhartii* under different culture conditions

To demonstrate the screening functionality of the developed platform, growth and oil accumulation of *C. reinhardtii* cells under two different culture media conditions (N-replete condition: 100% nitrogen (TAP media), N-deplete condition: 0% nitrogen (TAP-N media)) were monitored over time and compared each other. Droplets containing a single *C. reinhardtii* cell suspended in N-replete and N-deplete conditions were generated by preparing each sample solution with a density of 1.38 x 10^5 cells/ml in TAP and TAP-N media, respectively. Both cultures were carried out for 6 days under a light intensity of 80 μmol photons·m^{-2}·s^{-1} with a 12 hour light-dark cycle. Tracking the same droplets stored in the culture chamber allowed time-course growth analysis, where growth of *C. reinhardtii* was characterized by counting the number of cells inside droplets based on its chlorophyll autofluorescence. In addition, oil accumulation in *C. reinhardtii* cells was analyzed over time, which was estimated by measuring the fluorescence intensity per unit area in *C. reinhardtii* through sequential processes of on-chip Nile red staining, fluorescence microscopy, and image analysis (described in 'Characterization of on-chip staining for oil analysis' section).

Figure 36A showed the time-lapse microscopy where different growth rates of *C. reinhardtii* cells resulted from the two different culture conditions. In the N-replete condition, the average number of cells inside droplets increased up to 3 days of culture (day 3), and then the growth slowed down and started to saturate (Figure 36A-B). 8 – 12 hours of doubling time was observed between day 0 and day 3, which matches well with

previous studies. In the N-deplete condition, the increase in cell population inside droplets was observed during the first day of culture (day 1), but then these cell populations stopped to grow, resulting from the lack of nutrient (N source) in the culture condition (Figure 36A-B).

Time-course analysis of Nile red stained *C. reinhardtii* cells also showed differences in oil accumulation under two different culture environments (Figure 37A-B). Oil accumulation became higher as *C. reinhardtii* cells were exposed more to nutrient (N source) starvation condition (Figure 37B), while no oil was accumulated in N-replete condition (Figure 37A). Maximum increase of oil accumulation in the N-deplete condition was reached after 4 days of culture, followed by a subsequent decline at day 5 and day 6 (Figure 37C). This trend showing the oil accumulation inside droplets corresponds well with a recent report where maximum oil accumulation was studied 3 – 4 days after N starvation. Compared to *C. reinhardtii* cells in cultured N-replete condition, an increase in cell size (in other words, cell volume) was observed from the cells in N-deplete condition (Figure 37B), which would also be as a consequence of N starvation. Successful analysis of both growth and oil accumulation in *C. reinhardtii* cells demonstrates the capability of the developed droplet screening platform to be utilized as a high-throughput screening tool for microalgal strain studies.

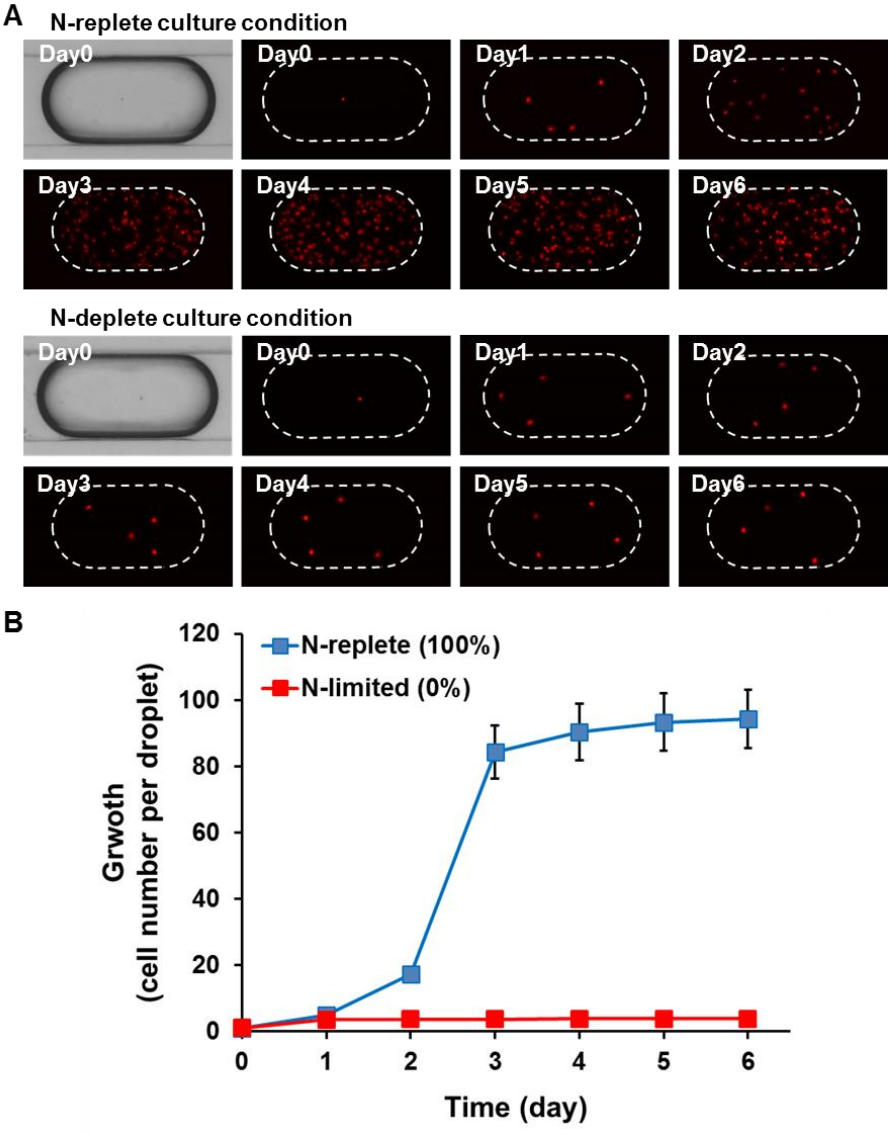

Figure 36. Growth analysis of *C. reinhartii* cells under different culture conditions (N-replete and N-limited environment). (A) Time-lapse microscopy showing different growth of *C. reinhartii* cells under N-replete and N-limited culture conditions. (B) Average number of *C. reinhartii* cells inside droplet analyzed for 6 days of culture under N-replete and N-limited conditions.

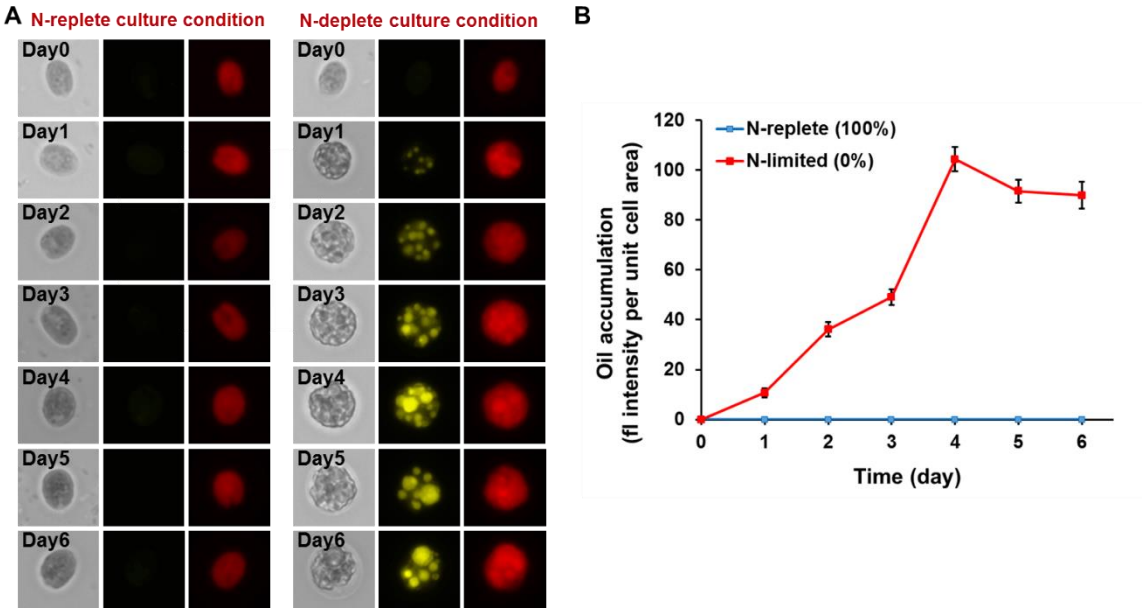

Figure 37. Analysis of oil accumulation in *C. reinhartii* cells under different culture conditions (N-replete and N-limited environment). (A) Time-lapse microscopy showing different oil accumulation of *C. reinhartii* cells under N-replete and N-limited culture conditions. (B) Average fluorescence intensity of Nile red stained *C. reinhartii* cells inside droplet analyzed for 6 days of culture under N-replete and N-limited conditions.

4.10. Automated high-throughput analysis of droplets

Although the developed droplet microfluidics-based screening platform has the capability of analyzing microalgal growth and oil production at high-throughput, these analysis methods were mainly based on fluorescence microscopy, which required relatively long analysis time, and thus limited the throughput as well. In order to reduce the analysis time and to further increase the throughput, a separate optical detection system was integrated into the previous droplet microfluidics-based screening platform. As shown in Figure 38, biomass and oil amount in microalgae can be quantified by measuring the intensity of autofluorescence from chlorophyll and emitting light from the on-chip Nile red staining. In addition, the droplet sorting schemes will be combined into this droplet-based screening platform, where all screening procedure from droplet formation with a single microalga to growth and oil analysis, followed by selective sorting can be conducted all together (Figure 38). In order to selectively retrieve particular droplets out of large numbers of samples, two different droplet sorting schemes were designed and their functionalities were tested (Figure 39). Droplets of interest (*e.g.,* higher miroalgal growth or oil accumulation) can be selectively collected for further analysis by applying a pneumatic actuation or an electric field, which moved particular droplets to a collection chamber while others flowed into a waste chamber.

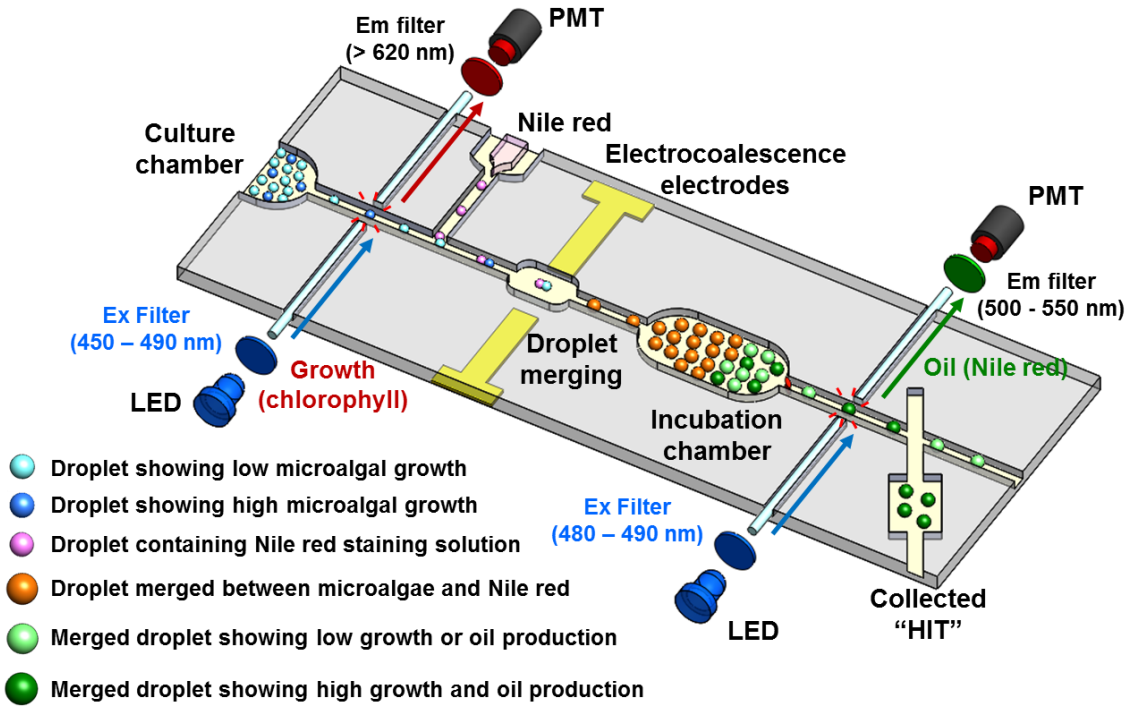

Figure 38. Illustration of the high-throughput droplet microfluidics-based microalgae screening platform for analyzing microalgal growth and oil production through the integrated optical detection system. Growth (biomass) can be analyzed by measuring microalgal chlorophyll autofluorescence intensity and oil amount can be quantified by evaluating Nile red fluorescence signal after on-chip staining process. Droplet sorting scheme is integrated at the downstream of the platform where droplets of interest can be collected for further analysis.

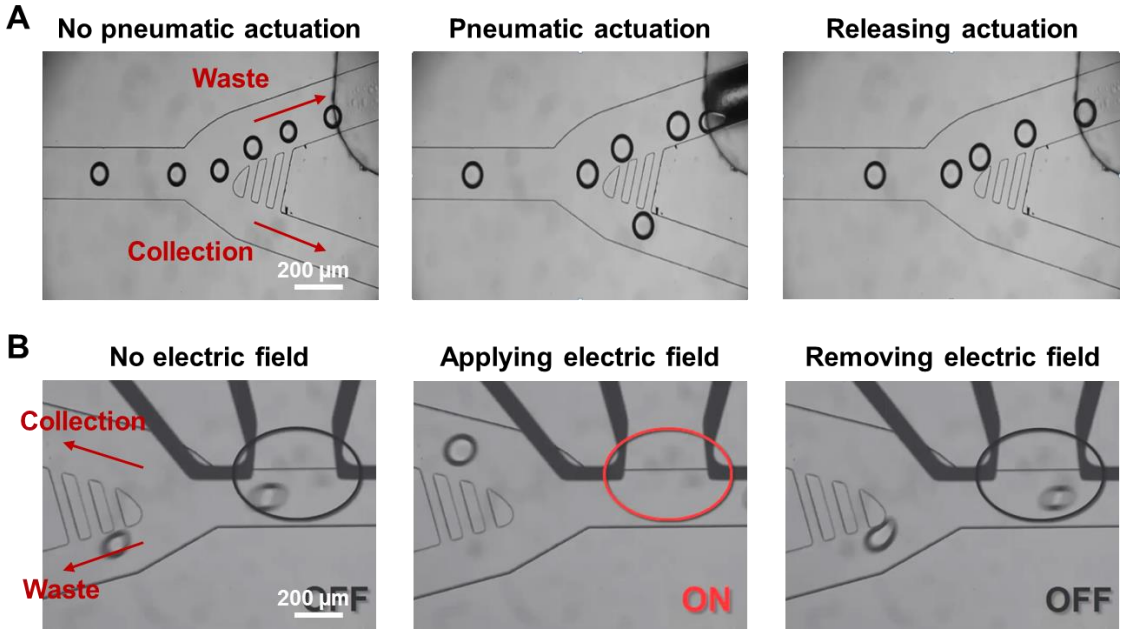

Figure 39. On-chip droplet sorting scheme. (A) Pneumatic actuation: droplets can selectively sorted at a collection chamber when pneumatic pressure is applied. (B) Electric field actuation: droplets can selectively extracted to a collection chamber when only electric field is applied.

4.11. Conclusion

A high-throughput droplet microfluidics-based microalgae screening platform was developed to investigate growth and oil production of numerous microalgal strains. Compared to the previously developed systems such as the growth condition screening photobioreactor array and the single-cell screening and selection platform, this platform has the capability of conducting the screening assay with much higher throughput (two or three orders higher), where large numbers of microalgae samples can be screened with much reduced time. Microalgal growth was characterized by creating the independent bioreactors through the droplet generation, which allowed for isolating a single microalga as well as monitoring its behavior over time. Oil production in microalgae was quantified through the on-chip Nile red staining, the key features of the developed platform, followed by the droplet rinsing process. The capability of on-chip staining for various microalgal strains was successfully validated using the unicellular microalga *C. reinhartii* and the colonial microalga *B. braunii*. Also, growth and oil accumulation of *C. reinhartii* under different culture conditions were successfully analyzed and compared, demonstrating the screening capability of the platform. Optical detection system as well as droplet sorting scheme have been developed, and the integration with these components will further improve the throughput and screening capability of the droplet-based platform. We expect that this system will serve as a powerful high-throughput analysis and screening tool to investigate large numbers of algal strains at significantly lower costs and reduced time.

CHAPTER V

CONCLUSIONS AND FUTURE WORK

5.1. Conclusions

In this study, various high-throughput microfluidic microalgae screening platforms have been developed, which provided the capabilities of investigating microalgal growth and oil production under different culture conditions or among large numbers of microalgal library.

As a growth condition screening platform, the high-throughput microfluidic photobioreactor array was developed and successfully utilized to investigate how different culture conditions (light intensity, light cycle, and culture media/chemical composition) influence microalgal growth and oil production with single cell/colony resolution. Through characterization of *B. braunii* colonies using the developed platform, the light condition showing 1.8-fold higher oil production compared to conditions typically used in conventional cultures was successfully identified. Also, screening was achieved with less cost (850 times less reagent consumption) and much higher throughput (250 times higher).

As a microalgal library screening platform, the high-throughput microfluidic single-cell screening and selection platform was developed, capable of capturing, culturing, and analyzing microalgae with single-cell resolution, followed by selectively extracting particular microalgae showing desired traits (faster growth or higher oil production) off-chip for further study. Two microfluidic control layers regulated by a

binary demultiplexer scheme and a microfluidic OR logic gate enabled independent control of the opening and closing of each of 1024 trapping sites with a much reduced complexity. Growth and oil accumulation of unicellular microalga *C. reinhardtii* was successfully examined using the platform, and the capability of selective cell extraction of the platform was also demonstrated by retrieving *C. reinhardtii* cells from particular trapping sites.

The high-throughput droplet microfluidics-based microalgae screening platform with the capabilities of investigating the growth and the oil production of numerous microalgal library was developed. This droplet-based platform can carry out the screening assay with much higher throughput (two or three orders higher) compared to the first and second microfluidic screening platforms. Large numbers of independent bioreactors were easily created by encapsulating a single microalga into a droplet within a short period of time. Oil content in microalgae was characterized through the on-chip staining process, where oil bodies in microalgae were stained and measured through Nile red treatment. Growth and oil accumulation of *C. reinhardtii* cells under different culture conditions (N-replete and N-limited conditions) were successfully analyzed and compared, demonstrating the capability of the platform as a high-throughput screening tool.

These developed microfluidic microalgae screening platforms will be utilized as a powerful high-throughput analysis and screening tool to investigate growth and oil production among large numbers of microalgal strains as well as to optimize culture conditions against microalgal strains of interest, all at significantly lower cost and

shorter time, which can dramatically accelerate the development of renewable microalgal energy systems.

5.2. Future work

Various microfluidic microalgae screening platforms were successfully developed and utilized to examine microalgal growth and oil production under different culture conditions or among different microalgal strains. Following are some suggestions for future studies with the microfluidic microalgae screening platforms.

5.2.1. Platform design and system operation

The high-throughput droplet microfluidics-based microalgae screening platform needs to be further developed. First, separate optical detection system, currently under development, will be characterized and integrated with current droplet-based screening platform, where biomass and oil amount can be quantified by measuring the intensity of autofluorescence from chlorophyll and emitting light from the on-chip Nile red staining. In addition, the droplet sorting schemes will be combined into the droplet-based screening platform, where all screening procedure from droplet formation with a single microalga to growth and oil analysis, followed by selective sorting can be conducted. In the growth condition screening photobioreactor array, the bottom microalgal culture layer will be modified to conduct droplet-based microaglae cultivation, and this will be

combined with the current dynamic light controller array module to investigate growth and oil production under various light conditions.

5.2.2. Microalgae screening

Large numbers of *C. reinhardtii* mutants will be created using transformation or EMS/UV mutation in order to acquire strains showing increased oil production or faster growth rate. The droplet microfluidics-based screening platform will be used to investigate this *C. reinhardtii* mutant library. The traditional mutant screening based on plating cells and analyzing colonies will be conducted in parallel with the droplet microfluidics-based screening. Once a few *C. reinhardtii* transgenic lines are identified through this screening, those strains will be grown in flask-scale or large-scale cultures, followed by analyzing their properties (*e.g.,* growth and oil production) to confirm whether these properties can be maintained over the passage. To identify optimal culture conditions for improved growth and oil production, the modified photobioreactor array, which has the bottom droplet-based culture layer will be utilized by altering light intensities as well as light cycles in a combinatorial manner. Different nutrient composition will also be tested, for example, growth and oil production under various levels of nitrogen and acetate in the culture media. Once the optimal growth conditions are investigated, these conditions will be applied to flask-scale or large-scale cultures, and the correlation between the microfluidic photobioreactor array and these cultures will be examined to confirm whether the screening results from the microfluidic screening platform can be translated to large-scale cultures.

REFERENCES

1. BP Statistical Review of World Energy June 2014.

2. Brennan, L. & Owende, P. Biofuels from microalgae - a review of technologies for production, processing, and extractions of biofuels and co-products. *Renewable and Sustainable Energy Reviews* **14**, 557-577 (2010).

3. Hu, Q. et al. Microalgal triacylglycerols as feedstocks for biofuel production: perspectives and advances. *The Plant Journal* **54**, 621-639 (2008).

4. Li, Y., Horsman, M., Wu, N., Lan, C.Q. & Dubois Calero, N. Biofuels from microalgae. *Biotechnology Progress* **24**, 815-820 (2008).

5. Georgianna, D.R. & Mayfield, S.P. Exploiting diversity and synthetic biology for the production of algal biofuels. *Nature* **488**, 329-335 (2012).

6. Chisti, Y. Biodiesel from microalgae. *Biotechnology Advances* **25**, 294-306 (2007).

7. Chisti, Y. Biodiesel from microalgae beats bioethanol. *Trends in Biotechnology* **26**, 126-131 (2008).

8. Mata, T.M., Martins, A.A. & Caetano, N.S. Microalgae for biodiesel production and other applications: a review. *Renewable and Sustainable Energy Reviews* **14**, 217-232 (2010).

9. Scott, S.A. et al. Biodiesel from algae: challenges and prospects. *Current Opinion in Biotechnology* **21**, 277-286 (2010).

10. Sharma, Y.C., Singh, B. & Korstad, J. A critical review on recent methods used for economically viable and eco-friendly development of microalgae as a potential feedstock for synthesis of biodiesel. *Green Chemistry* **13**, 2993 (2011).

11. Bilanovic, D., Andargatchew, A., Kroeger, T. & Shelef, G. Freshwater and marine microalgae sequestering of CO2 at different C and N concentrations-response surface methodology analysis. *Energy Conversion and Management* **50**, 262-267 (2009).

12. Schenk, P.M. et al. Second generation biofuels: high-efficiency microalgae for biodiesel production. *Bioenergy Research* **1**, 20-43 (2008).

13. Gouveia, L. & Oliveira, A.C. Microalgae as a raw material for biofuels production. *Journal of Industrial Microbiology and Biotechnology* **36**, 269-274 (2009).

14. Miao, X. & Wu, Q. Biodiesel production from heterotrophic microalgal oil. *Bioresource Technology* **97**, 841-846 (2006).

15. Spolaore, P., Joannis-Cassan, C., Duran, E. & Isambert, A. Commercial applications of microalgae. *Journal of Bioscience and Bioengineering* **101**, 87-96 (2006).

16. de Morais, M.G. & Costa, J.A. Carbon dioxide fixation by Chlorella kessleri, C. vulgaris, Scenedesmus obliquus and Spirulina sp. cultivated in flasks and vertical tubular photobioreactors. *Biotechnology Letters* **29**, 1349-1352 (2007).

17. Ugwu, C.U., Aoyagi, H. & Uchiyama, H. Photobioreactors for mass cultivation of algae. *Bioresource Technology* **99**, 4021-4028 (2008).

18. Demirbas, A. Progress and recent trends in biodiesel fuels. *Energy Conversion and Management* **50**, 14-34 (2009).

19. Renaud, S.M., Thinh, L.-V. & Parry, D.L. The gross chemical composition and fatty acid composition of 18 species of tropical Australian microalgae for possible use in mariculture. *Aquaculture* **170**, 147-159 (1999).

20. Minowa, T., Yokoyama, S.-y., Kishimoto, M. & Okakura, T. Oil production from algal cells of Dunaliella tertiolecta by direct thermochemical liquefaction. *Fuel* **74**, 1735-1738 (1995).

21. Eriksen, N.T. The technology of microalgal culturing. *Biotechnology Letters* **30**, 1525-1536 (2008).

22. Gouveia, L. & Oliveira, A.C. Microalgae as a raw material for biofuels production. *Journal of Industrial Microbiology and Biotechnology* **36**, 269-274 (2009).

23. Callaway, J. Hempseed as a nutritional resource: an overview. *Euphytica* **140**, 65-72 (2004).

24. Reijnders, L. & Huijbregts, M. Biogenic greenhouse gas emissions linked to the life cycles of biodiesel derived from European rapeseed and Brazilian soybeans. *Journal of Cleaner Production* **16**, 1943-1948 (2008).

25. Peterson, C.L. & Hustrulid, T. Carbon cycle for rapeseed oil biodiesel fuels. *Biomass and Bioenergy* **14**, 91-101 (1998).

26. Dismukes, G.C., Carrieri, D., Bennette, N., Ananyev, G.M. & Posewitz, M.C. Aquatic phototrophs: efficient alternatives to land-based crops for biofuels. *Current Opinion in Biotechnology* **19**, 235-240 (2008).

27. Searchinger, T. et al. Use of US croplands for biofuels increases greenhouse gases through emissions from land-use change. *Science* **319**, 1238 (2008).

28. Pulz, O. Photobioreactors: production systems for phototrophic microorganisms. *Applied Microbiology and Biotechnology* **57**, 287-293 (2001).

29. Kim, H.S., Weiss, T.L., Thapa, H.R., Devarenne, T.P. & Han, A. A microfluidic photobioreactor array demonstrating high-throughput screening for microalgal oil production. *Lab on a Chip* **14**, 1415-1425 (2014).

30. Tourovskaia, A., Figueroa-Masot, X. & Folch, A. Differentiation-on-a-chip: a microfluidic platform for long-term cell culture studies. *Lab on a Chip* **5**, 14-19 (2005).

31. Andersson, H. & van den Berg, A. Microfluidic devices for cellomics: a review. *Sensors and Actuators B: Chemical* **92**, 315-325 (2003).

32. Nevill, J.T., Cooper, R., Dueck, M. & Breslauer, D.N. Integrated microfluidic cell culture and lysis on a chip. *Lab on a Chip* **7**, 1689-1695 (2007).

33. Hung, P.J. et al. A novel high aspect ratio microfluidic design to provide a stable and uniform microenvironment for cell growth in a high throughput mammalian cell culture array. *Lab on a Chip* **5**, 44-48 (2005).

34. Shackman, J.G., Dahlgren, G.M., Peters, J.L. & Kennedy, R.T. Perfusion and chemical monitoring of living cells on a microfluidic chip. *Lab on a Chip* **5**, 56-63 (2005).

35. Hong, J.W., Chen, Y., Anderson, W.F. & Quake, S.R. Molecular biology on a microfluidic chip. *Journal of Physics: Condensed Matter* **18**, S691-S701 (2006).

36. Zhang, Z. et al. Microchemostat-microbial continuous culture in a polymer-based, instrumented microbioreactor. *Lab on a Chip* **6**, 906-913 (2006).

37. Campbell, K. & Groisman, A. Generation of complex concentration profiles in microchannels in a logarithmically small number of steps. *Lab on a Chip* **7**, 264-272 (2007).

38. Figallo, E. et al. Micro-bioreactor array for controlling cellular microenvironments. *Lab on a Chip* **7**, 710-719 (2007).

39. Ingham, C.J. et al. The micro-Petri dish, a million-well growth chip for the culture and high-throughput screening of microorganisms. *Proceedings of the National Academy of Sciences of the United States of America* **104**, 18217-18222 (2007).

40. Nevill, J.T., Cooper, R., Dueck, M., Breslauer, D.N. & Lee, L.P. Integrated microfluidic cell culture and lysis on a chip. *Lab on a Chip* **7**, 1689-1695 (2007).

41. Walker, G.M., Monteiro-Riviere, N., Rouse, J. & O'Neill, A.T. A linear dilution microfluidic device for cytotoxicity assays. *Lab on a Chip* **7**, 226-232 (2007).

42. Weibel, D.B., Diluzio, W.R. & Whitesides, G.M. Microfabrication meets microbiology. *Nature reviews. Microbiology* **5**, 209-218 (2007).

43. Bennett, M.R. et al. Metabolic gene regulation in a dynamically changing environment. *Nature* **454**, 1119-1122 (2008).

44. Dertinger, S.K., Chiu, D.T., Jeon, N.L. & Whitesides, G.M. Generation of gradients having complex shapes using microfluidic networks. *Analytical Chemistry* **73**, 1240-1246 (2001).

45. Chen, C.S., Jiang, X. & Whitesides, G.M. Microengineering the environment of mammalian cells in culture. *Mrs Bulletin* **30**, 194-201 (2005).

46. Whitesides, G.M. What comes next? *Lab on a Chip* **11**, 191-193 (2011).

47. Salieb-Beugelaar, G.B., Simone, G., Arora, A., Philippi, A. & Manz, A. Latest developments in microfluidic cell biology and analysis systems. *Analytical Chemistry* **82**, 4848-4864 (2010).

48. Mark, D., Haeberle, S., Roth, G., von Stetten, F. & Zengerle, R. Microfluidic lab-on-a-chip platforms: requirements, characteristics and applications. *Chemical Society Reviews* **39**, 1153-1182 (2010).

49. Yin, H. & Marshall, D. Microfluidics for single cell analysis. *Current Opinion in Biotechnology* **23**, 110-119 (2012).

50. Lindstrom, S. & Andersson-Svahn, H. Overview of single-cell analyses: microdevices and applications. *Lab on a Chip* **10**, 3363-3372 (2010).

51. Lecault, V., White, A.K., Singhal, A. & Hansen, C.L. Microfluidic single cell analysis: from promise to practice. *Current Opinion in Chemical Biology* **16**, 381-390 (2012).

52. Teh, S.Y., Lin, R., Hung, L.H. & Lee, A.P. Droplet microfluidics. *Lab on a Chip* **8**, 198-220 (2008).

53. Lagus, T.P. & Edd, J.F. A review of the theory, methods and recent applications of high-throughput single-cell droplet microfluidics. *Journal of Physics D: Applied Physics* **46**, 114005 (2013).

54. Han, A., Hou, H., Li, L., Kim, H.S. & de Figueiredo, P. Microfabricated devices in microbial bioenergy sciences. *Trends in Biotechnology* **31**, 225-232 (2013).

55. Han, A., Yang, L. & Frazier, A.B. Quantification of the heterogeneity in breast cancer cell lines using whole-cell impedance spectroscopy. *Clinical Cancer Research* **13**, 139 (2007).

56. Cho, Y. et al. Whole-cell impedance analysis for highly and poorly metastatic cancer cells. *Microelectromechanical Systems, Journal of* **18**, 808-817 (2009).

57. Sorokin, C. & Krauss, R.W. The effects of light intensity on the growth rates of green algae. *Plant Physiology* **33**, 109 (1958).

58. Foy, R., Gibson, C. & Smith, R. The influence of daylength, light intensity and temperature on the growth rates of planktonic blue-green algae. *British Phycological Journal* **11**, 151-163 (1976).

59. Meseck, S.L., Alix, J.H. & Wikfors, G.H. Photoperiod and light intensity effects on growth and utilization of nutrients by the aquaculture feed microalga, *Tetraselmis chui* (PLY429). *Aquaculture* **246**, 393-404 (2005).

60. Banerjee, A., Sharma, R., Chisti, Y. & Banerjee, U. Botryococcus braunii: a renewable source of hydrocarbons and other chemicals. *Critical Reviews in Biotechnology* **22**, 245-279 (2002).

61. Metzger, P. & Largeau, C. Botryococcus braunii: a rich source for hydrocarbons and related ether lipids. *Applied Microbiology and Biotechnology* **66**, 486-496 (2005).

62. Li, Y. & Qin, J.G. Comparison of growth and lipid content in three Botryococcus braunii strains. *Journal of Applied Phycology* **17**, 551-556 (2005).

63. Yeesang, C. & Cheirsilp, B. Effect of nitrogen, salt, and iron content in the growth medium and light intensity on lipid production by microalgae isolated from freshwater sources in Thailand. *Bioresource Technology* **102**, 3034-3040 (2011).

64. Weiss, T.L. et al. Raman spectroscopy analysis of botryococcene hydrocarbons from the green microalga Botryococcus braunii. *Journal of Biological Chemistry* **285**, 32458-32466 (2010).

65. Weiss, T.L. et al. Colony organization in the green alga Botryococcus braunii (Race B) is specified by a complex extracellular matrix. *Eukaryotic cell* **11**, 1424-1440 (2012).

66. Okada, S., Devarenne, T.P., Murakami, M., Abe, H. & Chappell, J. Characterization of botryococcene synthase enzyme activity, a squalene synthase-like activity from the green microalga Botryococcus braunii, Race B. *Archives of Biochemistry and Biophysics* **422**, 110-118 (2004).

67. Yoshimura, T., Okada, S. & Honda, M. Culture of the hydrocarbon producing microalga Botryococcus braunii strain Showa: optimal CO2, salinity, temperature, and irradiance conditions. *Bioresource Technology* **133**, 232-239 (2013).

68. Hashemi, N., Erickson, J.S., Golden, J.P. & Ligler, F.S. Optofluidic characterization of marine algae using a microflow cytometer. *Biomicrofluidics* **5**, 32009-320099 (2011).

69. Schaap, A., Bellouard, Y. & Rohrlack, T. Optofluidic lab-on-a-chip for rapid algae population screening. *Biomedical Optics Express* **2**, 658-664 (2011).

70. Schaap, A., Rohrlack, T. & Bellouard, Y. Optical classification of algae species with a glass lab-on-a-chip. *Lab on a Chip* **12**, 1527-1532 (2012).

71. Erickson, R.A. & Jimenez, R. Microfluidic cytometer for high-throughput measurement of photosynthetic characteristics and lipid accumulation in individual algal cells. *Lab on a Chip* **13**, 2893-2901 (2013).

72. Lee, D.H., Bae, C.Y., Han, J.I. & Park, J.K. In situ analysis of heterogeneity in the lipid content of single green microalgae in alginate hydrogel microcapsules. *Analytical Chemistry* **85**, 8749-8756 (2013).

73. Holcomb, R.E., Mason, L.J., Reardon, K.F., Cropek, D.M. & Henry, C.S. Culturing and investigation of stress-induced lipid accumulation in microalgae

using a microfluidic device. *Analytical and Bioanalytical Chemistry* **400**, 245-253 (2011).

74. Pan, J. et al. Quantitative tracking of the growth of individual algal cells in microdroplet compartments. *Integrative Biology : Quantitative Biosciences from Nano to Macro* **3**, 1043-1051 (2011).

75. Dewan, A., Kim, J., McLean, R.H., Vanapalli, S.A. & Karim, M.N. Growth kinetics of microalgae in microfluidic static droplet arrays. *Biotechnology and Bioengineering* **109**, 2987-2996 (2012).

76. Au, S.H., Shih, S.C. & Wheeler, A.R. Integrated microbioreactor for culture and analysis of bacteria, algae and yeast. *Biomedical Microdevices* **13**, 41-50 (2011).

77. Chen, M., Mertiri, T., Holland, T. & Basu, A.S. Optical microplates for high-throughput screening of photosynthesis in lipid-producing algae. *Lab on a Chip* **12**, 3870-3874 (2012).

78. Jeon, N.L. et al. Generation of solution and surface gradients using microfluidic systems. *Langmuir* **16**, 8311-8316 (2000).

79. Lee, K. et al. Generalized serial dilution module for monotonic and arbitrary microfluidic gradient generators. *Lab on a Chip* **9**, 709-717 (2009).

80. Thorsen, T., Maerkl, S.J. & Quake, S.R. Microfluidic large-scale integration. *Science* **298**, 580-584 (2002).

81. Xia, Y. & Whitesides, G.M. Soft lithography. *Annual Review of Materials Science* **28**, 153-184 (1998).

82. Lee, K. et al. Generalized serial dilution module for monotonic and arbitrary microfluidic gradient generators. *Lab on a chip* **9**, 709-717 (2008).

83. Beebe, D.J., Mensing, G.A. & Walker, G.M. Physics and applications of microfluidics in biology. *Annual Review of Biomedical Engineering* **4**, 261-286 (2002).

84. Wolf, F.R. & Cox, E.R. Ultrastructure of active and resting colonies of Botryococcus braunii (Chlorophyceae) 1. *Journal of Phycology* **17**, 395-405 (1981).

85. Maxwell, J., Douglas, A., Eglinton, G. & McCormick, A. The botryococcenes — hydrocarbons of novel structure from the alga Botryococcus braunii, Kützing. *Phytochemistry* **7**, 2157-2171 (1968).

86. Knights, B., Brown, A., Conway, E. & Middleditch, B. Hydrocarbons from the green form of the freshwater alga Botryococcus braunii. *Phytochemistry* **9**, 1317-1324 (1970).

87. Templier, J., Largeau, C. & Casadevall, E. Mechanism of non-isoprenoid hydrocarbon biosynthesis in Botryococcus braunii. *Phytochemistry* **23**, 1017-1028 (1984).

88. Metzger, P., Casadevall, E., Pouet, M. & Pouet, Y. Structures of some botryococcenes: branched hydrocarbons from the B-race of the green alga Botryococcus braunii. *Phytochemistry* **24**, 2995-3002 (1985).

89. Metzger, P., Templier, J., Largeau, C. & Casadevall, E. An n-alkatriene and some n-alkadienes from the A race of the green alga Botryococcus braunii. *Phytochemistry* **25**, 1869-1872 (1986).

90. Metzger, P., Allard, B., Casadevall, E., Berkaloff, C. & Coute, A. structure and chemistry of a new chemical race of Botryococcus braunii (Chlorophyceae) that prodcues lycopadiene, a tetraterpenoid hycrocarbon. *Journal of Phycology* **26**, 258-266 (1990).

91. Templier, J., Largeau, C. & Casadevall, E. Biosynthesis of n-alkatrienes in Botryococcus braunii. *Phytochemistry* **30**, 2209-2215 (1991).

92. Casadevall, E. et al. Studies on batch and continuous cultures of Botryococcus braunii: hydrocarbon production in relation to physiological state, cell ultrastructure, and phosphate nutrition. *Biotechnology and Bioengineering* **27**, 286-295 (1985).

93. Metzger, P., Casadevall, E. & Coute, A. Botryococcene distribution in strains of the green alga Botryococcus braunii. *Phytochemistry* **27**, 1383-1388 (1988).

94. Moldowan, J.M. & Seifert, W.K. First discovery of botryococcane in petroleum. *Journal of the Chemical Society, Chemical Communications*, 912-914 (1980).

95. Hillen, L., Pollard, G., Wake, L. & White, N. Hydrocracking of the oils of Botryococcus braunii to transport fuels. *Biotechnology and Bioengineering* **24**, 193-205 (1982).

96. Kitazato, H., Asaoka, S. & Iwamoto, H. Catalytic cracking of hydrocarbons from microalgae. *Journal of The Japan Petroleum Institute* **32**, 28-34 (1989).

97. Brown, A., Knights, B. & Conway, E. Hydrocarbon content and its relationship to physiological state in the green alga Botryococcus braunii. *Phytochemistry* **8**, 543-547 (1969).

98. Nonomura, A.M. Botryococcus braunii var. showa (Chlorophyceae) from Berkeley, California, United States of America. *Japanese Journal of Phycology* **36**, 285-291 (1988).

99. Grung, M., Metzger, P. & Liaaen-jensen, S. Primary and secondary carotenoids in two races of the green alga Botryococcus braunii. *Biochemical Systematics and Ecology* **17**, 263-269 (1989).

100. Merkel, T., Bondar, V., Nagai, K., Freeman, B. & Pinnau, I. Gas sorption, diffusion, and permeation in poly (dimethylsiloxane). *Journal of Polymer Science Part B: Polymer Physics* **38**, 415-434 (2000).

101. Elsey, D., Jameson, D., Raleigh, B. & Cooney, M.J. Fluorescent measurement of microalgal neutral lipids. *Journal of Microbiological Methods* **68**, 639-642 (2007).

102. Lee, S.J., Yoon, B.-D. & Oh, H.-M. Rapid method for the determination of lipid from the green alga Botryococcus braunii. *Biotechnology Techniques* **12**, 553-556 (1998).

103. Toepke, M.W. & Beebe, D.J. PDMS absorption of small molecules and consequences in microfluidic applications. *Lab on a Chip* **6**, 1484-1486 (2006).

104. Tyystjärvi, E. & Aro, E.-M. The rate constant of photoinhibition, measured in lincomycin-treated leaves, is directly proportional to light intensity. *Proceedings of the National Academy of Sciences* **93**, 2213-2218 (1996).

105. Wahal, S. & Viamajala, S. Maximizing algal growth in batch reactors using sequential change in light intensity. *Applied Biochemistry and Biotechnology* **161**, 511-522 (2010).

106. Watson, S., McCauley, E. & Downing, J.A. Sigmoid relationships between phosphorus, algal biomass, and algal community structure. *Canadian Journal of Fisheries and Aquatic Sciences* **49**, 2605-2610 (1992).

107. Falkowski, P. & Kiefer, D.A. Chlorophyll a fluorescence in phytoplankton: relationship to photosynthesis and biomass. *Journal of Plankton Research* **7**, 715-731 (1985).

108. Vonshak, A., Abeliovich, A., Boussiba, S., Arad, S. & Richmond, A. Production of Spirulina biomass: effects of environmental factors and population density. *Biomass* **2**, 175-185 (1982).

109. Qiang, H. & Richmond, A. Productivity and photosynthetic efficiency of Spirulina platensis as affected by light intensity, algal density and rate of mixing in a flat plate photobioreactor. *Journal of Applied Phycology* **8**, 139-145 (1996).

110. Dayananda, C., Sarada, R., Usha Rani, M., Shamala, T. & Ravishankar, G. Autotrophic cultivation of Botryococcus braunii for the production of hydrocarbons and exopolysaccharides in various media. *Biomass and Bioenergy* **31**, 87-93 (2007).

111. Hsieh, C.H. & Wu, W.T. Cultivation of microalgae for oil production with a cultivation strategy of urea limitation. *Bioresource Technology* **100**, 3921-3926 (2009).

112. Haines, K.C. & Guillard, R.R.L. Growth of vitamin B12 requiring marine diatoms in mixed laboratory cultures with vitamin B12 producing marine bacteria. *Journal of Phycology* **10**, 245-252 (1974).

113. Parker, B.C. & Bold, H.C. Biotic relationships between soil algae and other microorganisms. *American Journal of Botany* **48**, 185-197 (1961).

114. Saks, N.M. & Kahn, E.G. Substrate competition between a salt marsh diatom and a bacterial population. *Journal of Phycology* **15**, 17-21 (1979).

115. Fallon, R.D. & Brock, T.D. Decomposition of blue-green algal (cyanobacterial) blooms in Lake Mendota, Wisconsin. *Applied and Environmental Microbiology* **37**, 820 (1979).

116. Chisti, Y. Constraints to commercialization of algal fuels. *Journal of Biotechnology* **167**, 201-214 (2013).

117. Autebert, J. et al. Microfluidic: an innovative tool for efficient cell sorting. *Methods* **57**, 297-307 (2012).

118. Huh, D., Gu, W., Kamotani, Y., Grotberg, J.B. & Takayama, S. Microfluidics for flow cytometric analysis of cells and particles. *Physiological Measurement* **26**, R73-98 (2005).

119. Sun, T. & Morgan, H. Single-cell microfluidic impedance cytometry: a review. *Microfluidics and Nanofluidics* **8**, 423-443 (2010).

120. Mazutis, L. et al. Single-cell analysis and sorting using droplet-based microfluidics. *Nature Protocols* **8**, 870-891 (2013).

121. Kovac, J.R. & Voldman, J. Intuitive, image-based cell sorting using optofluidic cell sorting. *Analytical Chemistry* **79**, 9321-9330 (2007).

122. Tan, W.H. & Takeuchi, S. A trap-and-release integrated microfluidic system for dynamic microarray applications. *Proceedings of the National Academy of Sciences of the United States of America* **104**, 1146-1151 (2007).

123. Tan, W.H. & Takeuchi, S. Dynamic microarray system with gentle retrieval mechanism for cell-encapsulating hydrogel beads. *Lab on a Chip* **8**, 259-266 (2008).

124. Taff, B.M., Desai, S.P. & Voldman, J. Electroactive hydrodynamic weirs for microparticle manipulation and patterning. *Applied Physics Letters* **94**, 84102 (2009).

125. Zhu, Z., Frey, O., Ottoz, D.S., Rudolf, F. & Hierlemann, A. Microfluidic single-cell cultivation chip with controllable immobilization and selective release of yeast cells. *Lab on a Chip* **12**, 906-915 (2012).

126. Mayfield, S.P., Franklin, S.E. & Lerner, R.A. Expression and assembly of a fully active antibody in algae. *Proceedings of the National Academy of Sciences of the United States of America* **100**, 438-442 (2003).

127. Leon-Banares, R., Gonzalez-Ballester, D., Galvan, A. & Fernandez, E. Transgenic microalgae as green cell-factories. *Trends in Biotechnology* **22**, 45-52 (2004).

128. Griesbeck, C., Kobl, I. & Heitzer, M. Chlamydomonas reinhardtii. *Molecular Biotechnology* **34**, 213-223 (2006).

129. Hallmann, A. Algal transgenics and biotechnology. *Transgenic Plant Journal* **1**, 81-98 (2007).

130. Grossman, A.R. et al. Novel metabolism in Chlamydomonas through the lens of genomics. *Current Opinion in Plant Biology* **10**, 190-198 (2007).

131. Merchant, S.S. et al. The Chlamydomonas genome reveals the evolution of key animal and plant functions. *Science* **318**, 245-250 (2007).

132. Grossman, A.R. Transgenic microalgae as green cell factories. 54-76 (Springer, 2007).

133. Castruita, M. et al. Systems biology approach in Chlamydomonas reveals connections between copper nutrition and multiple metabolic steps. *The Plant Cell* **23**, 1273-1292 (2011).

134. Harris, E.H., Stern, D.B. & Witman, G. The Chlamydomonas sourcebooksourcebook: introduction to chlamydomonas and its laboratory use. (2009).

135. Gorman, D.S. & Levine, R.P. Cytochrome f and plastocyanin: their sequence in the photosynthetic electron transport chain of Chlamydomonas reinhardtii. *Proceedings of the National Academy of Sciences* **54**, 1665-1669 (1965).

136. Moellering, E.R. & Benning, C. RNA interference silencing of a major lipid droplet protein affects lipid droplet size in Chlamydomonas reinhardtii. *Eukaryot Cell* **9**, 97-106 (2010).

137. Lee do, Y. & Fiehn, O. High quality metabolomic data for Chlamydomonas reinhardtii. *Plant Methods* **4**, 7 (2008).

138. Huebner, A. et al. Microdroplets: a sea of applications? *Lab on a Chip* **8**, 1244-1254 (2008).

139. Casadevall i Solvas, X. & deMello, A. Droplet microfluidics: recent developments and future applications. *Chemical Communications* **47**, 1936-1942 (2011).

140. Dittrich, P.S. & Manz, A. Lab-on-a-chip: microfluidics in drug discovery. *Nature Reviews. Drug Discovery* **5**, 210-218 (2006).

141. Seemann, R., Brinkmann, M., Pfohl, T. & Herminghaus, S. Droplet based microfluidics. *Reports on Progress in Physics. Physical Society* **75**, 016601 (2012).

142. Baroud, C.N., Gallaire, F. & Dangla, R. Dynamics of microfluidic droplets. *Lab on a Chip* **10**, 2032-2045 (2010).

143. Park, J. et al. Microdroplet-enabled highly parallel co-cultivation of microbial communities. *PloS One* **6**, e17019 (2011).

144. Lagus, T.P. & Edd, J.F. High-throughput co-encapsulation of self-ordered cell trains: cell pair interactions in microdroplets. *Rsc Advances* **3**, 20512-20522 (2013).

145. Huebner, A. et al. Quantitative detection of protein expression in single cells using droplet microfluidics. *Chemical Communications*, 1218-1220 (2007).

146. Koster, S. et al. Drop-based microfluidic devices for encapsulation of single cells. *Lab on a Chip* **8**, 1110-1115 (2008).

147. Brouzes, E. et al. Droplet microfluidic technology for single-cell high-throughput screening. *Proceedings of the National Academy of Sciences of the United States of America* **106**, 14195-14200 (2009).

148. Srisa-Art, M. et al. Identification of rare progenitor cells from human periosteal tissue using droplet microfluidics. *The Analyst* **134**, 2239-2245 (2009).

149. Markey, A.L., Mohr, S. & Day, P.J. High-throughput droplet PCR. *Methods* **50**, 277-281 (2010).

150. Guo, M.T., Rotem, A., Heyman, J.A. & Weitz, D.A. Droplet microfluidics for high-throughput biological assays. *Lab on a Chip* **12**, 2146-2155 (2012).

151. Agresti, J.J. et al. Ultrahigh-throughput screening in drop-based microfluidics for directed evolution. *Proceedings of the National Academy of Sciences* **107**, 4004-4009 (2010).

152. Ahn, B., Lee, K., Lee, H., Panchapakesan, R. & Oh, K.W. Parallel synchronization of two trains of droplets using a railroad-like channel network. *Lab on a Chip* **11**, 3956-3962 (2011).

153. Zagnoni, M., Le Lain, G. & Cooper, J.M. Electrocoalescence mechanisms of microdroplets using localized electric fields in microfluidic channels. *Langmuir* **26**, 14443-14449 (2010).

154. Chen, Y.Y., Chen, Z.M. & Wang, H.Y. Enhanced fluorescence detection using liquid-liquid extraction in a microfluidic droplet system. *Lab on a Chip* **12**, 4569-4575 (2012).

APPENDIX

1. Mask designs (unit: μm)

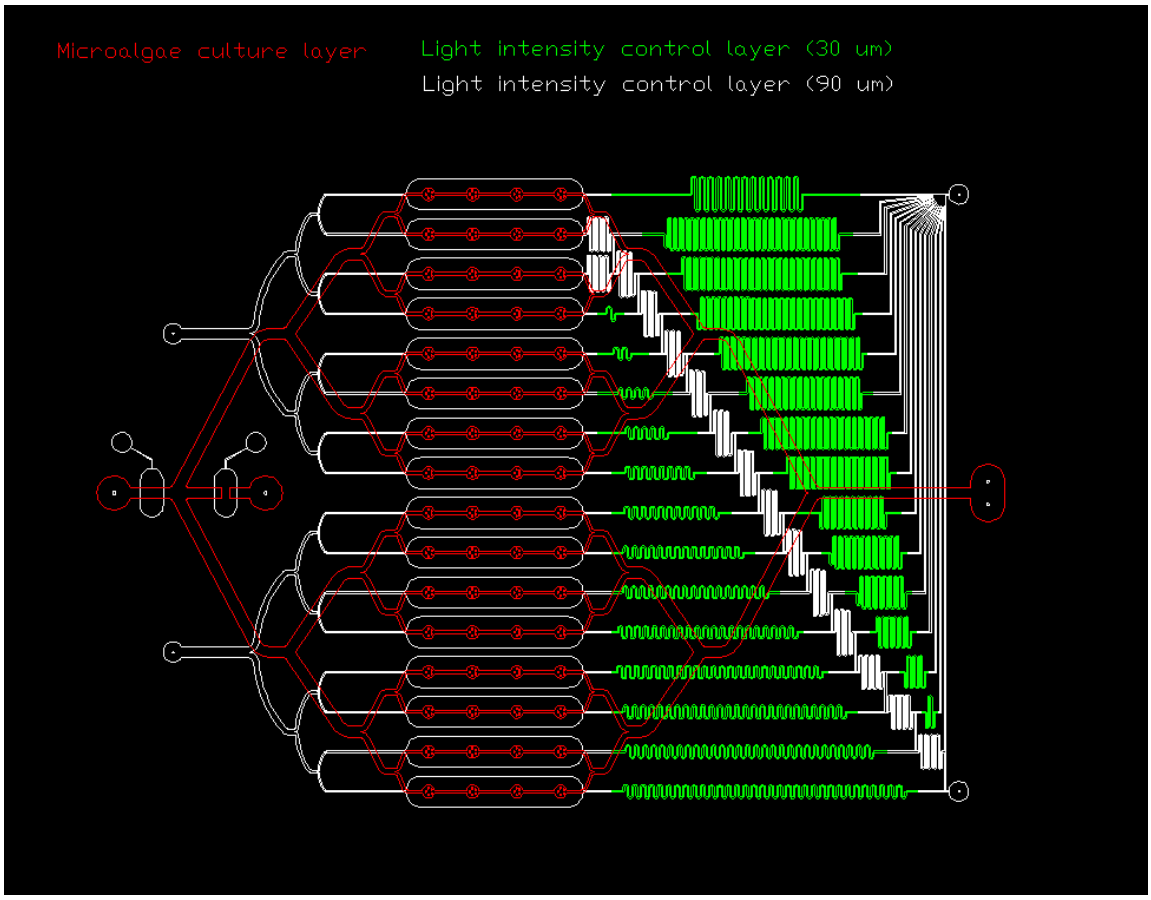

Figure A1.1. A high-throughput microfluidic photobioreactor array capable of screening 16 different light intensity conditions, assembled device

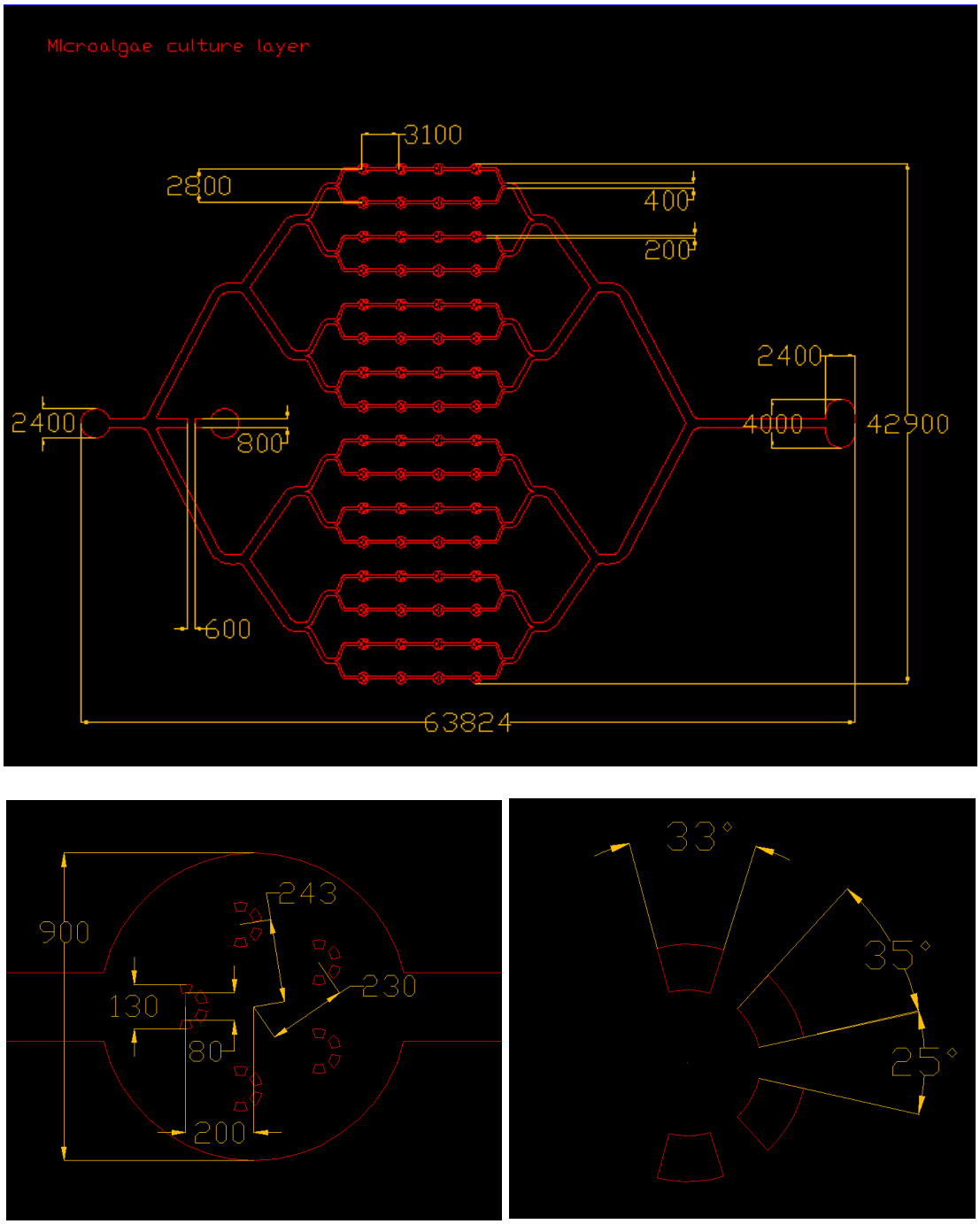

Figure A1.2. A high-throughput microfluidic photobioreactor array capable of screening 16 different light intensity conditions, microalgae culture layer

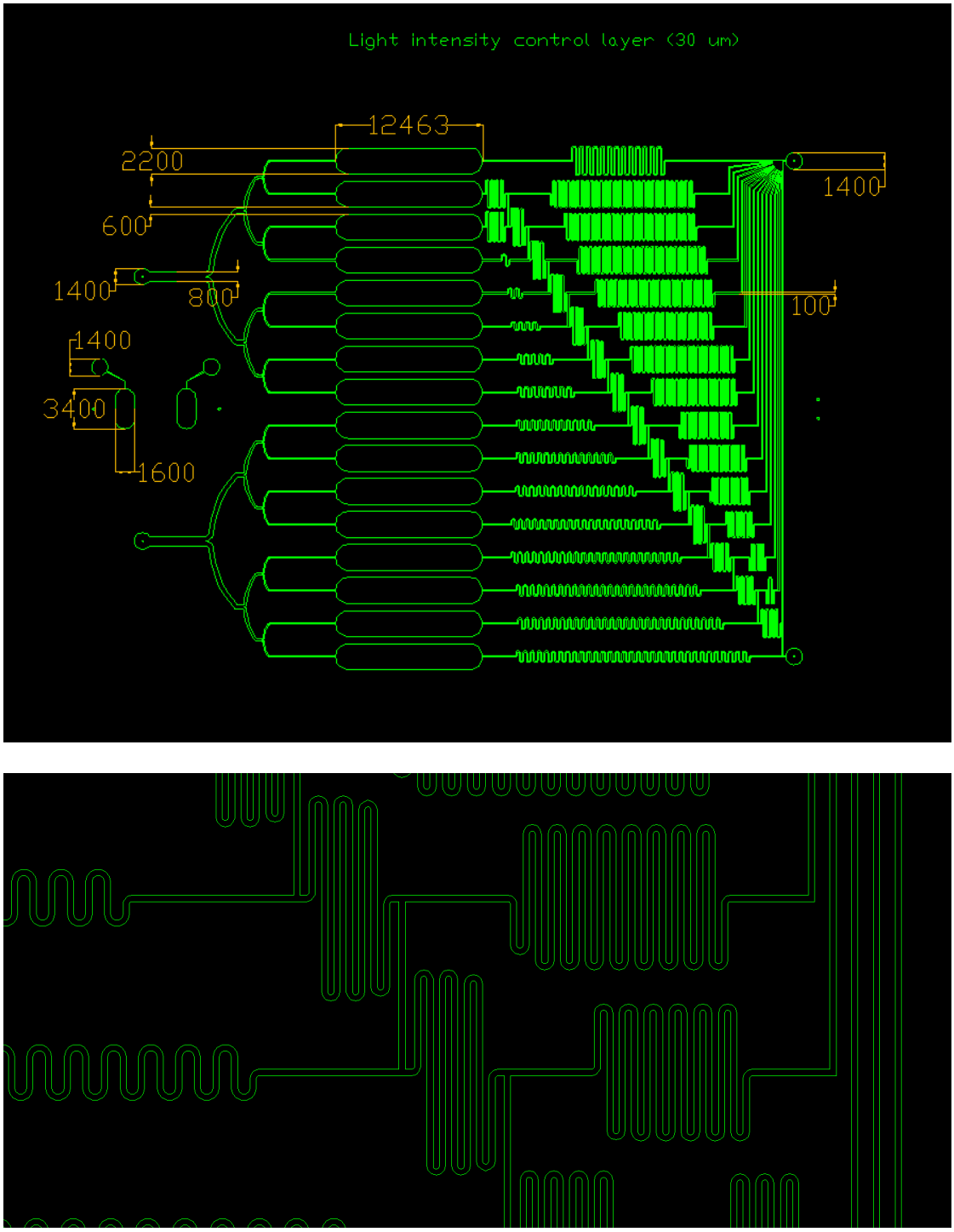

Figure A1.3. A high-throughput microfluidic photobioreactor array capable of screening 16 different light intensity conditions, light intensity control layer (30 µm thick)

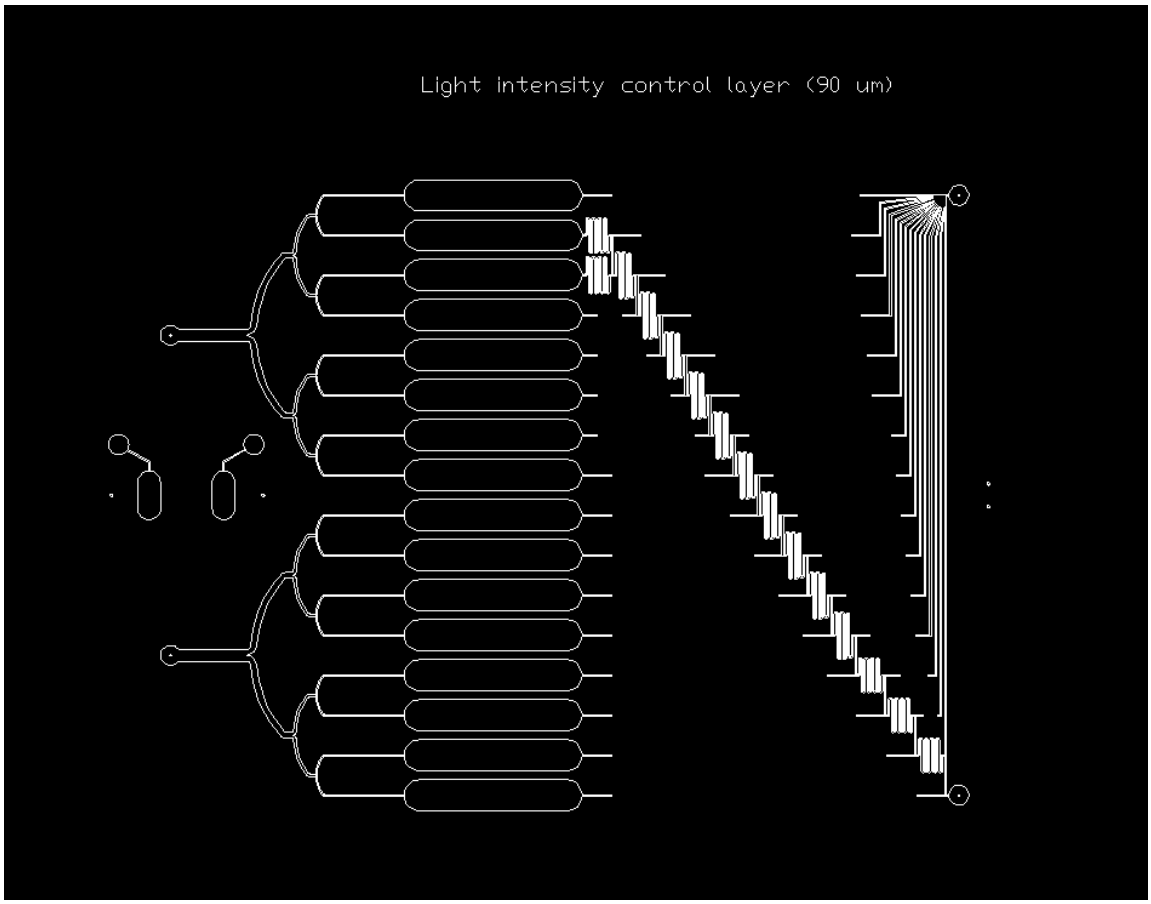

Figure A1.4. A high-throughput microfluidic photobioreactor array capable of screening 16 different light intensity conditions, light intensity control layer (90 μm thick)

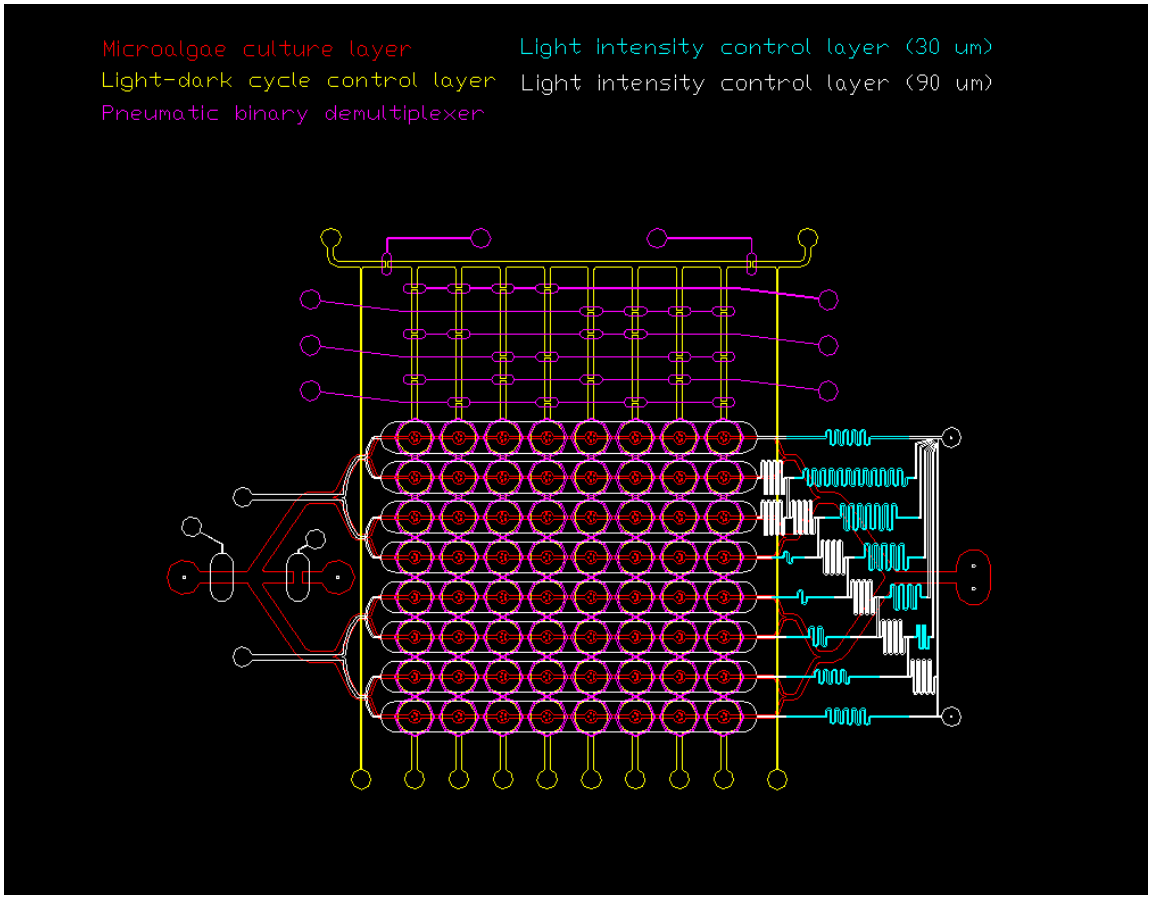

Figure A1.5. A high-throughput microfluidic photobioreactor array capable of screening 64 different light intensity conditions, assembled device

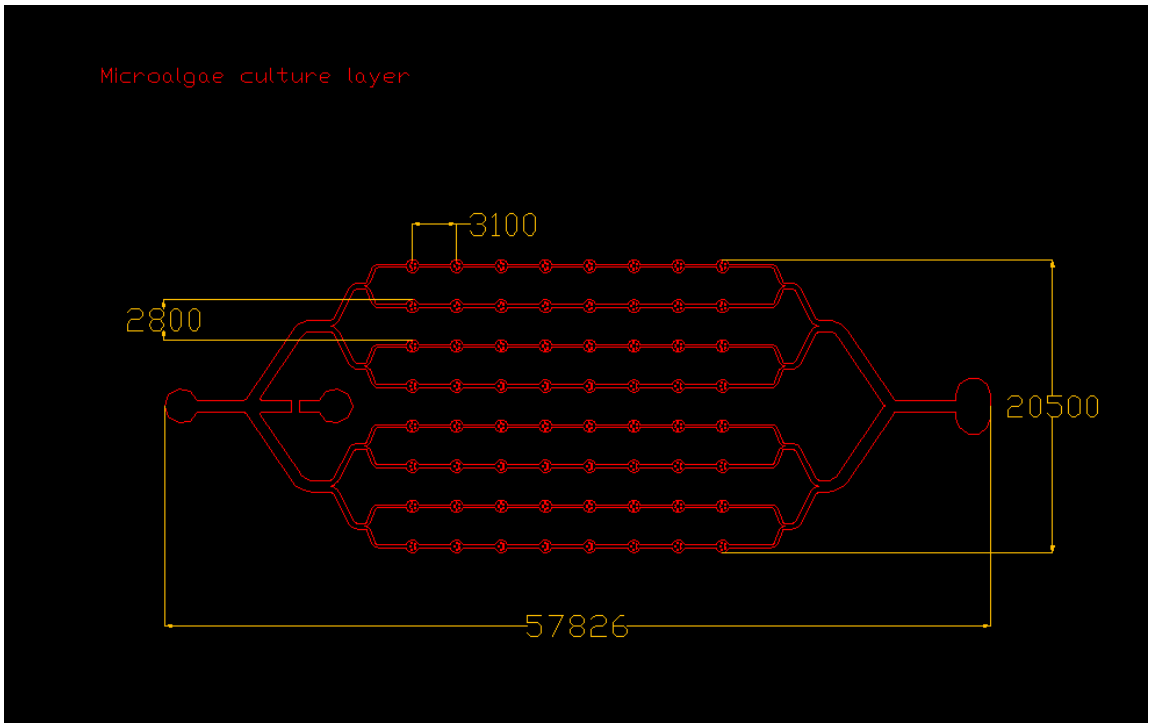

Figure A1.6. A high-throughput microfluidic photobioreactor array capable of screening 64 different light intensity conditions, microalgae culture layer

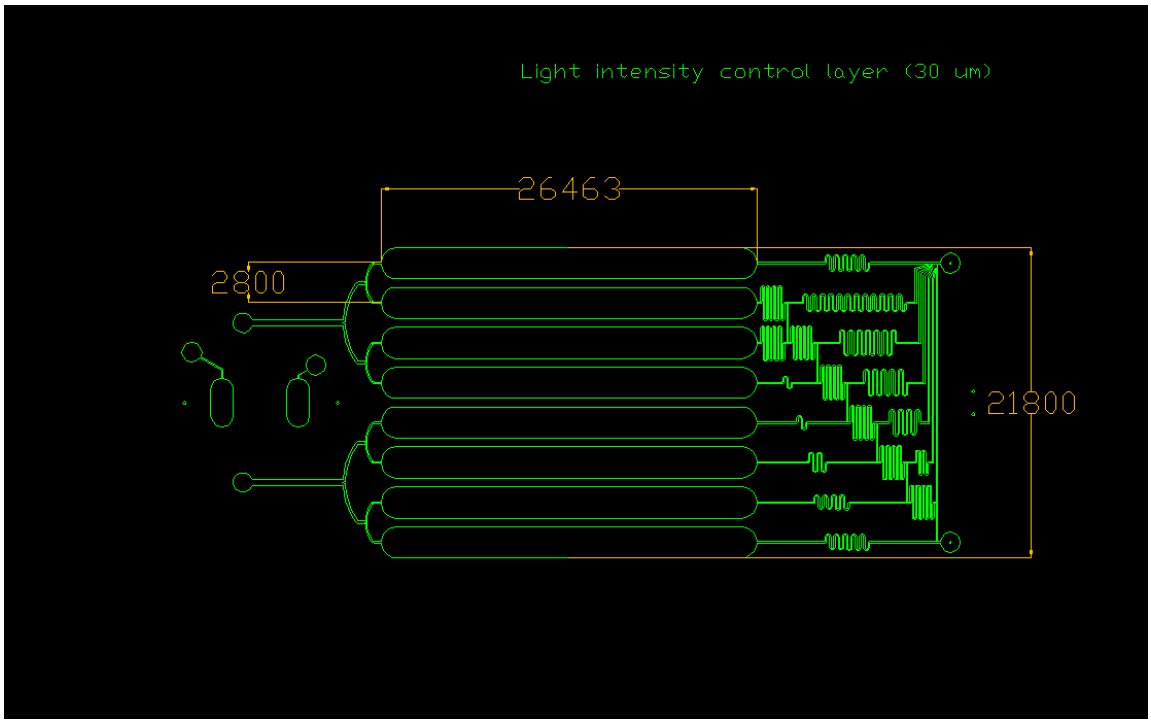

Figure A1.7. A high-throughput microfluidic photobioreactor array capable of screening 64 different light intensity conditions, light intensity control layer (30 μm thick)

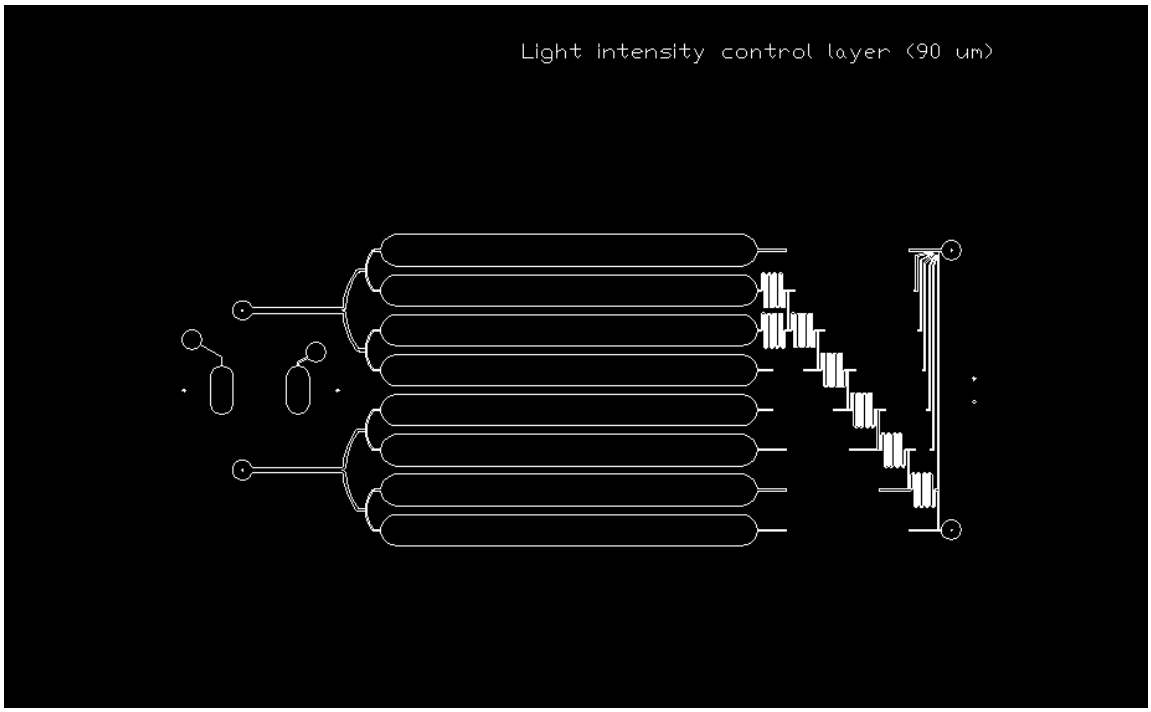

Figure A1.8. A high-throughput microfluidic photobioreactor array capable of screening 64 different light intensity conditions, light intensity control layer (90 μm thick)

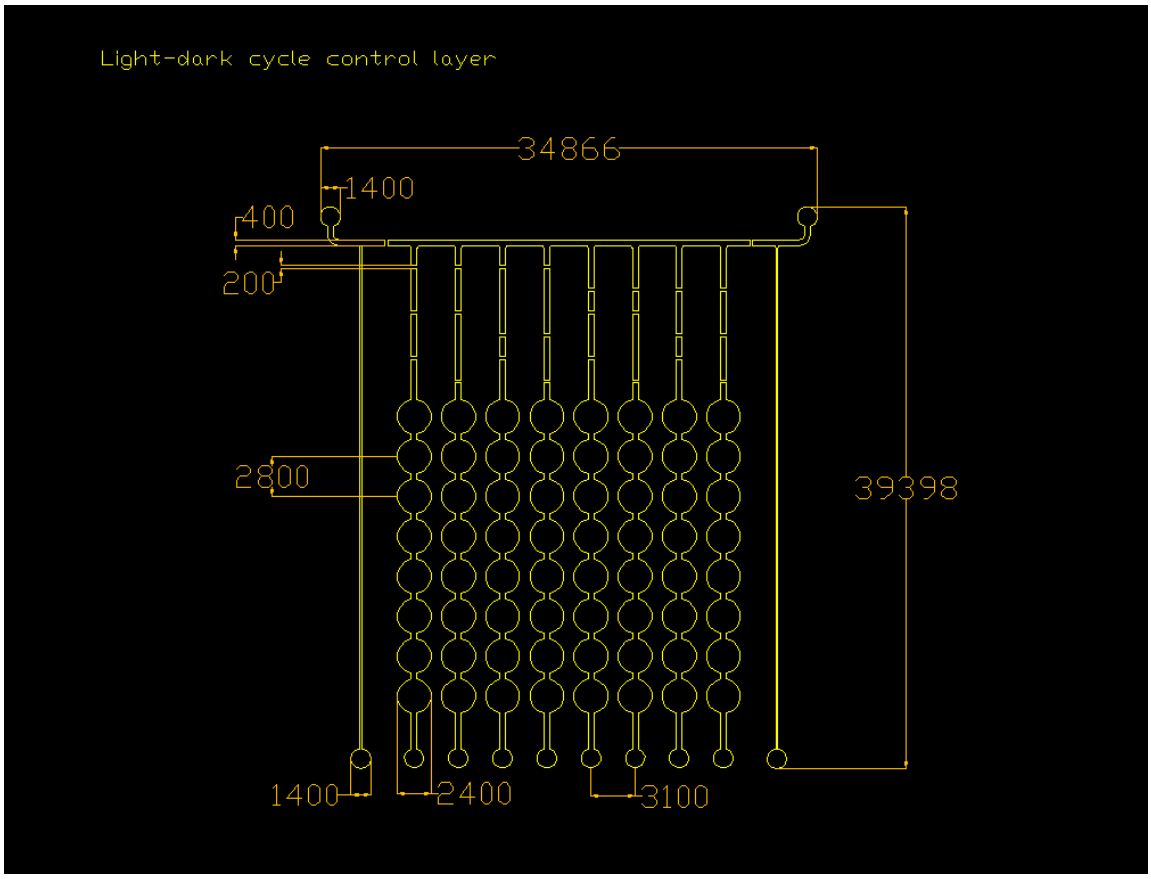

Figure A1.9. A high-throughput microfluidic photobioreactor array capable of screening 64 different light intensity conditions, light-dark cycle control layer

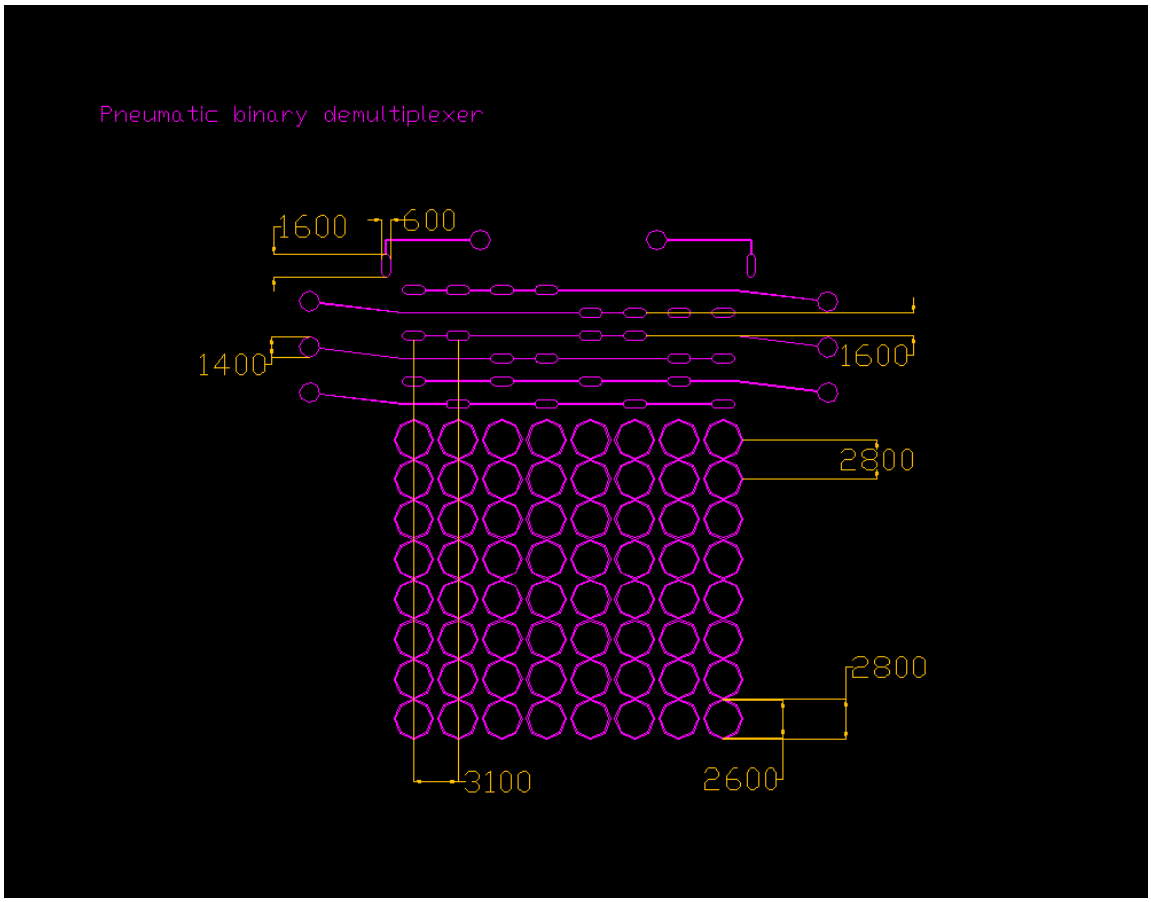

Figure A1.10. A high-throughput microfluidic photobioreactor array capable of screening 64 different light intensity conditions, light-dark cycle control layer

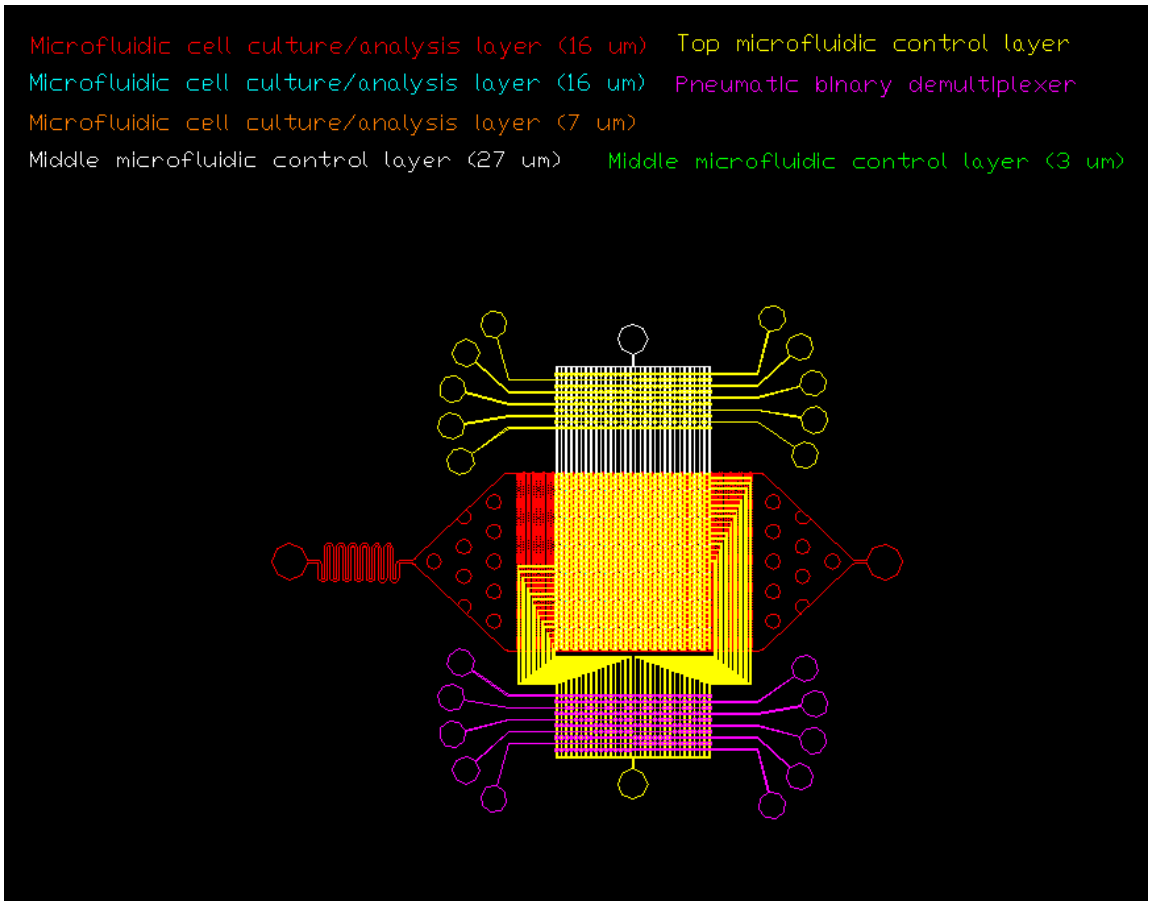
Microfluidic cell culture/analysis layer (16 um)
Top microfluidic control layer
Microfluidic cell culture/analysis layer (16 um)
Pneumatic binary demultiplexer
Microfluidic cell culture/analysis layer (7 um)
Middle microfluidic control layer (27 um)
Middle microfluidic control layer (3 um)

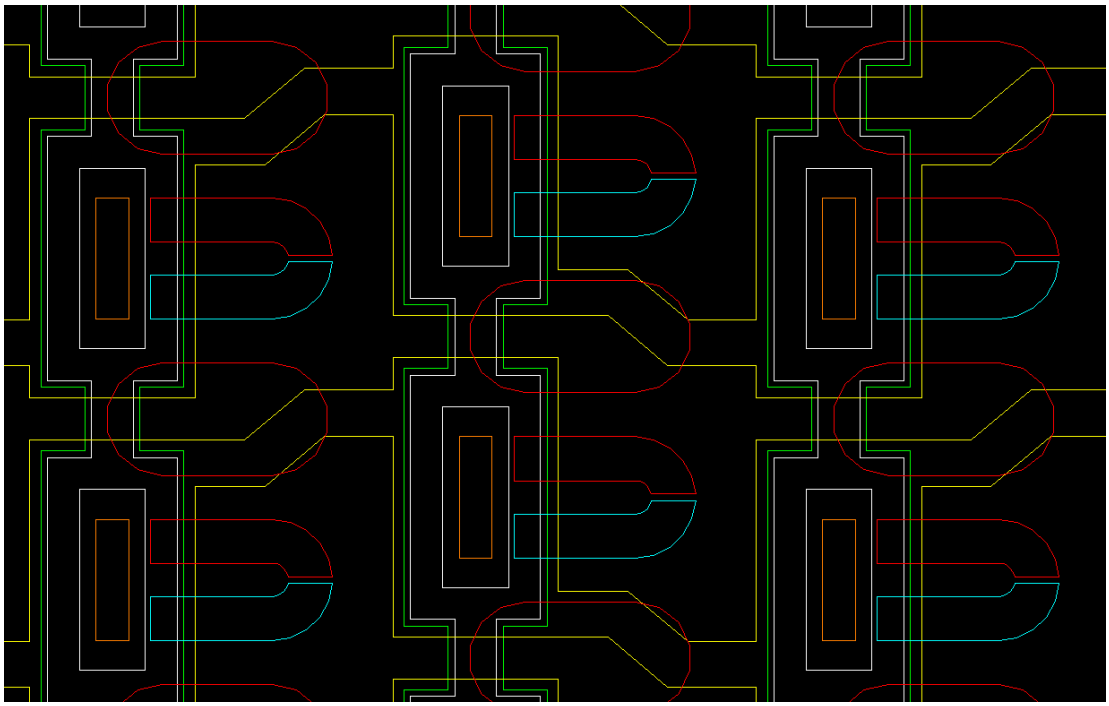

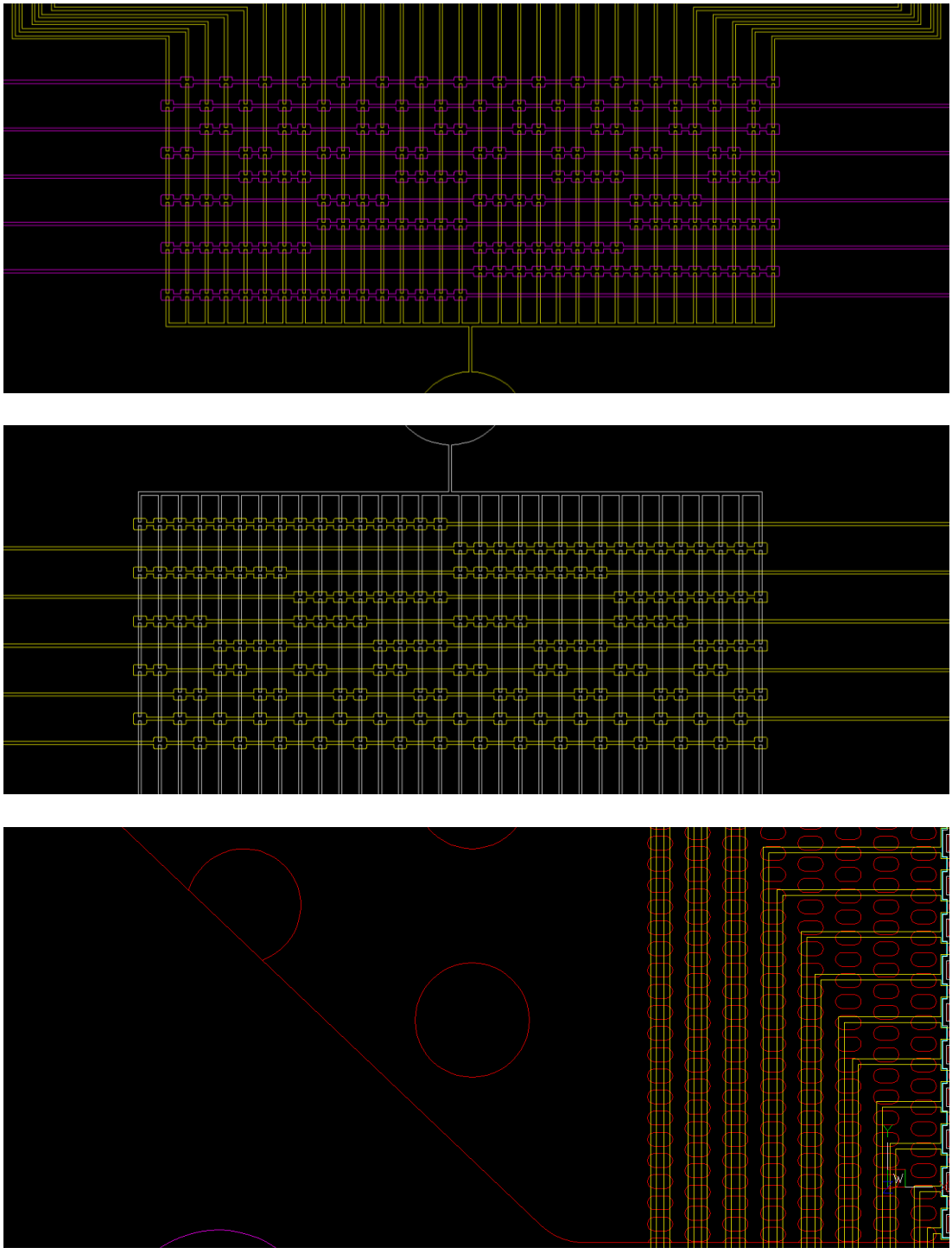

Figure A1.11. A high-throughput microfluidic single-cell screening and selection platform, assembled device

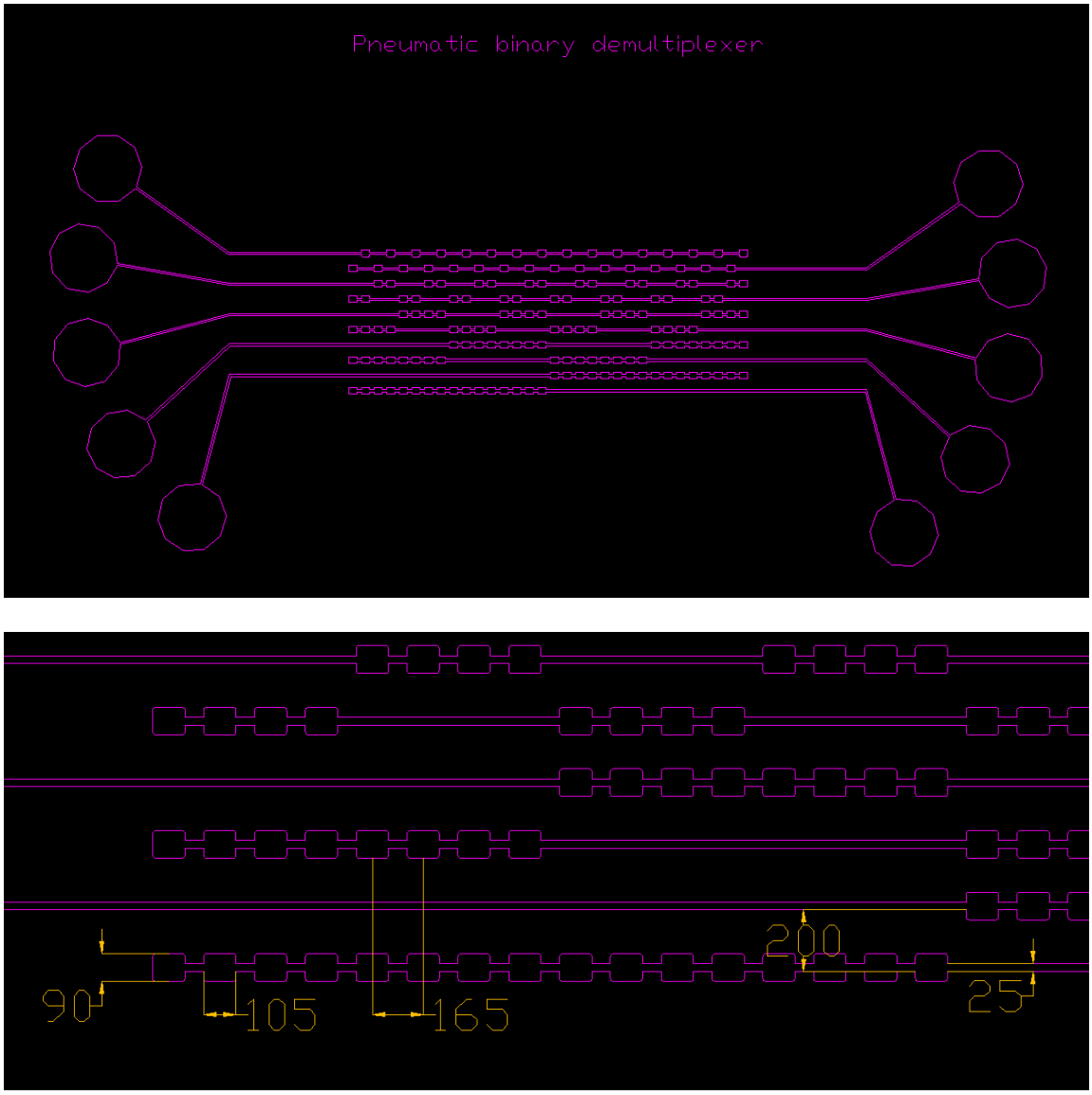

Figure A1.12. A high-throughput microfluidic single-cell screening and selection platform, pneumatic binary demultiplexer

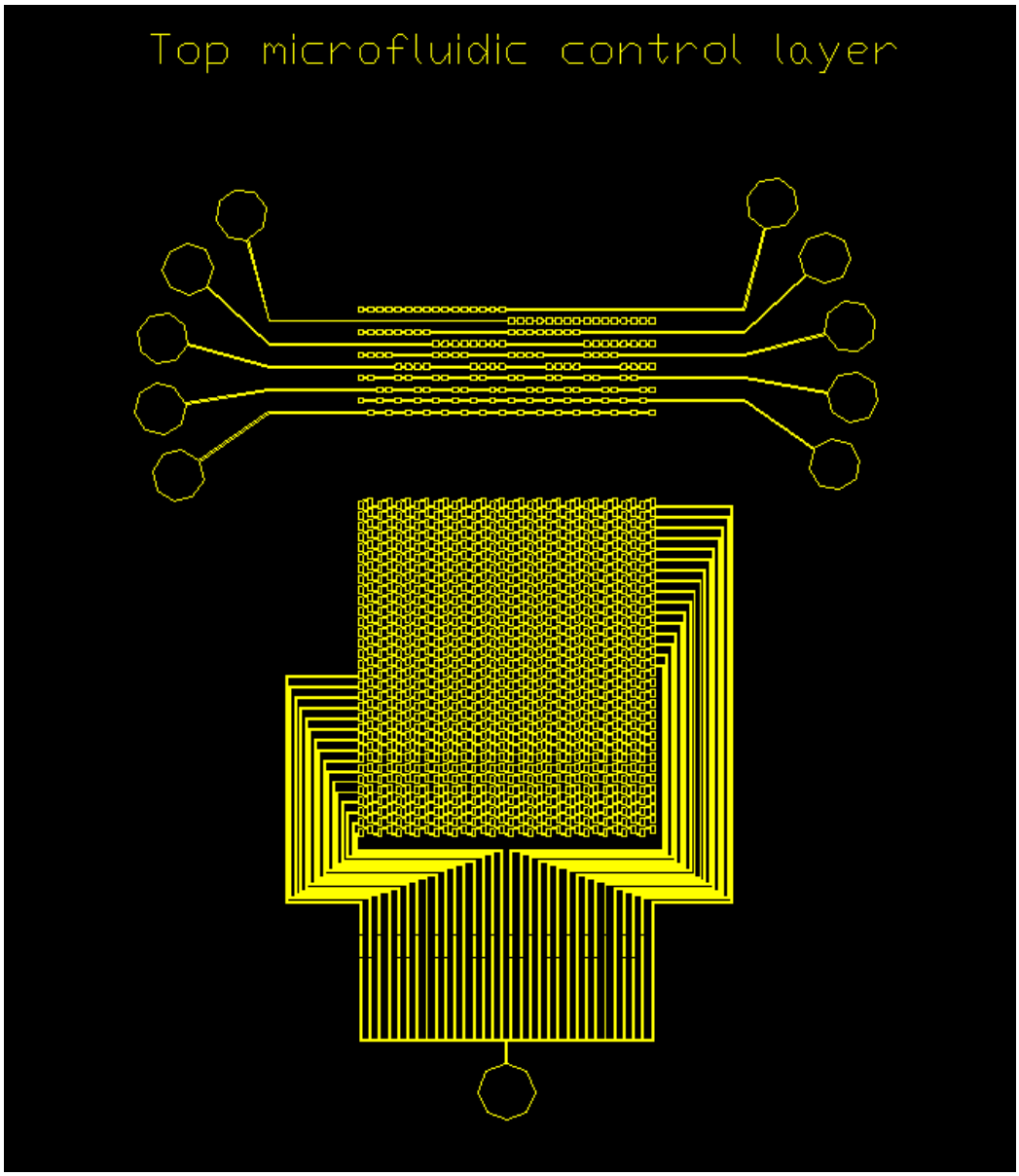
Top microfluidic control layer

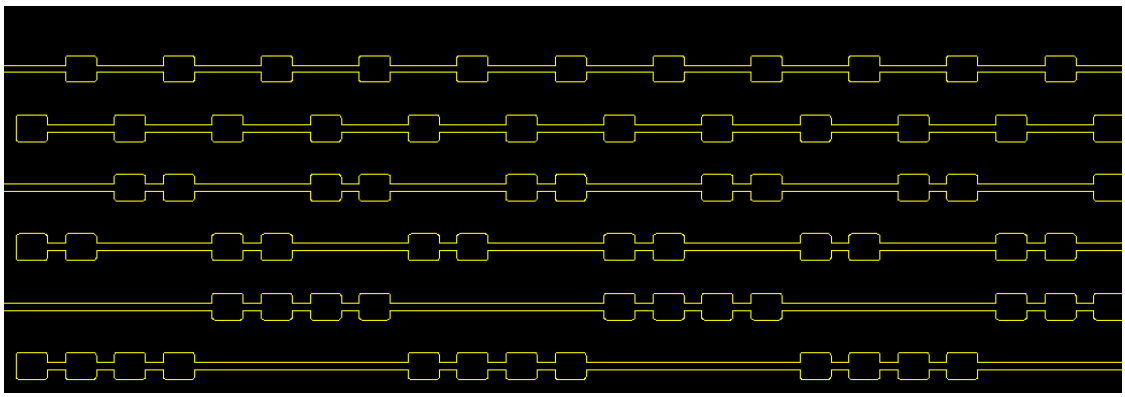

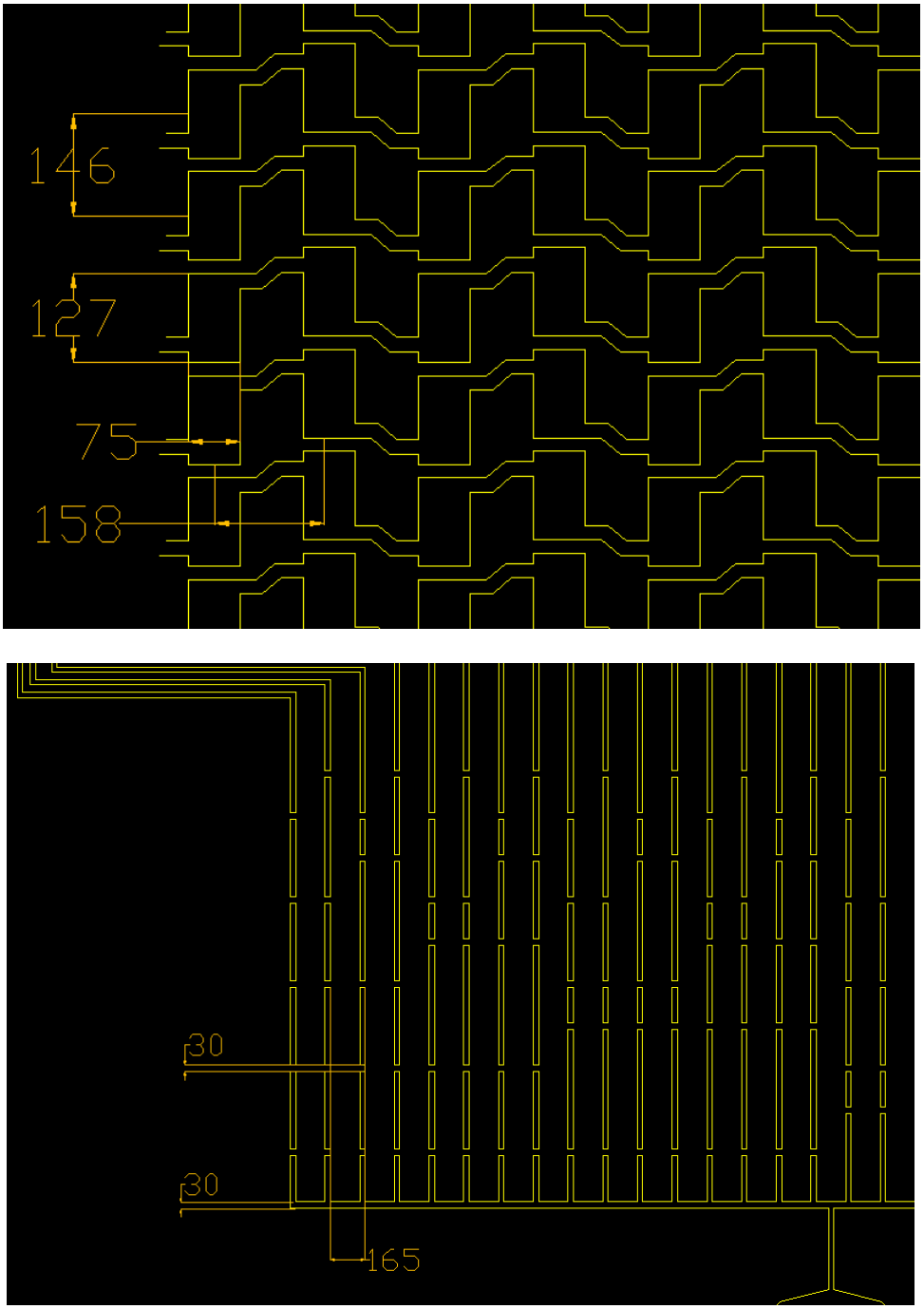

Figure A1.13. A high-throughput microfluidic single-cell screening and selection platform, top microfluidic control layer

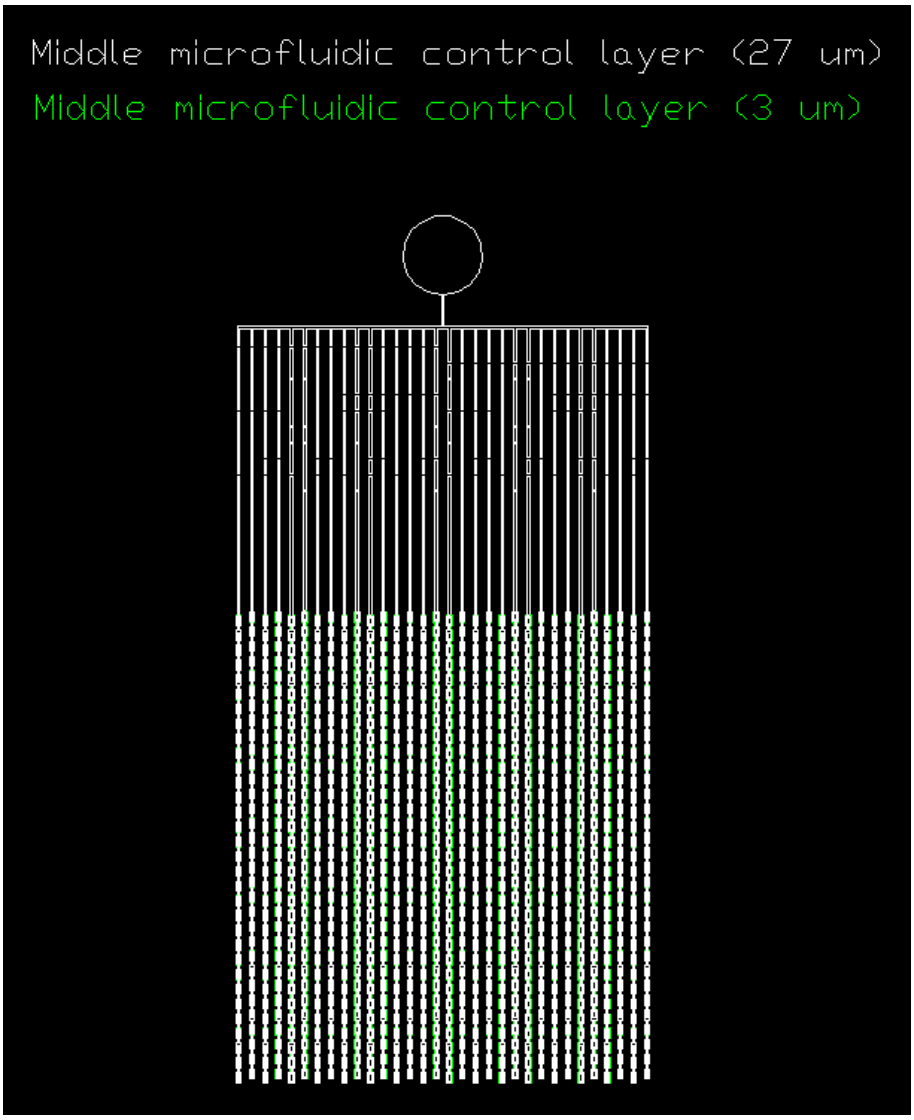
Middle microfluidic control layer (27 um)
Middle microfluidic control layer (3 um)

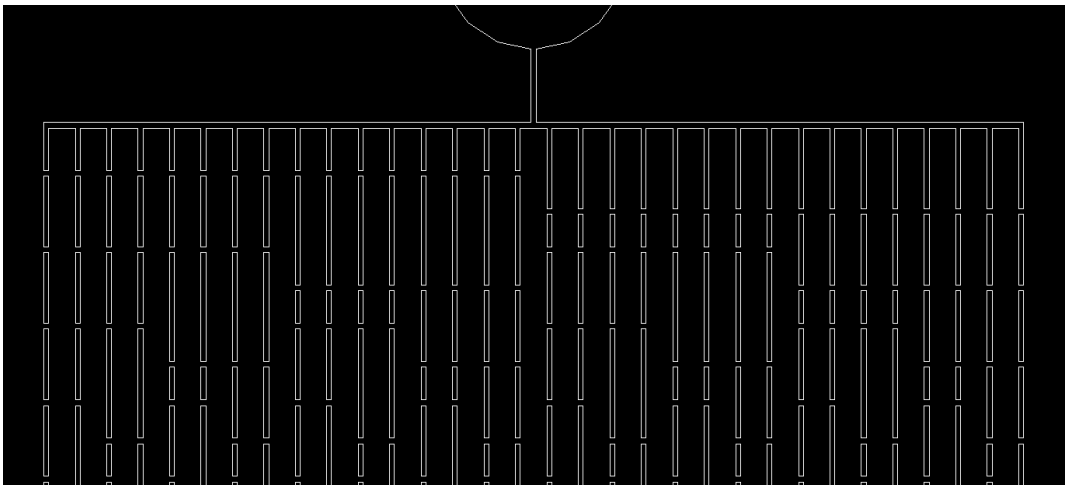

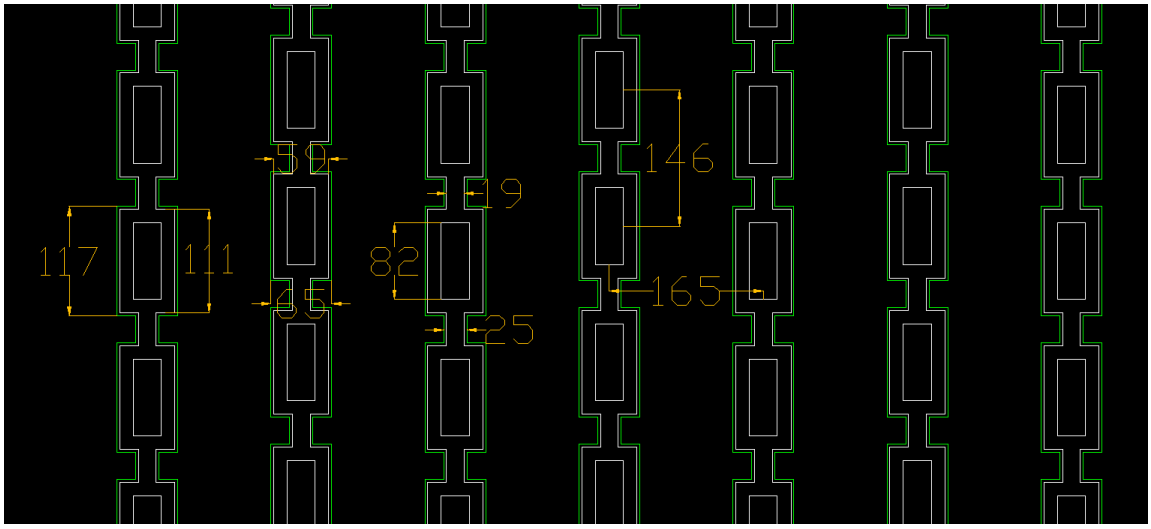

Figure A1.14. A high-throughput microfluidic single-cell screening and selection platform, middle microfluidic control layer

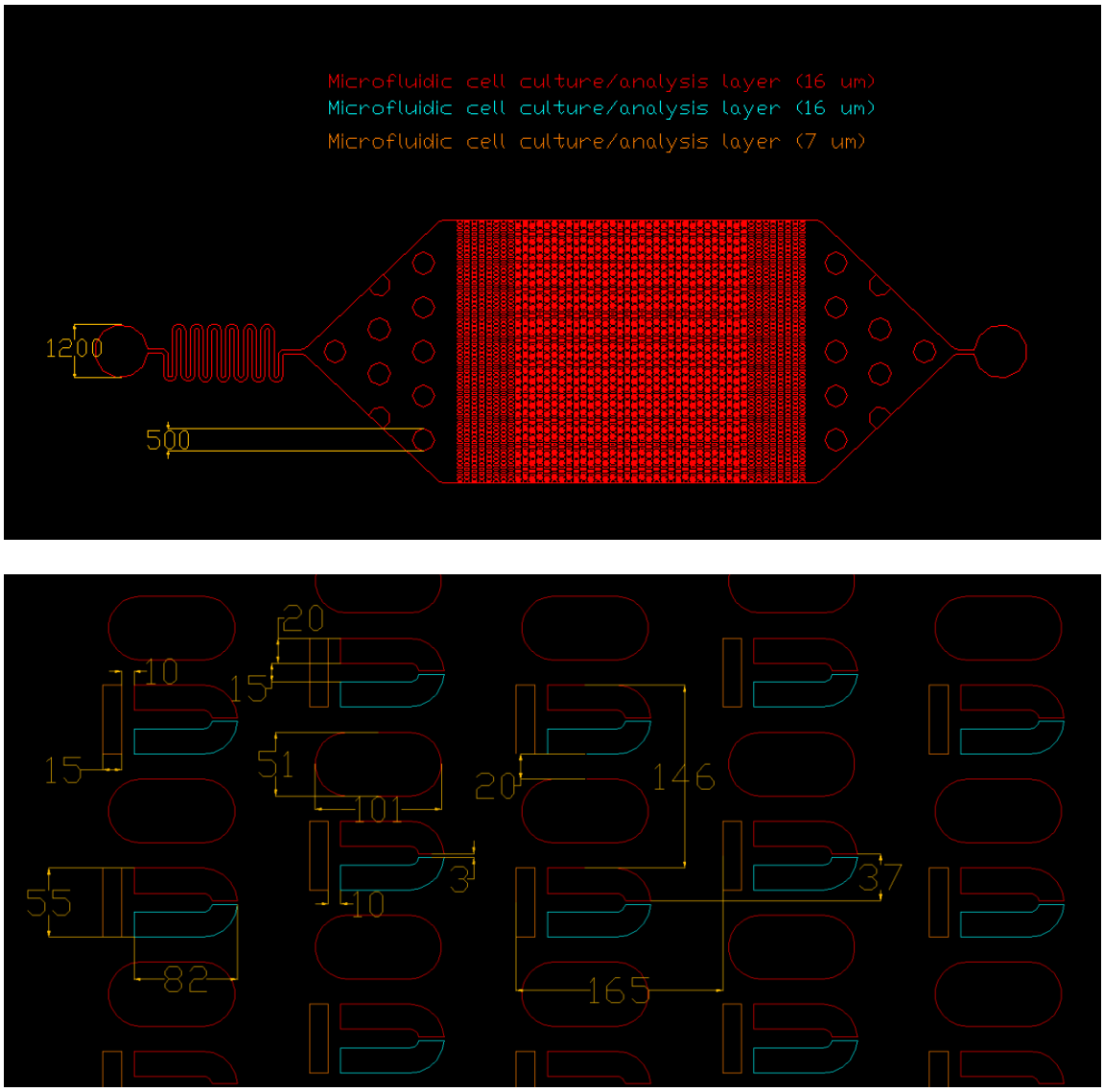

Figure A1.15. A high-throughput microfluidic single-cell screening and selection platform, microfluidic cell culture/analysis layer

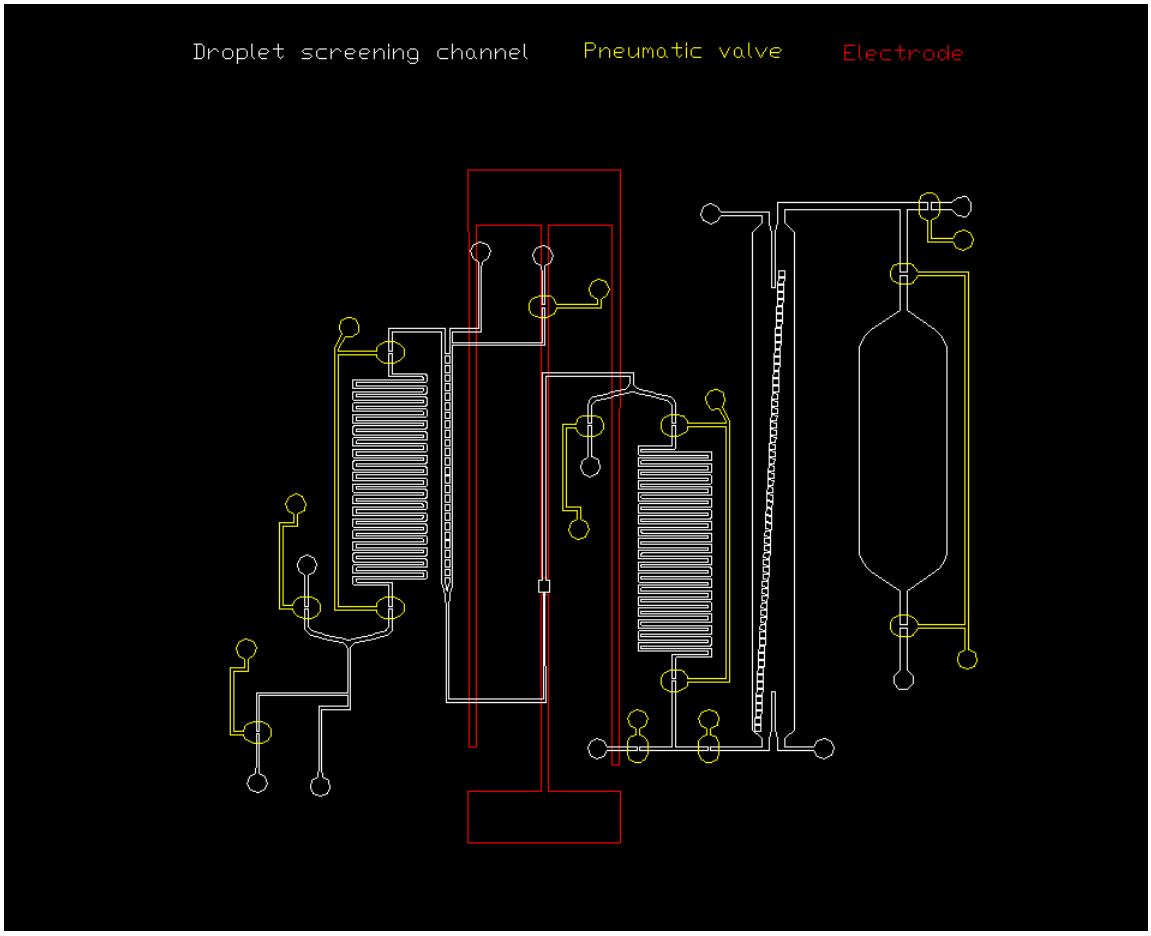

Figure A1.16. A high-throughput droplet microfluidics-based microalgae screening platform, assembled device

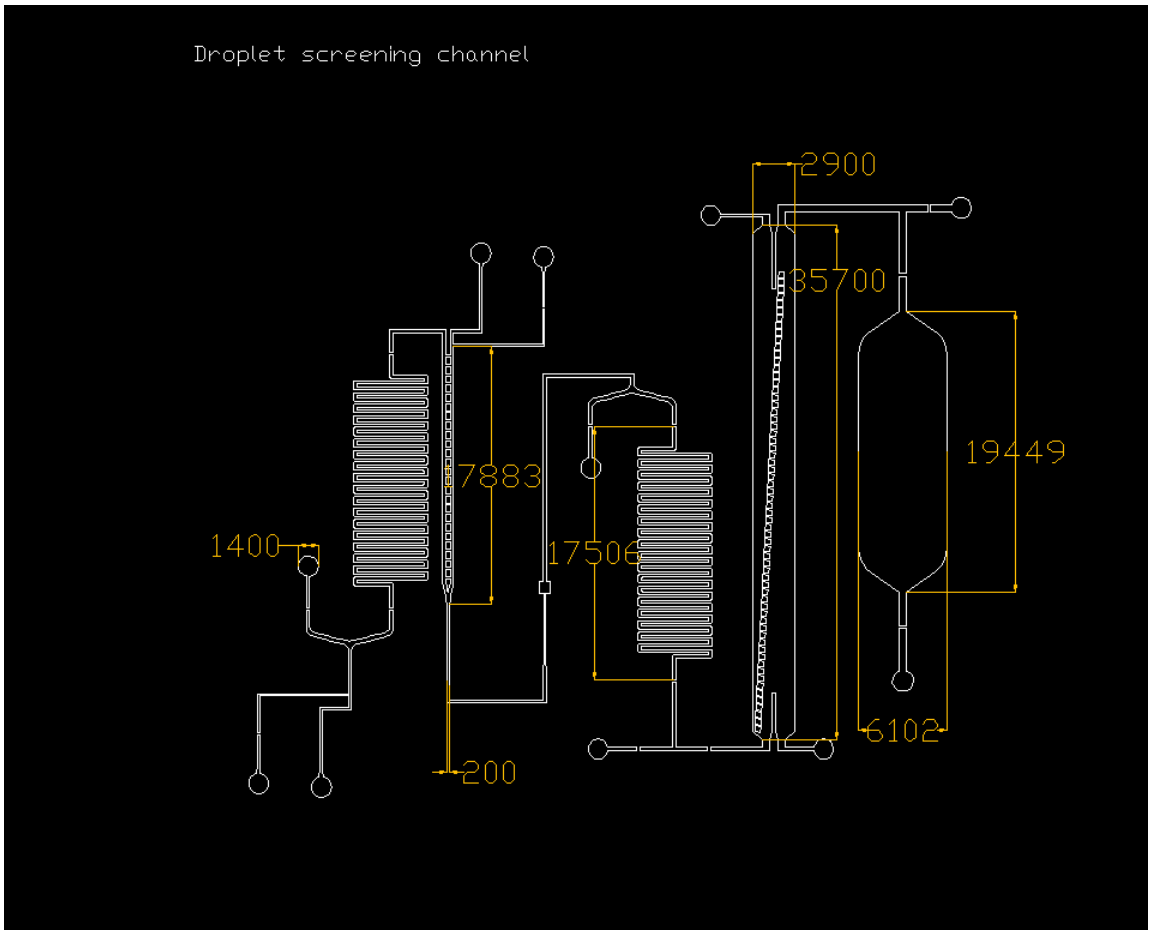
Droplet screening channel
2900
35700
19449
7883
1400
17506
6102
200

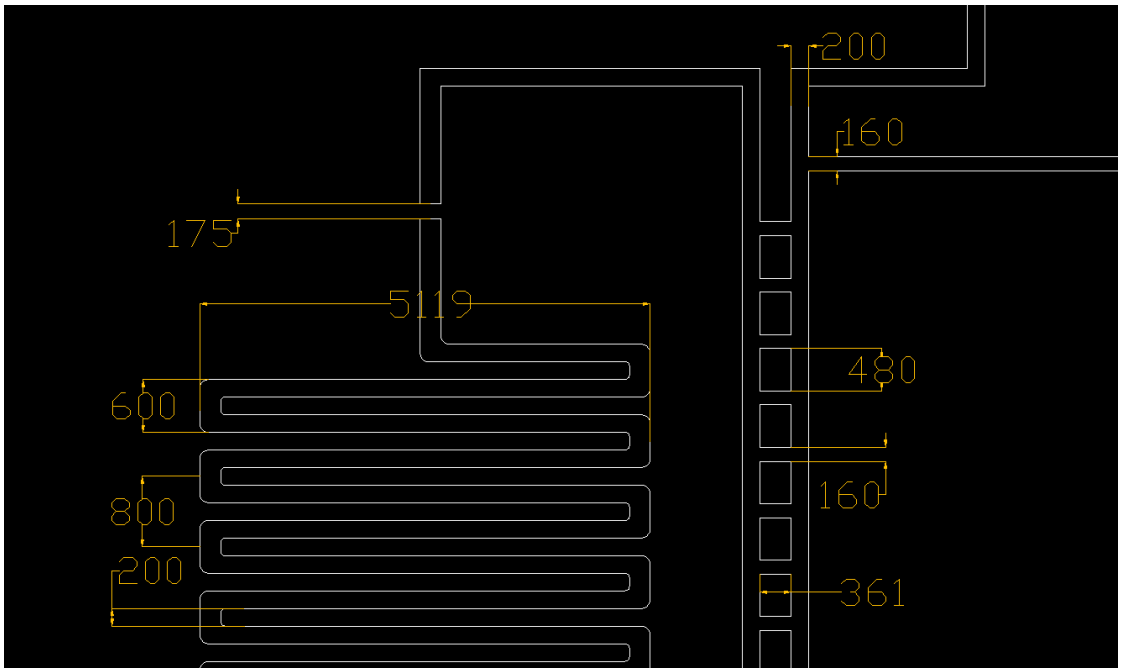
200
160
175
5119
480
600
160
800
200
361

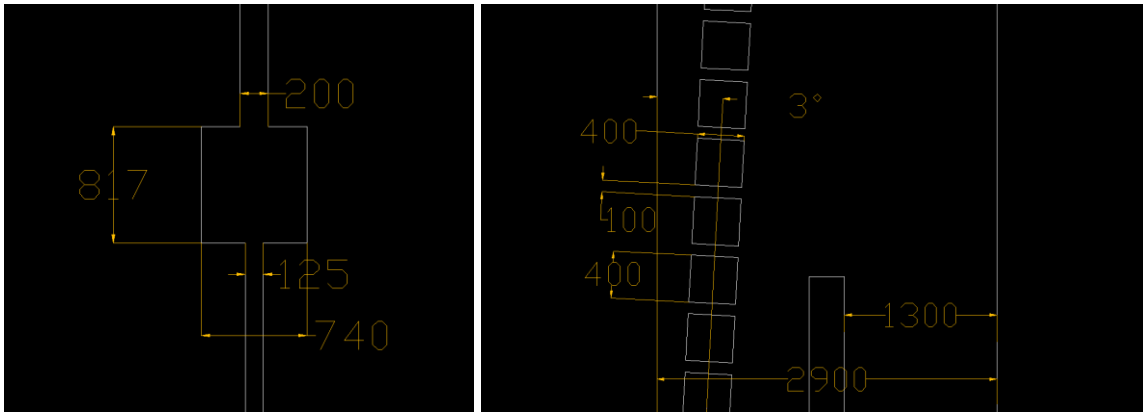

Figure A1.17. A high-throughput droplet microfluidics-based microalgae screening platform, droplet screening channel

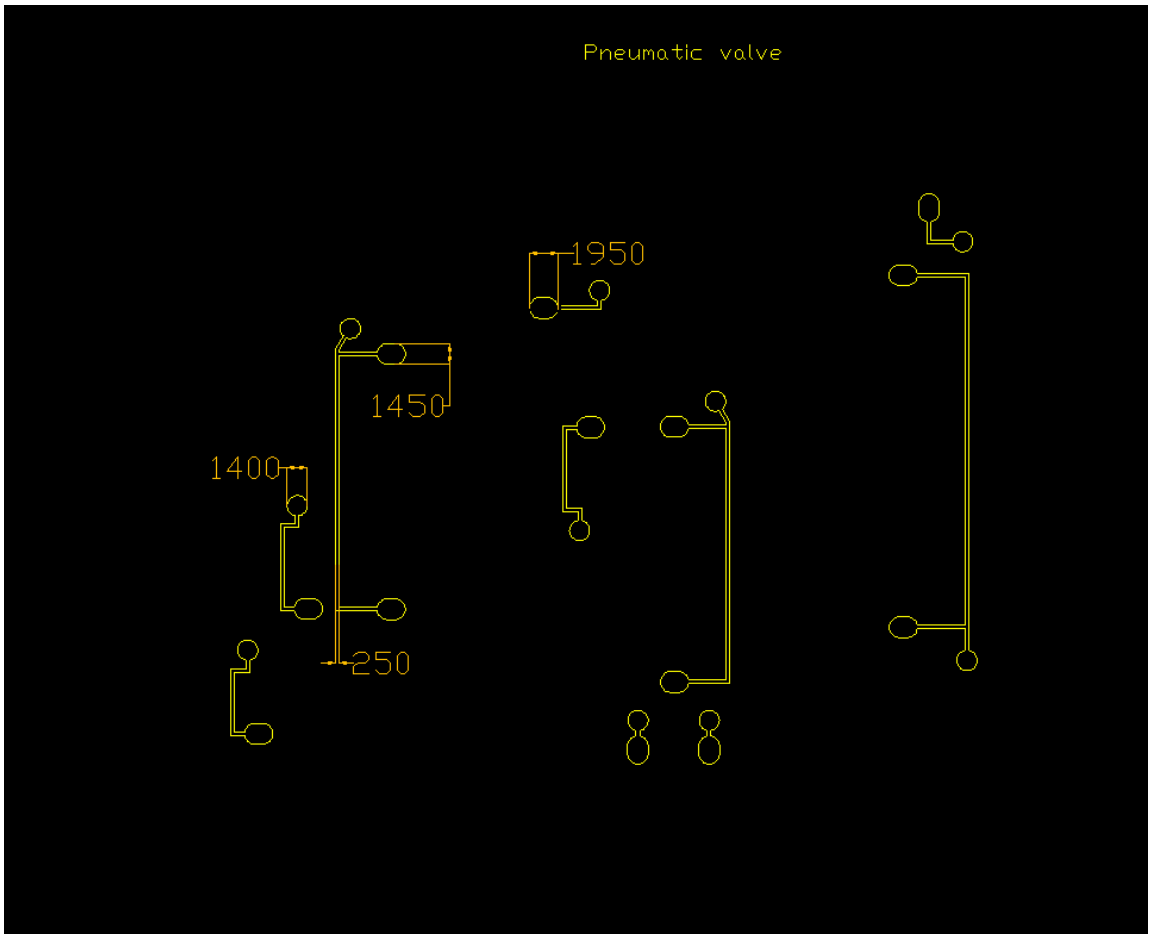

Figure A1.18. A high-throughput droplet microfluidics-based microalgae screening platform, pneumatic valve

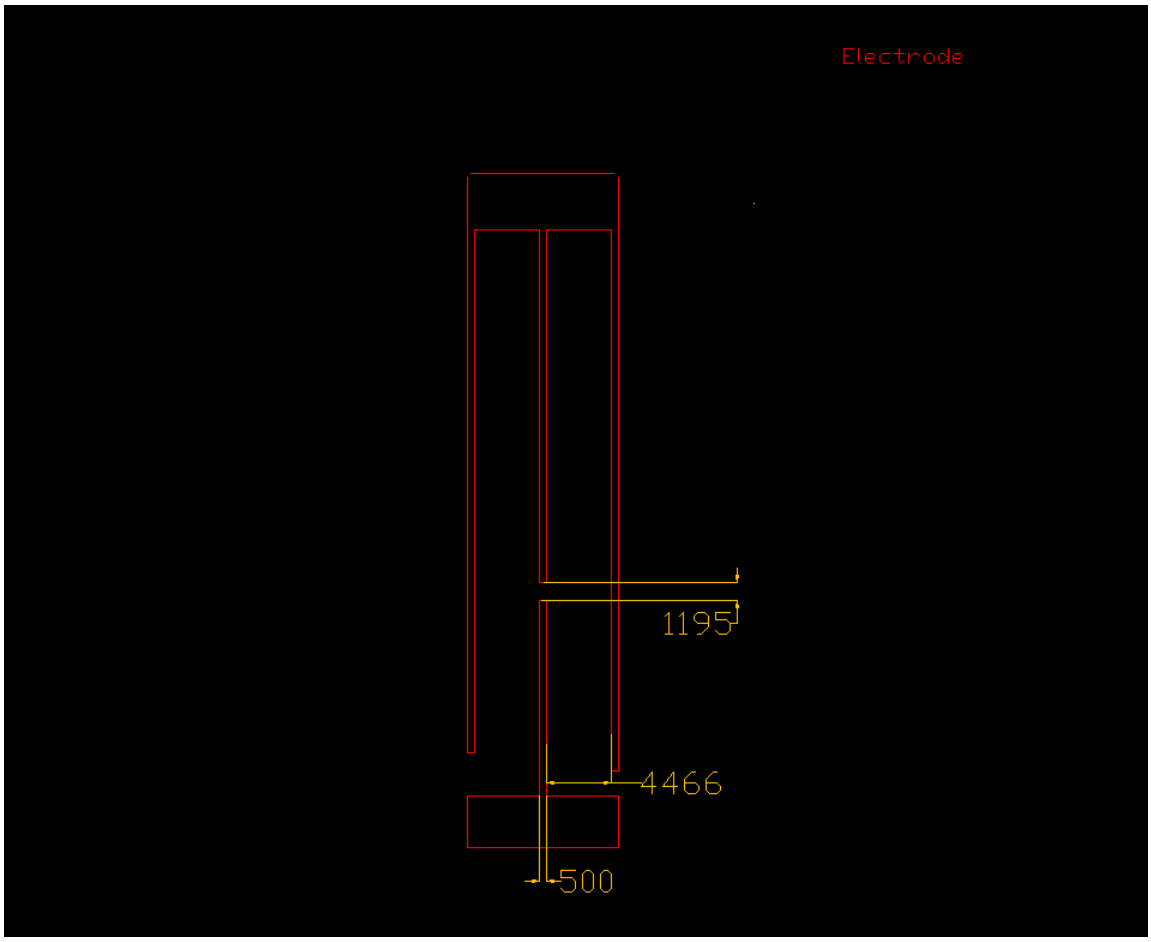

Figure A1.19. A high-throughput droplet microfluidics-based microalgae screening platform, electrode

2. PMMA mold designs (unit: mm)

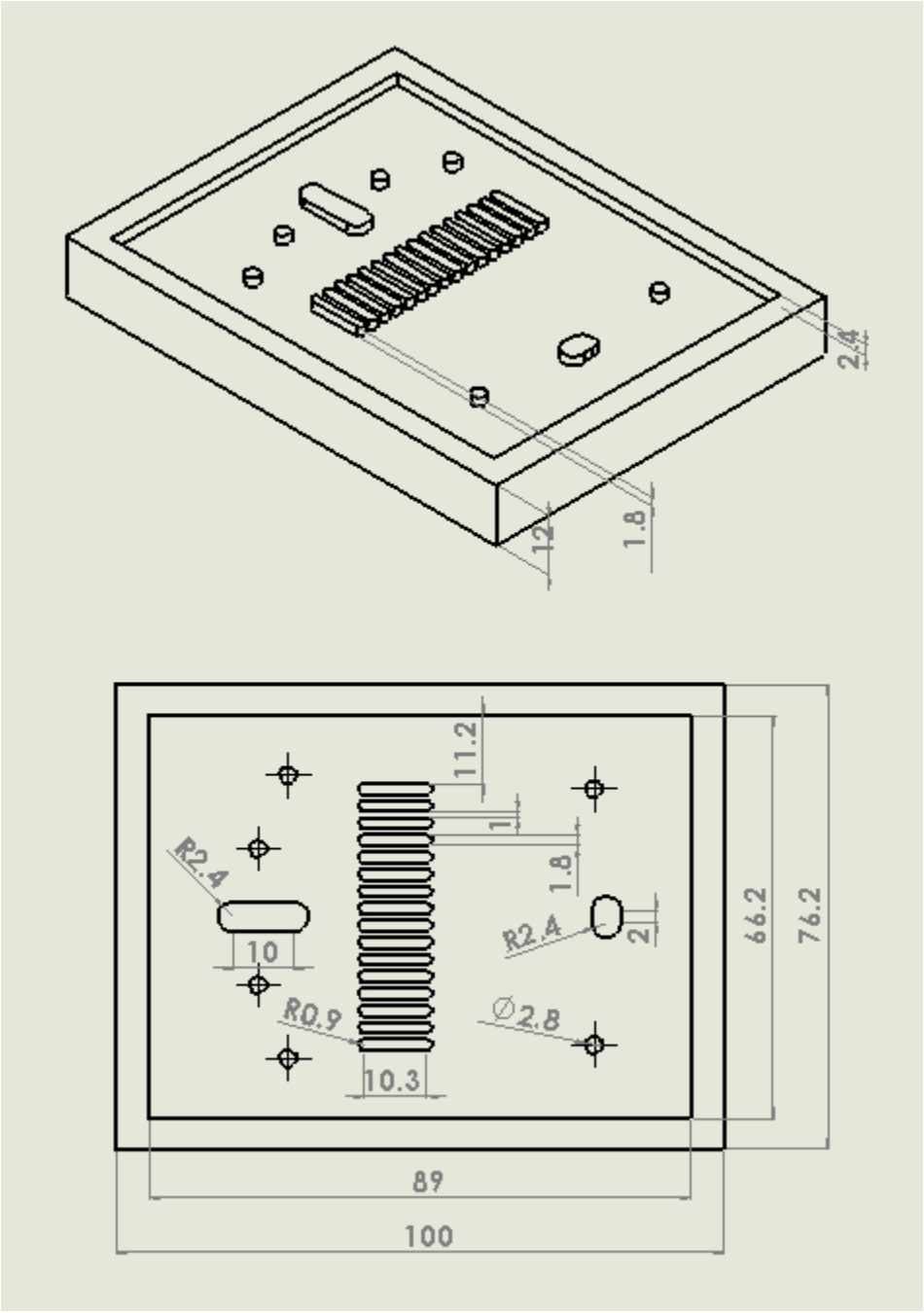

Figure A2.1. A high-throughput microfluidic photobioreactor array capable of screening 16 different light intensity conditions, light blocking layer mold

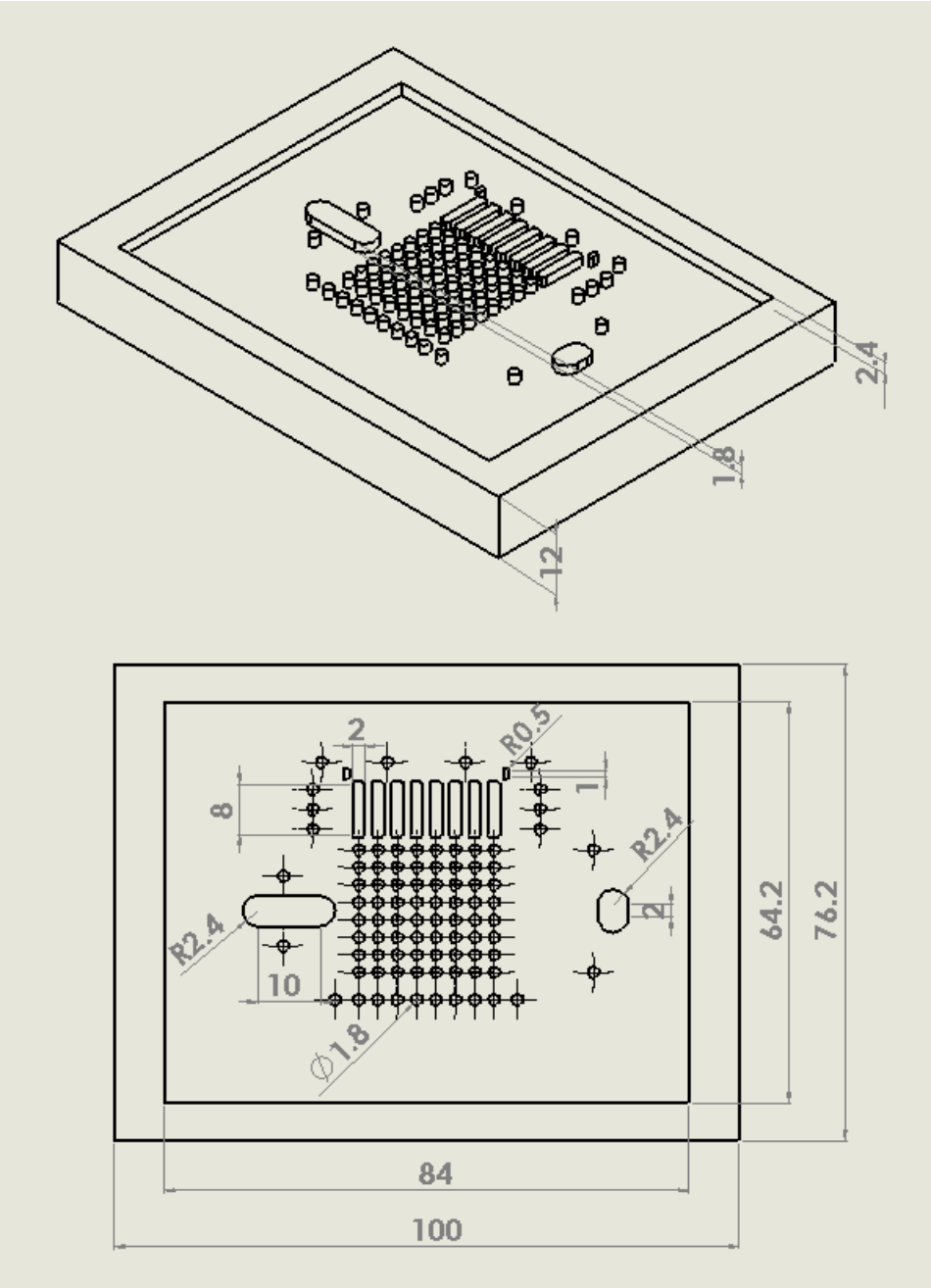

Figure A2.2. A high-throughput microfluidic photobioreactor array capable of screening 64 different light intensity conditions, light blocking layer mold

3. Fabrication protocol

(A) PDMS Soft-lithography

- Vapor coat PDMS soft-lithography master mold with (tridecafluoro-1,1,2,2-tetrahydrooctyl) trichlorosilane for 15 minutes
- Rinse the soft-lithography master mold with IPA, and dry with N_2 gas
- Mix PDMS pre-polymer with curing agent (10:1, w/w)
- Pour the PDMS mixture over the soft-lithography master mold
- Remove bubbles by degassing the PDMS mixture inside a vacuum chamber for 10-20 minutes
- Curing the PDMS inside a leveled 85°C oven for 3-12 hours for polymerization
- Cool down and peel off the polymerized PDMS layer from the master mold

(B) Master molds for a high-throughput microfluidic photobioreactor array

- Microalgae culture layer

  - Photoresist: SU-8™ 2050
  - Spin-coat: 60 seconds at 1500 rpm (acceleration: 10 seconds)
  - Soft bake: 60 minutes at 65 °C + 20 minutes at 95 °C
  - Exposure: 235 mJ/cm^2 (MA6, Karl Suss)
  - Post exposure bake: 10 minutes at 65 °C + 20 minutes at 95 °C
  - Develop in Thinner P

- Light intensity control layer

  - Photoresist: SU-8™ 2025
  - 1st spin-coat: 60 seconds at 2200 rpm (acceleration: 10 seconds)
  - 1st soft bake: 60 minutes at 65 °C + 20 minutes at 95 °C
  - 1st exposure: 205 mJ/cm^2 (MA6, Karl Suss)
  - 1st post exposure bake: 10 minutes at 65 °C + 20 minutes at 95 °C
  - Photoresist: SU-8™ 2075
  - 2nd spin-coat: 60 seconds at 1950 rpm (acceleration: 10 seconds)
  - 2nd soft bake: 24 hours at 65 °C + 40 minutes at 95 °C
  - 2nd exposure: 235 mJ/cm^2 (MA6, Karl Suss)
  - 2nd post exposure bake: 40 minutes at 65 °C + 20 minutes at 95 °C
  - Develop in Thinner P

- Light-dark cycle control layer

  - Photoresist: SU-8™ 2075

- Spin-coat: 60 seconds at 1950 rpm (light-dark control channels) and 1000 rpm (pneumatic binary demultiplexer), both with 10 second acceleration
- Soft bake: 24 hours at 65 °C + 40 minutes at 95 °C
- Exposure: 235 mJ/cm^2 (light-dark control channels) and 325 (pneumatic binary demultiplexer) mJ/cm^2 (MA6, Karl Suss)
- Post exposure bake: 40 minutes at 65 °C + 20 minutes at 95 °C
- Develop in Thinner P

- Light blocking layer
  - Design 3D schematic of the master mold using Solidworks or other 3D CAD design software
  - Print the design with 3D printer or Cut it using a CNC milling machine

(C) Master molds for a high-throughput microfluidic single-cell screening and selection platform

- Microfluidic cell culture/analysis layer

  - Photoresist: SU-8™ 2007
  - 1st spin-coat: 40 seconds at 3500 rpm
  - 1st soft bake: 10 minutes at 95 °C
  - 1st exposure: 175 mJ/cm^2 (MA6, Karl Suss)
  - 1st post exposure bake: 10 minutes at 95 °C
  - Develop in Thinner P
  - Photoresist: SU-8™ 2015
  - 2nd spin-coat: 40 seconds at 3000 rpm
  - 2nd soft bake: 10 minutes at 95 °C
  - 2nd exposure: 215 mJ/cm^2 (MA6, Karl Suss)
  - 2nd post exposure bake: 10 minutes at 95 °C
  - Develop in Thinner P

- Middle microfluidic control layer

  - Photoresist: SU-8™ 2002
  - 1st spin-coat: 40 seconds at 1000 rpm
  - 1st soft bake: 4 minutes at 95 °C
  - 1st exposure: 200 mJ/cm^2 (MA6, Karl Suss)
  - 1st post exposure bake: 4 minutes at 95 °C
  - Develop in Thinner P

- Photoresist: SU-8™ 2025
- 2nd spin-coat: 60 seconds at 3000 rpm (acceleration: 10 seconds)
- 2nd soft bake: 60 minutes at 65 °C + 20 minutes at 95 °C
- 2nd exposure: 205 mJ/cm^2 (MA6, Karl Suss)
- 2nd post exposure bake: 10 minutes at 65 °C + 20 minutes at 95 °C
- Develop in Thinner P

- Top microfluidic control layer & binary multiplexer
  - Photoresist: SU-8™ 2050
  - Spin-coat: 60 seconds at 3500 rpm (acceleration: 10 seconds)
  - Soft bake: 60 minutes at 65 °C + 20 minutes at 95 °C
  - Exposure: 220 mJ/cm^2 (MA6, Karl Suss)
  - Post exposure bake: 10 minutes at 65 °C + 20 minutes at 95 °C
  - Develop in Thinner P

(D) Master molds for a high-throughput droplet microfluidics-based microalgae screening platform

- Droplet screening channel layer

  - Photoresist: SU-8™ 2075
  - Spin-coat: 60 seconds at 1000 rpm (acceleration: 10 seconds)
  - Soft bake: 24 hours at 65 °C + 40 minutes at 95 °C
  - Exposure: 325 mJ/cm2 (MA6, Karl Suss)
  - Post exposure bake: 40 minutes at 65 °C + 20 minutes at 95 °C
  - Develop in Thinner P

- Pneumatic valve layer

  - Photoresist: SU-8™ 2075
  - 1st spin-coat: 60 seconds at 1000 rpm (acceleration: 10 seconds)
  - 1st soft bake: 24 hours at 65 °C + 40 minutes at 95 °C
  - 2nd spin-coat: 60 seconds at 1500 rpm (acceleration: 10 seconds)
  - 2nd soft bake: 24 hours at 65 °C + 40 minutes at 95 °C
  - Exposure: 370 mJ/cm2 (MA6, Karl Suss)
  - Post exposure bake: 40 minutes at 65 °C + 20 minutes at 95 °C
  - Develop in Thinner P

- Electrode layer

  - Deposit Cr/Cu on a glass slide (50.8 mm x 76.2 mm)
  - Photoresist: S1818
  - Spin-coat: 30 seconds at 4000 rpm

- Soft bake: 5 minutes at 110 °C
- Exposure: 84 mJ/cm2 (MA6, Karl Suss)
- Develop in MF-319
- Selective Cr/Cu etching (TFE and CE-100)
- Remove S1818 pattern by rinsing with acetone